

Herbich, John B.¹

Scour around pipelines, piles and sea walls

1991

¹ W.H. Bauer professor, Civil and Ocean Engineering, Texas A&M University

CONTENTS

SCOUR AROUND PIPELINES

- Scour DepthMaximum Scour Depth
- Pipelines Buried Near the Shoreline
- Pipelines in Intermediate and Deep Water

SCOUR AROUND PILES

- Dynamics of Scour
- Scour Around Pipelines Caused by Currents
- Scour Around Pile Groups Caused by Wave Action
- Scour Around Piles Due to Waves and Currents
- General Scour Depth and Critical Conditions for the Initiation of Scour,
- Analysis of "Total" and Net "Local" Scour Depth
- Summary
- Scour About a Single, Cylindrical Pile Due to Combined Random Waves and a Current

SCOUR AROUND LARGE DIAMETER PILES

- Local Scour Around Pile Groups Due to Waves and Currents
- Criteria for Local Scour Around Piles
- Dishpan Scour

SCOUR IN FRONT OF SEAWALLS

- Experimental Studies
- Mechanics of Sediment Movement
- Boundary Layer Along a Flat Sand Bed
- Dimensional Analysis
- General Observations
- Results
- Uncertainties Involved in Scour Prediction

REFERENCES

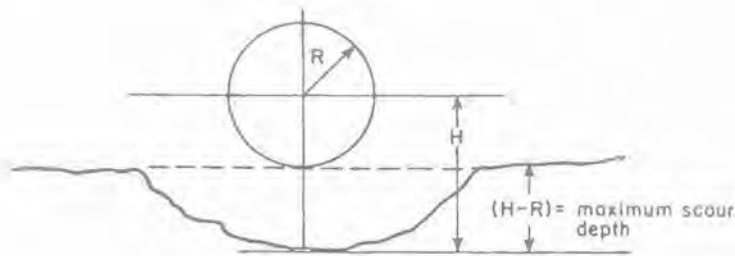


Figure 1. Graphical illustration of the problem.

Scour Around Pipelines*

Scour around pipelines may be caused by currents and/or waves and may be either long-term or short-term. Long-term changes in shallow water involve a general erosion or accretion of sediment over decades or hundreds of years. Shallow-water relates to a condition where wavelength-to-water-depth ratio is greater than 2. The short-term changes are associated with a variable-wave climate and the direction of sediment motion depends on the direction of wave approach angle.

If the currents near the pipeline are sufficiently strong to produce scour, the overburden will gradually erode as shown in Figure 1.

Storm waves produce appreciable horizontal and vertical velocities in shallow water. If the ocean bed is composed of erodible materials, the dynamic equilibrium of granular sediments may be disturbed and scour and deposition of sediments will occur. The pipe itself may trigger (or initiate) scour or cause additional local scour. Because of large horizontal drag and inertial forces as the storm intensifies, the scour may eventually uncover and expose the pipeline. The exposed pipe may be broken or damaged in such a case, because, generally, pipelines are not designed to withstand spanning and vibration due to vortex shedding. The subsiding storm may fill the trench, pushing the pipe upward or downward. If the pipe becomes buried again, a visual observation by a diver after the storm will not show that the pipe had moved closer to the ocean bottom or that it had been exposed during the storm.

Scour Depth

Kjeldsen, et al. [26] proposed a formula for estimating the equilibrium scour depth based on experiments with pipes having diameters 6 to 50 cm resting on a bed of sediment with a mean grain size of 0.074 mm.

The equilibrium scour depth in meters below the bottom of the pipeline, S , is

$$S = 0.972 \left(\frac{U^2}{g} \right)^{0.2} D^{0.80} \quad (1)$$

* From Chapter 3, "Scour Around Pipelines and Other Objects," *Offshore Pipeline Design Elements* (with permission from Marcel Dekker, Inc.) [20].

where U = flow velocity in m/sec
 g = acceleration due to gravity = 9.81 m/sec^2
 D = pipe diameter in m

In subsequent studies Kjeldsen found that the ratio of water depth to pipe diameter has no influence for values greater than 3 to 5.

Bijker [7] assumed that the velocity just outside the viscous sublayer for the undisturbed flow is

$$V_b = q_w V_R \quad (2)$$

where $q_w = 1/\ln(33 y_h/k_b)$

$y_h = h_0 + 2R$, with a positive or negative value of h_0

k_b = bottom roughness

V_R = mean velocity over the height of the pipe above the seafloor

h_0 = distance between the bottom of the pipe and seabed (Figure 2)

The velocity profile underneath the pipe is not logarithmic and the velocity V_b just outside the viscous sublayer under the pipe may be expressed as

$$V_b = s_w V_B \quad (3)$$

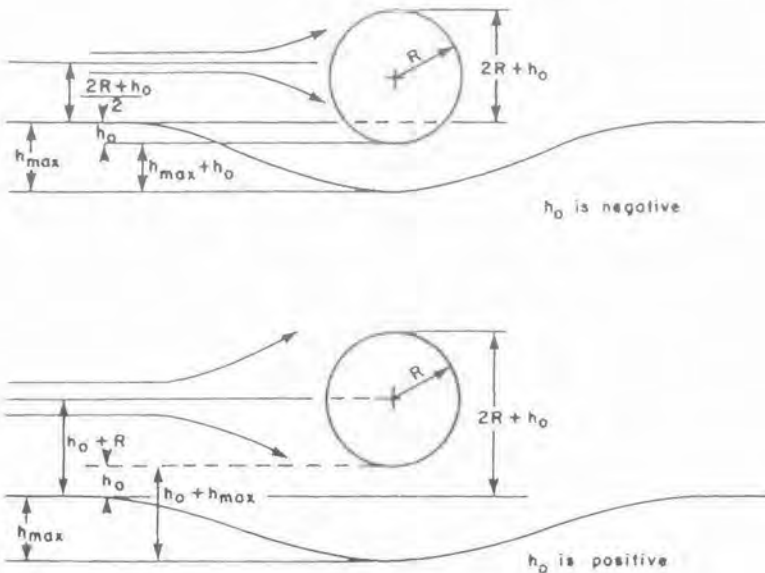


Figure 2. Flow pattern around pipes [7].

where $s_w = \sqrt{f'/(2\kappa^2)}$
 f' = wave friction factor [25]
 κ = von Karman's constant

and V_B just outside the boundary layer under the pipe is

$$V_B = V_R [1 + R^2/(h_0 + h_{max} + R)^2] \quad (4)$$

where h_{max} = distance from the seabed to the bottom of the scour hole (Figure 2).
 The velocity V_b just outside the viscous sublayer under the pipe is given by

$$V_b = s_w V_R [1 + R^2/(h_0 + h_{max} + R)^2] \quad (5)$$

Because this velocity must be equal to $q_w V_R$, the velocities under the pipe must be decreased by V_d , or

$$V_d = V_R [1 + R^2/(h_0 + h_{max} + R)^2] - \frac{q_w}{s_w} V_R \quad (6)$$

The scour measured under the pipe for uniform flow is shown in Figure 3.

Carstens [10] measured localized scour around horizontal cylinders in oscillatory flow. The scour depth, S , function was related to the sediment number, N_s , defined as

$$N_s = \frac{U_{max}}{\sqrt{(s-1)gd}} \quad (7)$$

where U_{max} = maximum velocity in oscillatory flow
 s = specific gravity of sediment
 d = grain diameter

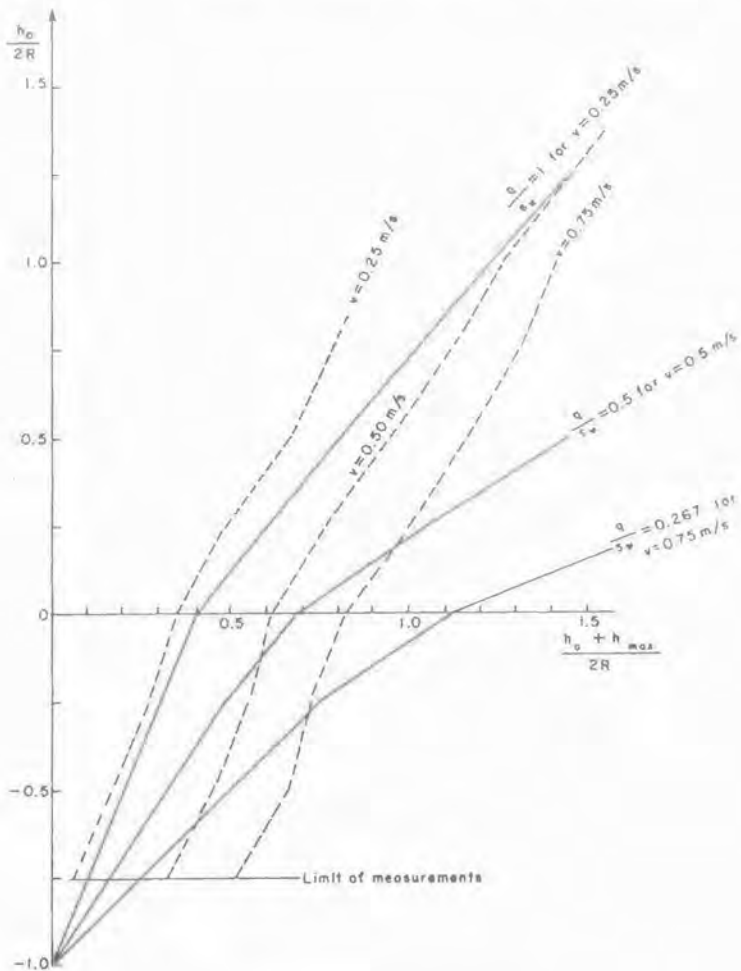
The dimensionless scour is

$$\frac{S}{L} = f \left[(N_s^2 - N_{sc}^2)^{5/2} \frac{d}{L} \left(\frac{U t}{L} \right) \right] \quad (8)$$

where L = characteristic length
 U = characteristic velocity
 t = time
 N_{sc} = zero transport sediment transport number (determined experimentally).

Bijker [7] indicated that the velocity distribution around the pipe may be expressed as

$$U_a = U_0 \left(1 + \frac{R^2}{a^2} \right) \quad (9)$$



LEGEND

- SCOUR MEASUREMENTS FOR CONSTANT VELOCITIES
- $\frac{q}{a_w}$ FOR CONSTANT VELOCITIES AND INCREASING $\frac{h_a + h_{max}}{2R}$

Figure 3. Pipeline scour caused by currents [7].

where U_a = velocity around the pipe
 a = distance from the center of the pipe
 R = radius of the pipe
 U_0 = orbital velocity at the bottom

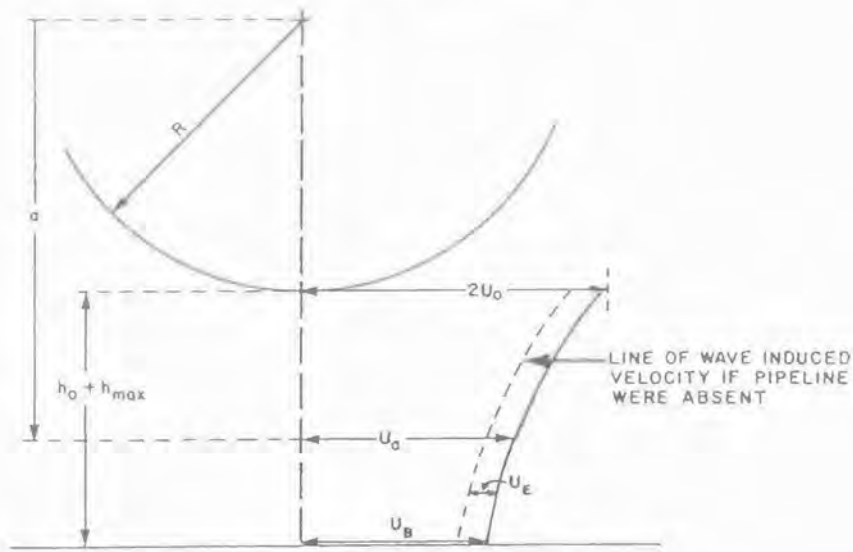


Figure 4. Velocity distribution around pipeline [7].

Based on the distances h_0 and h_{max} as shown in Figure 4, the velocity just outside the boundary layer under the pipe is

$$U_B = U_0 \left[1 + R^2 / (h_0 + h_{max} + R)^2 \right] \quad (10)$$

Because this velocity must be equal to U_0 , the velocities under the pipeline are decreased by a value, U_E , defined as

$$\begin{aligned} U_E &= U_0 \left[1 + R^2 / (h_0 + h_{max} + R)^2 \right] - U_0 \\ &= U_0 R^2 / (h_0 + H_{max} + R)^2 \end{aligned} \quad (11)$$

Van Ast and de Boer [52] employed the assumed distribution of flow to derive the following expressions for the scour depth ($h_0 + h_{max}$):

$$S^3 = S^2(3R - B) + S(R^2 - 2BR) - BR^2 = 0 \quad \text{for } h_0 \geq 0 \quad (12a)$$

$$S^3 - 2S^2R = SR^2 - R^3 = 0 \quad \text{for } h_0 = 0 \quad (12b)$$

$$S^3 + S^2(5R - B)/2 - BRS - (R^3 + BR^2)/2 = 0 \quad \text{for } h_0 \leq 0 \quad (12c)$$

$$\text{where } S = (h_0 + h_{max}) \text{ and } B = (h_0 + R) \quad (13)$$

It will be noted that this expression for scour depends only on the radius of the pipeline and not on the sediment or wave characteristics.

Experimental results conducted at the Delft University of Technology, the Netherlands and at the Hydraulic Research Station, Wallingford, U.K. are shown in Figure 5.

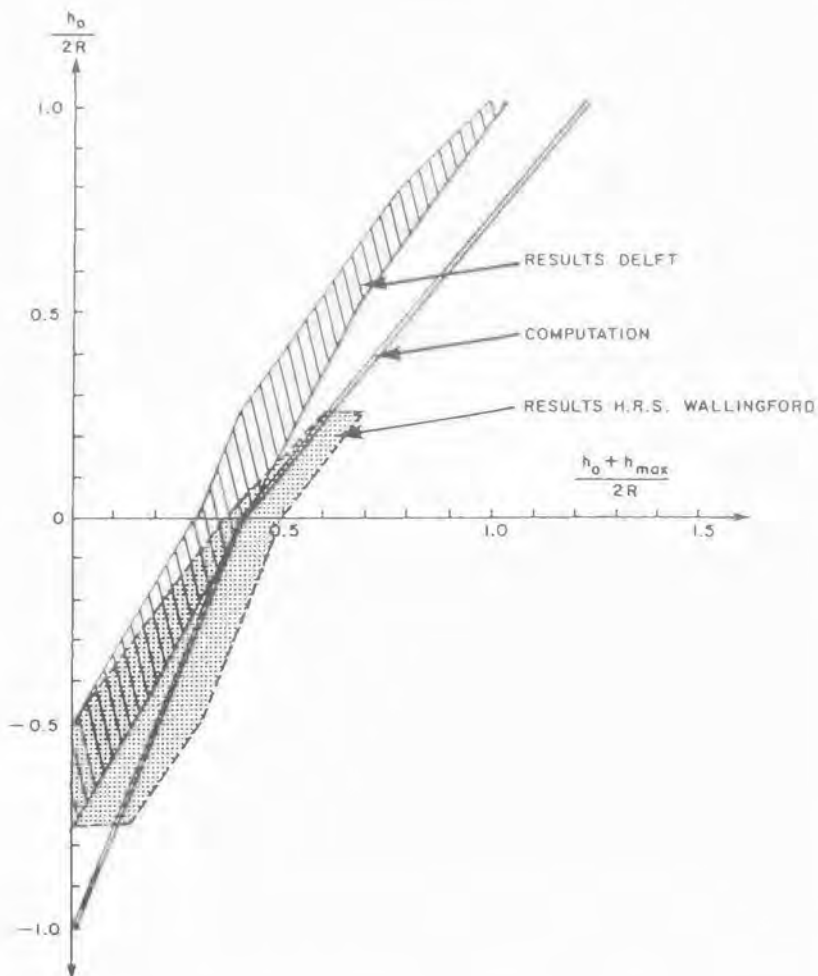


Figure 5. Pipeline scour caused by waves [7].

Maximum Scour Depth

An analytical method for estimating the maximum scour depth under the offshore pipelines due to currents was developed by Chao and Hennessy [11]. This method provides an order-of-magnitude estimation of the possible scour hole depth.

The subsurface current is assumed to flow perpendicular to the longitudinal axis of the pipeline. Based on two-dimensional potential flow theory and the assumptions outlined by Chao and Hennessy, the discharge through the scour hole is:

$$q = u_0 \left(H - \frac{R^2}{2H - R} \right) \quad \text{for } H \geq R \quad (14)$$

where u_0 = undisturbed subsurface current at the top of the pipe
 R = radius of the pipe
 H = scour hole depth from the center of the pipe

The average jet velocity is:

$$u_{\text{avg}} = \frac{q}{(H - R)} = u_0 \left[\frac{2 \left(\frac{H}{R} \right)^2 - \left(\frac{H}{R} \right) - 1}{2 \left(\frac{H}{R} \right)^2 - 3 \left(\frac{H}{R} \right) + 1} \right] \quad \text{for } H \geq R \quad (15)$$

If the velocity in the scour hole is greater than the free stream velocity, erosion may occur. The limit of scour is presumably reached when, because of the enlargement of the scour section, the velocity along the boundary has decreased to the point at which the boundary shear stress τ_b becomes equal to the critical tractive stress τ_c of the sediment composing the erodible beds.

The critical tractive stress for a given sand grain size is plotted in Figure 6, and required values of τ_c were obtained as shown in Table 1.

The boundary shear stress in the eroded channel is computed based on assumptions stated by Chao and Hennessy [11]. The friction factor f_r is estimated from the Reynolds number relationship reported by Lovera and Kennedy [29], by using a Reynolds number defined as:

$$R_n = \frac{u_{\text{avg}}(H - R)}{\nu} \quad (16)$$

where ν = kinematic viscosity of seawater. The roughness parameter is defined as $R_h/D_{50} \times 10^{-2}$, where R_h is the hydraulic radius, which is approximated as $(H - R)$. The friction factor f_r is determined from Figure 7.

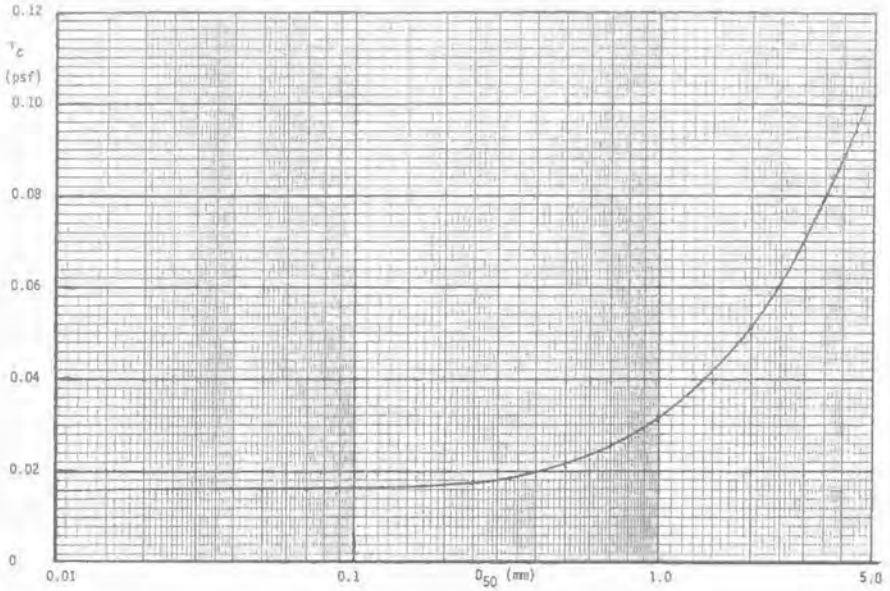


Figure 6. Critical tractive stress vs. grain size.

Table 1
Critical Tractive Stress for Various Grain Sizes

D_{50} , mm	τ_c , ^e psf
4.00	0.0890
2.00	0.0513
1.00	0.0316
0.75	0.0266
0.50	0.0215
0.25	0.0172
0.13	0.0166
0.10	0.0164
0.08	0.0162
0.05	0.0161

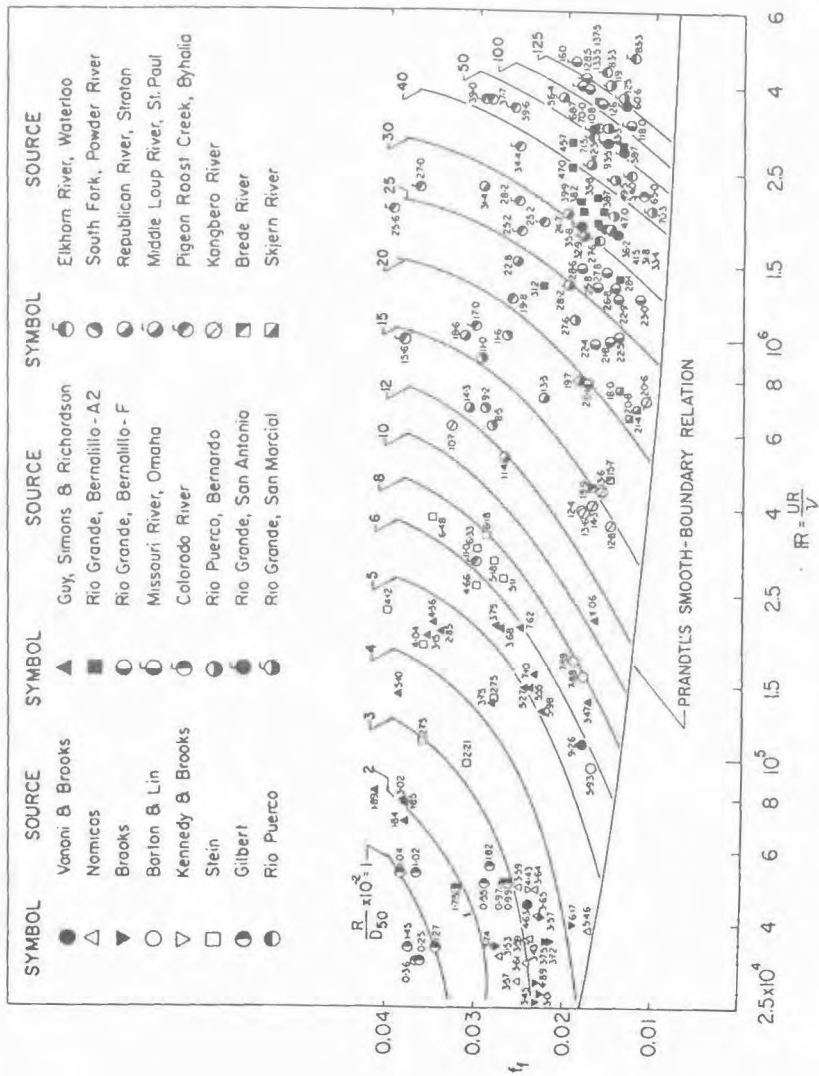


Figure 7. Friction factor predictor for flat-bed flows in alluvial channels. (From Lovera and Kennedy, 1969. Reprinted by permission.)

Once the friction factor is known, the boundary stress is calculated by using the relationship described by Streeter [12]:

$$\tau_b = \frac{f_r \rho (u_{avg})^2}{8} \quad (17)$$

where ρ is the density of seawater. These calculations were performed for bottom velocities of

$$u_0 = 0.5, 1.0, 1.5, \text{ and } 2.0 \text{ ft/sec}$$

and scour hole depths of

$$H = 1, 2, 3, 4, 5, 6, 7, 8, 9, \text{ and } 10 \text{ ft, for } H \geq R$$

The boundary shear stresses τ_b were plotted as a function of scour hole depth H (Figures 8-25). The maximum scour depth ($H - R$) was then plotted as a function of bottom current velocity.

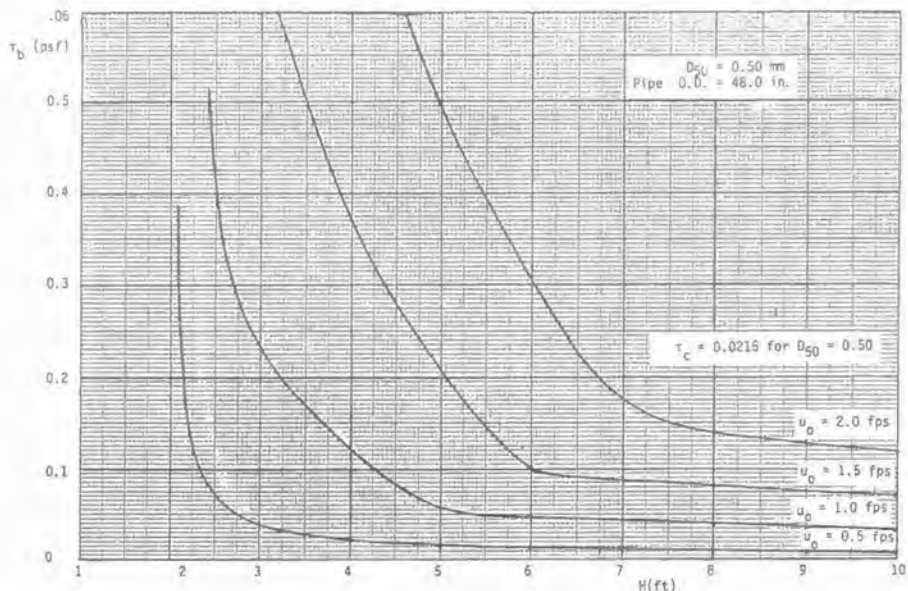


Figure 8. The boundary shear stress as a function of wave height; pipe O.D. = 48 in; $D_{50} = 0.5$ mm.

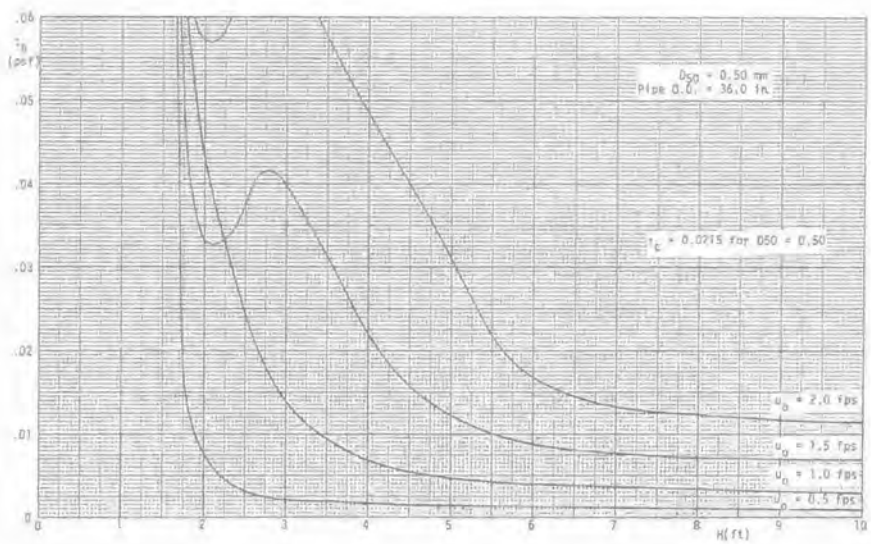


Figure 9. τ_b as a function of wave height; pipe O.D. = 36 in; $D_{50} = 0.50 \text{ mm}$.

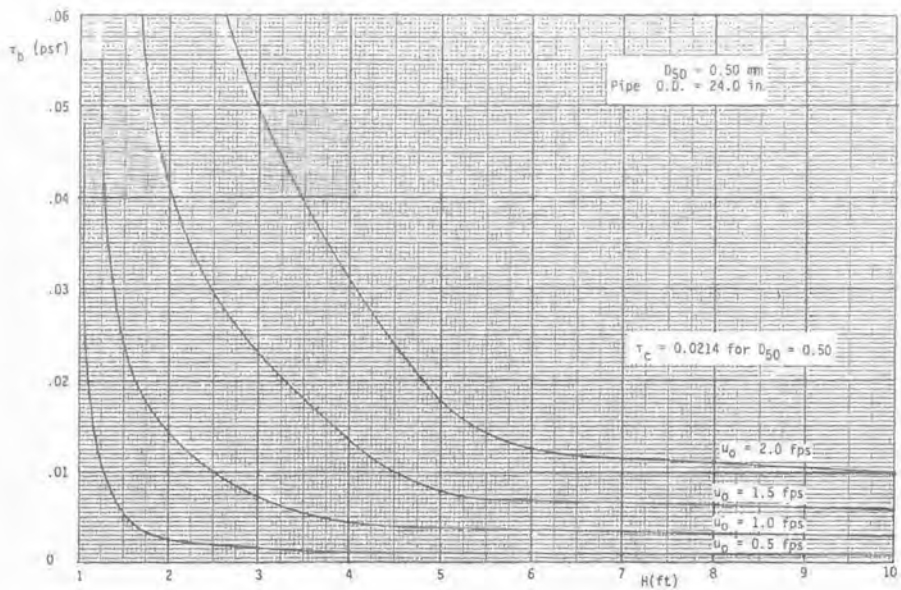


Figure 10. τ_b as a function of wave height; pipe O.D. = 24 in; $D_{50} = 0.50 \text{ mm}$.

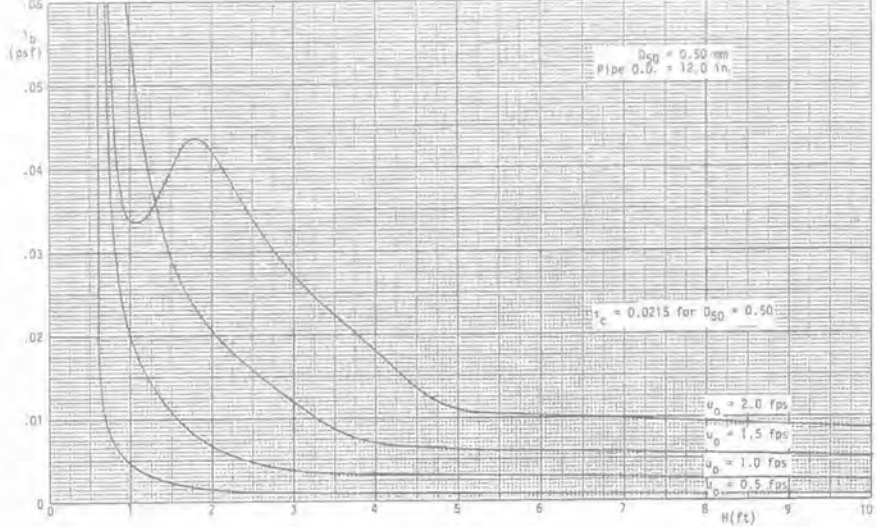


Figure 11. τ_b as a function of wave height; pipe O.D. = 12 in; $D_{50} = 0.5 \text{ mm}$.

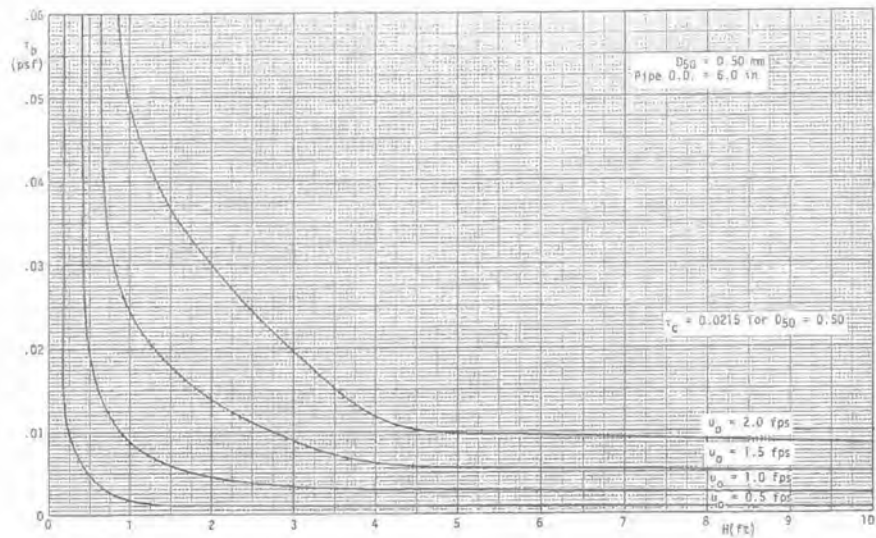


Figure 12. τ_b as a function of wave height; pipe O.D. = 6 in; $D_{50} = 0.5 \text{ mm}$.

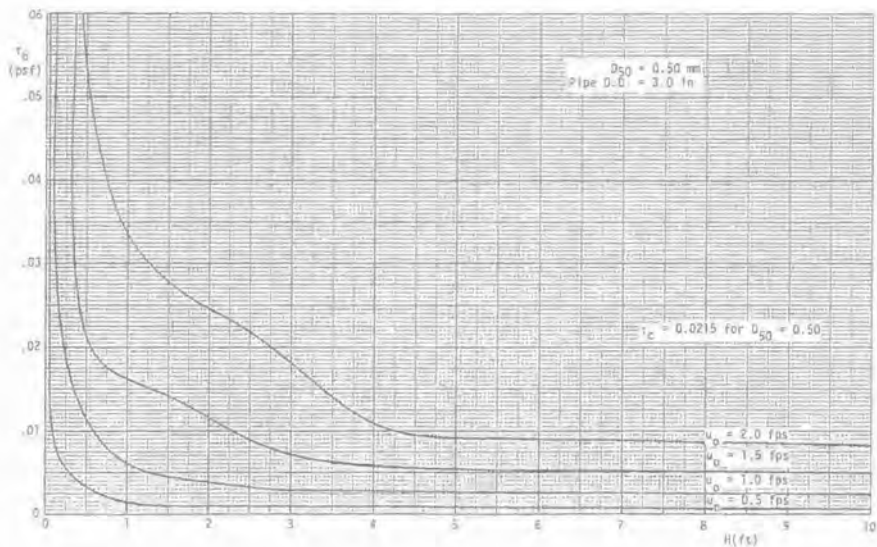


Figure 13. τ_b as a function of wave height; pipe O.D. = 3 in; $D_{50} = 50$ mm.

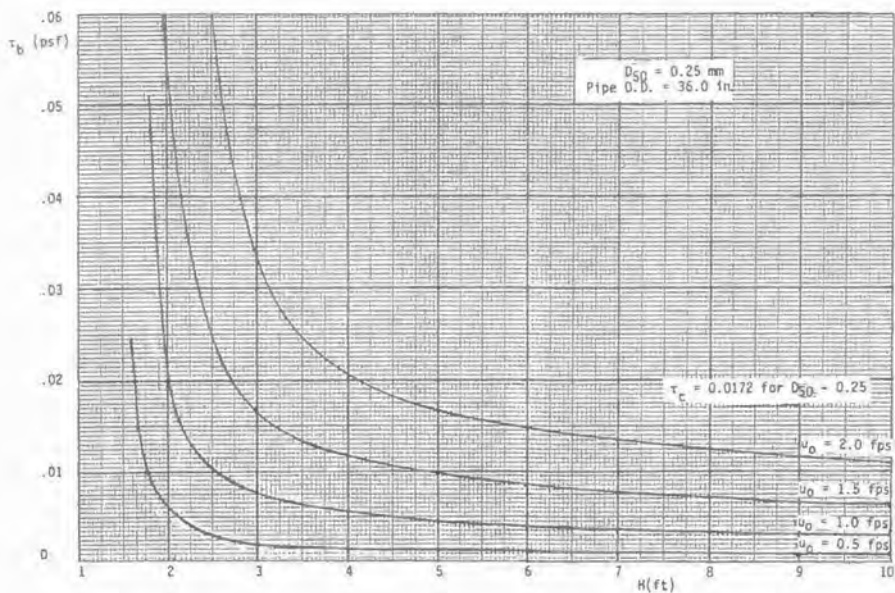


Figure 14. τ_b as a function of wave height; pipe O.D. = 48 in; $D_{50} = 0.25$ mm.

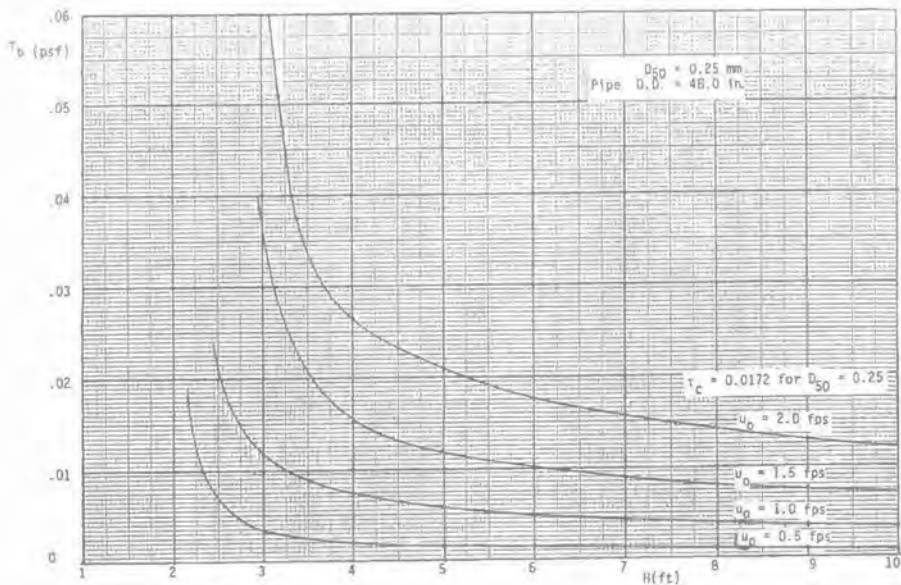


Figure 15. τ_b as a function of wave height; pipe O.D. = 36 in; $D_{50} = 0.25$ mm.

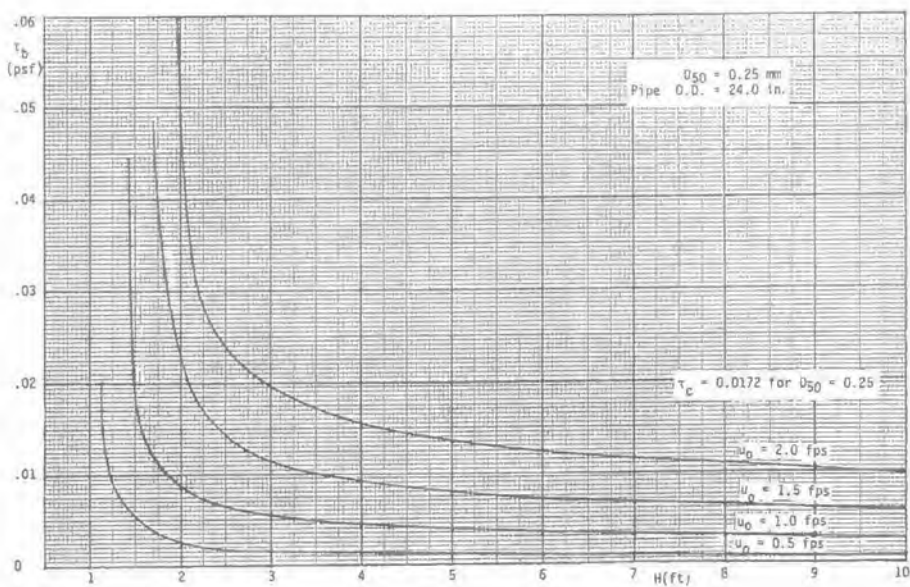


Figure 16. τ_b as a function of wave height; pipe O.D. = 24 in; $D_{50} = 0.25$ mm.

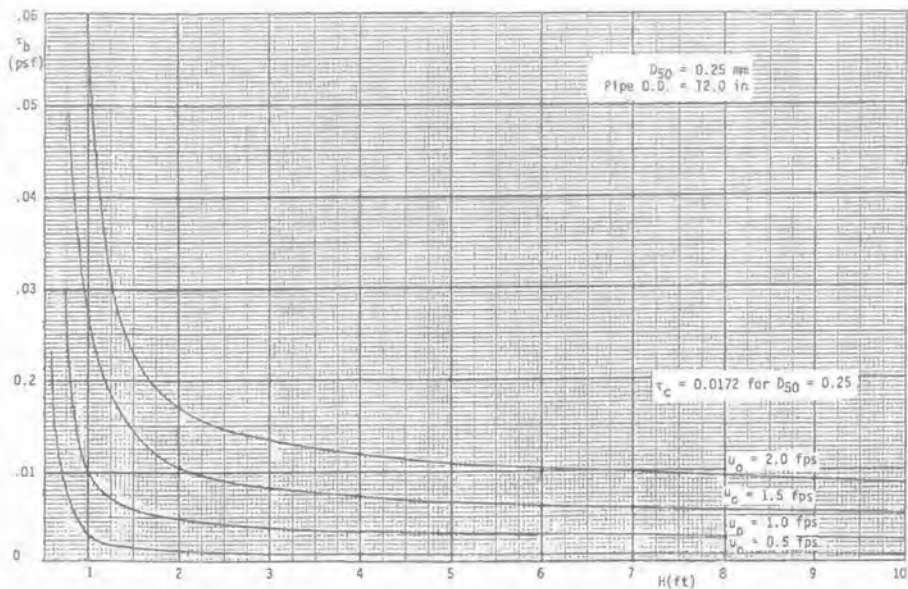


Figure 17. τ_b as a function of wave height; pipe O.D. = 12 in; $D_{50} = 0.25 \text{ mm}$.

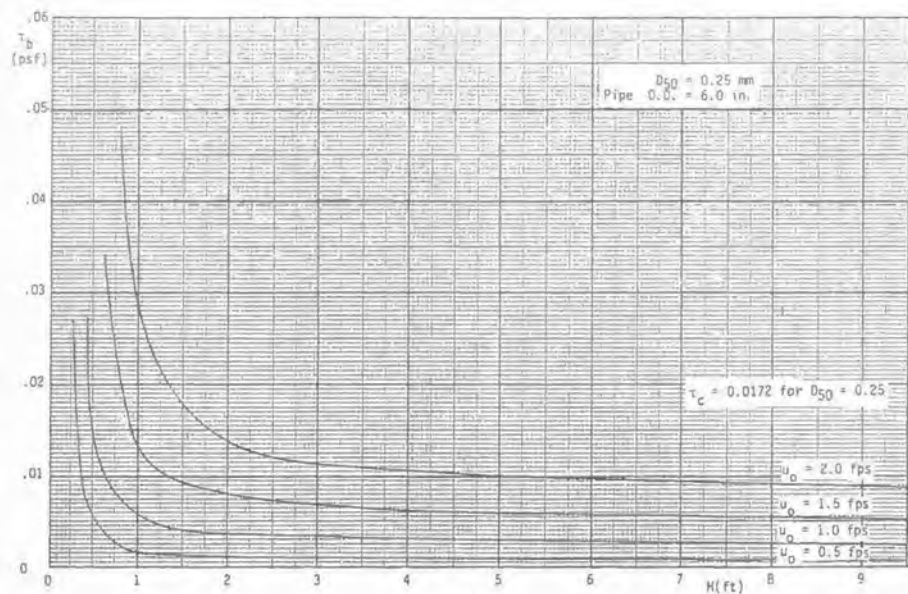


Figure 18. τ_b as a function of wave height; pipe O.D. = 6 in; $D_{50} = 0.25 \text{ mm}$.

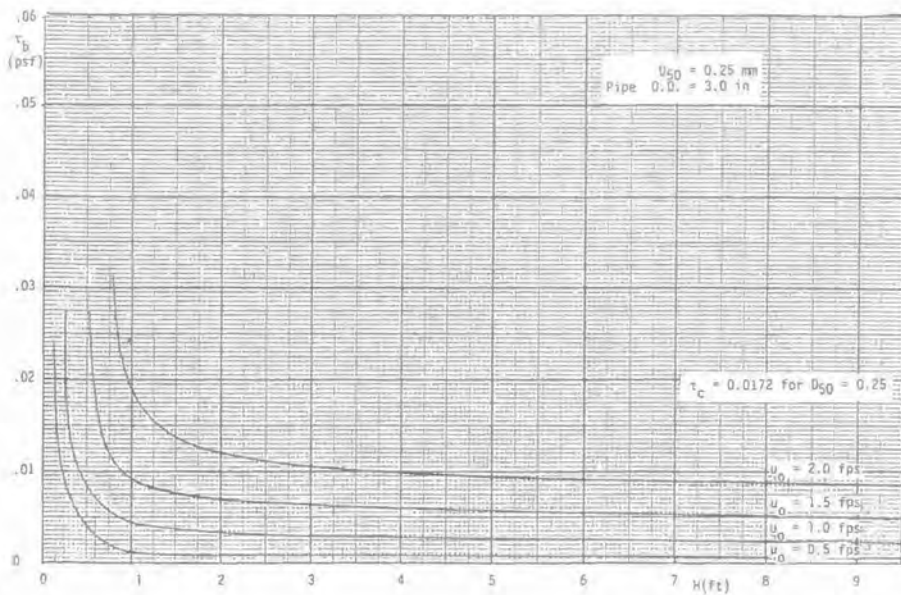


Figure 19. τ_b as a function of wave height; pipe O.D. = 3 in; $D_{50} = 0.25$ mm.

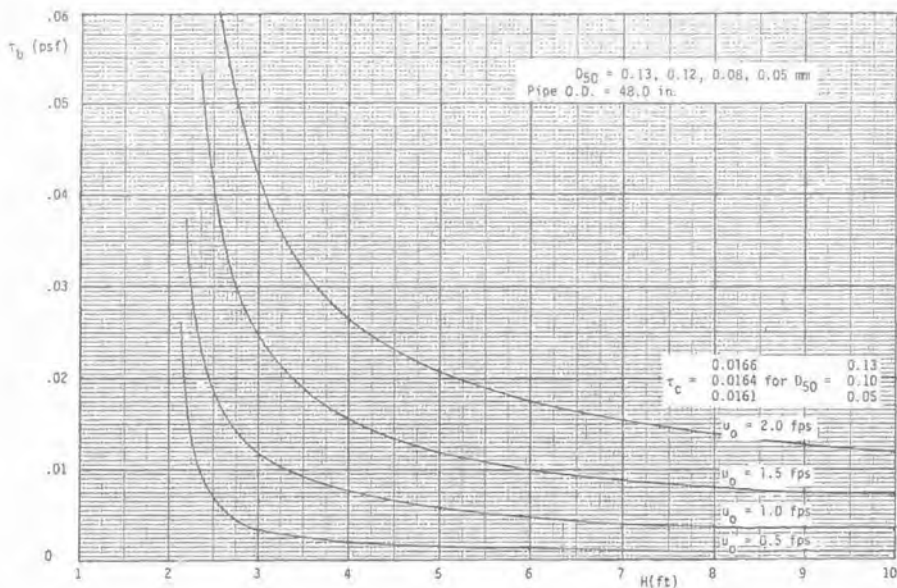


Figure 20. τ_b as a function of wave height; pipe O.D. = 48 in; $D_{50} = 0.13, 0.12, 0.08, 0.05$ mm.

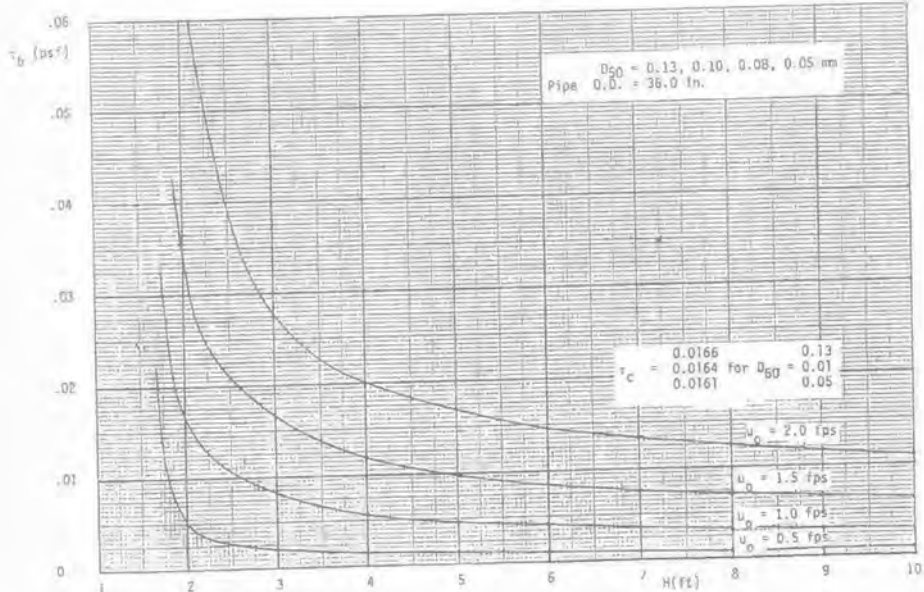


Figure 21. τ_b as a function of wave height; pipe O.D. = 36 in; $D_{50} = 0.13, 0.10, 0.08, 0.05$ mm.

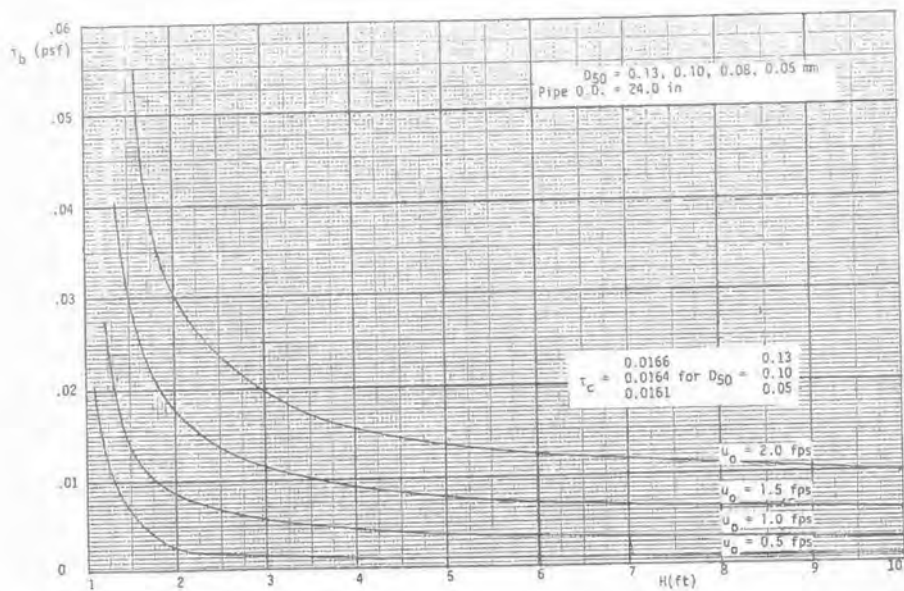


Figure 22. τ_b as a function of wave height; pipe O.D. = 24 in; $D_{50} = 0.13, 0.10, 0.08$ and 0.05 mm.

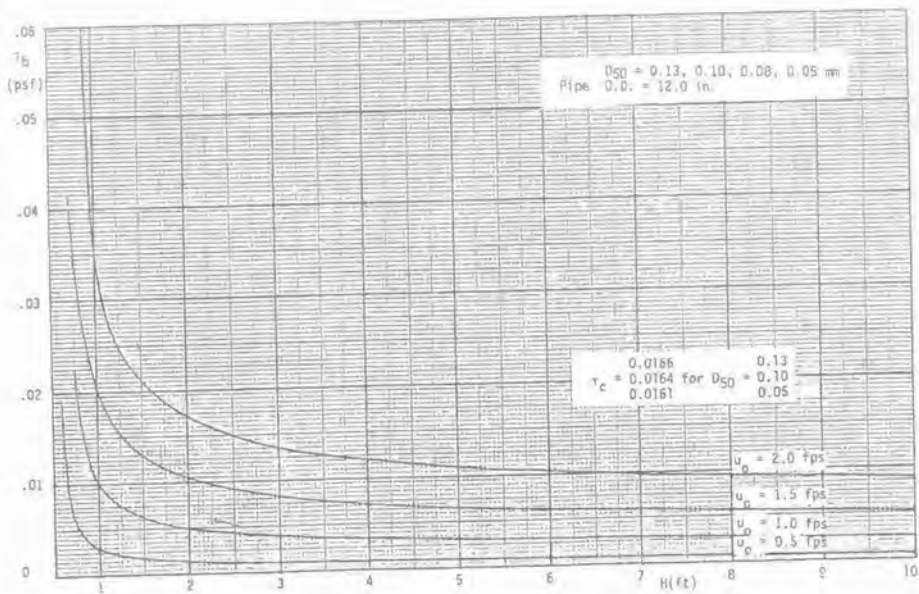


Figure 23. τ_b as a function of wave height; pipe O.D. = 12 in; $D_{50} = 0.13, 0.10, 0.08, 0.05 \text{ mm}$.

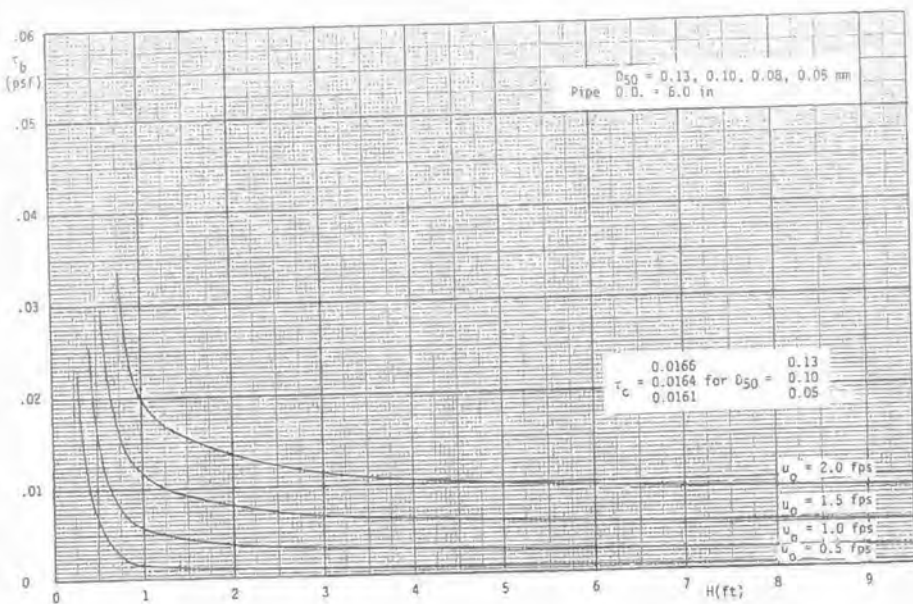


Figure 24. τ_b as a function of wave height; pipe O.D. = 6 in; $D_{50} = 0.13, 0.10, 0.08, 0.05 \text{ mm}$.

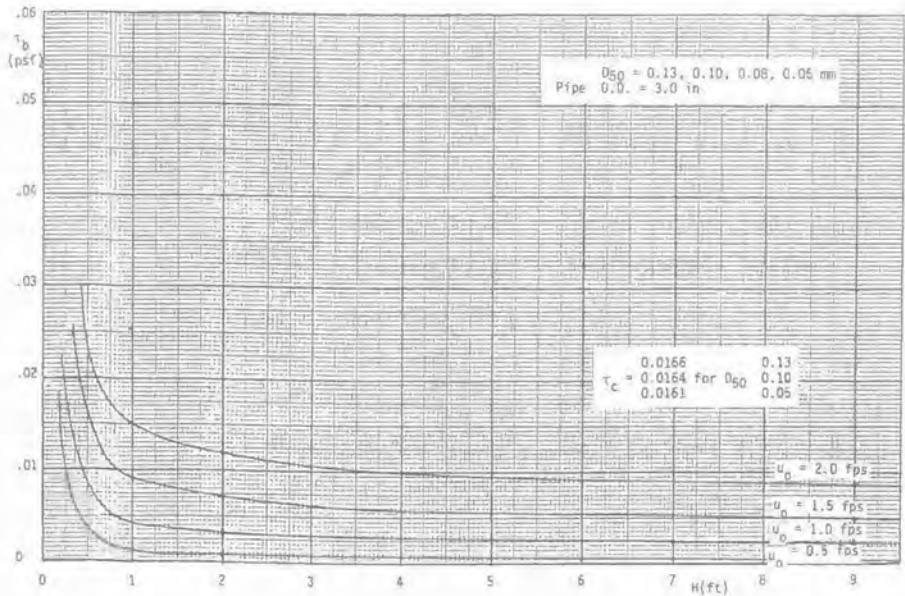


Figure 25. τ_b as a function of wave height; pipe O.D. = 3 in; D_{50} = 0.13, 0.10, 0.08, 0.05 mm.

Boundary Shear Stresses. Curves were plotted for the following cases:

$D_{50} = 0.50$ mm } O.D. = 48, 36, 24, 12, 6, 3, in.
(Figures 8-13)

= 0.25 mm } O.D. = 48, 36, 24, 12, 6, 3 in.
(Figures 14-19)

= 0.13 mm }
= 0.10 mm } identical curves
= 0.08 mm } O.D. = 48, 36, 24, 12, 6, 3, in.
= 0.05 mm } (Figures 20-25)

Curves for the other cases were not suitable for this analysis.

Maximum Scour Depth. Curves were plotted for the following cases:

- $D_{50} = 0.50$ mm (Figure 26a)
- = 0.25 mm (Figure 26b)
- = 0.13 mm (Figure 26c)
- = 0.10 mm (Figure 26d)
- = 0.05 mm (Figure 26e)

The curves for $D_{50} = 0.08$ mm are almost identical to those for $D_{50} = 0.05$ mm.

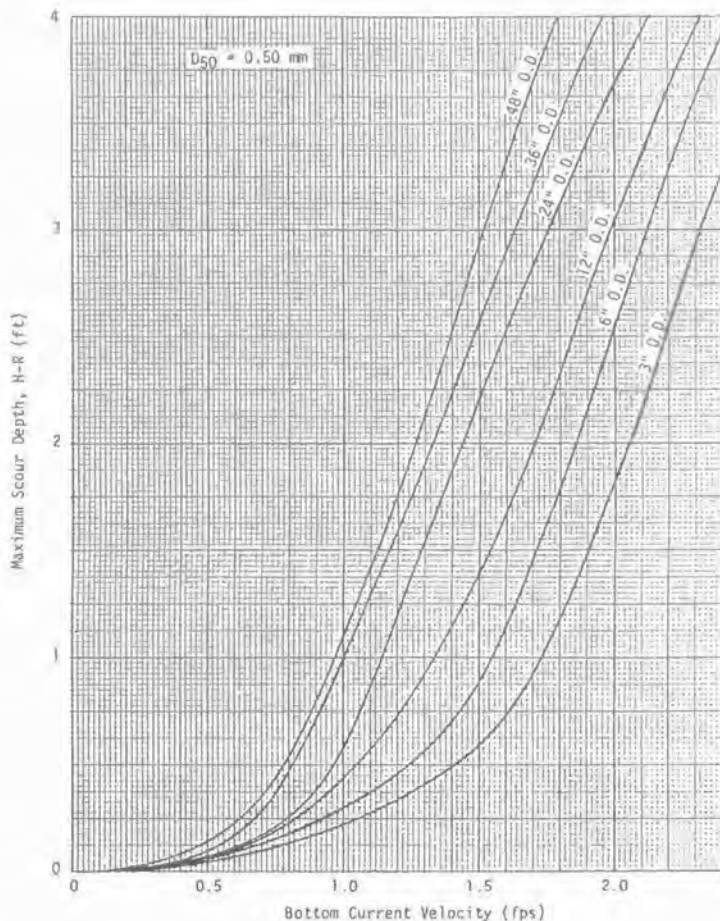


Figure 26a. Maximum scour depth as a function of bottom current velocity — $D_{50} = 0.50$ mm.

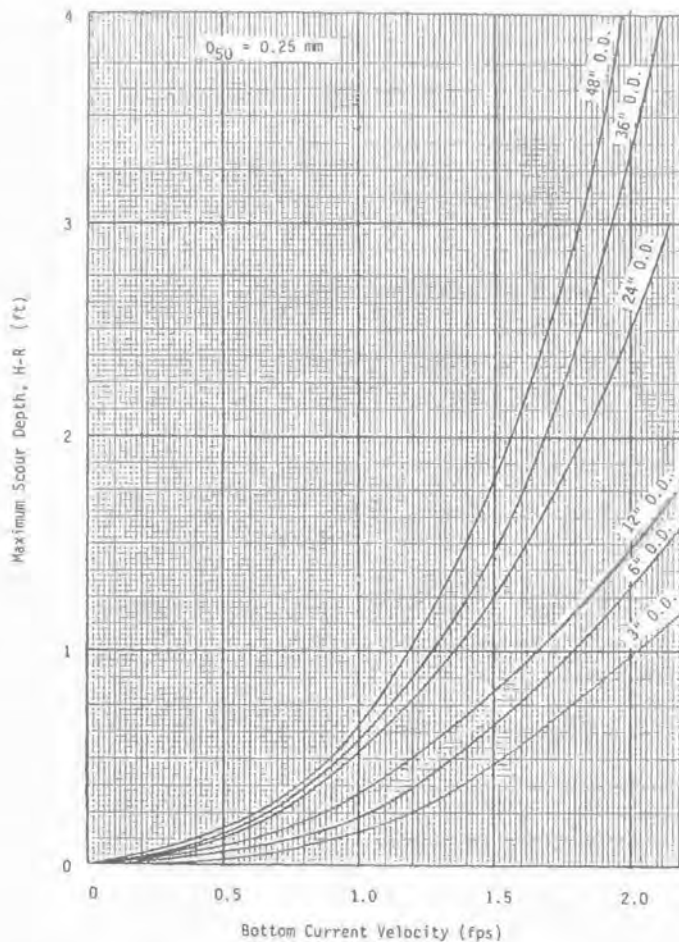


Figure 26b. Maximum scour depth as a function of bottom current velocity — $D_{50} = 0.25$ mm.

Pipelines Buried Near the Shoreline

The objective of this section is to determine, through physical modeling, the effect of storm waves on buried pipelines approaching the shoreline. Scour depth and scour patterns were evaluated in a 120-ft-long two-dimensional wave tank that was 2 ft wide and 3 ft deep. Three-dimensional effects were studied in a 32 × 86 ft wave basin that was 2.5 ft deep. The parameters varied including water depth, pipe burial

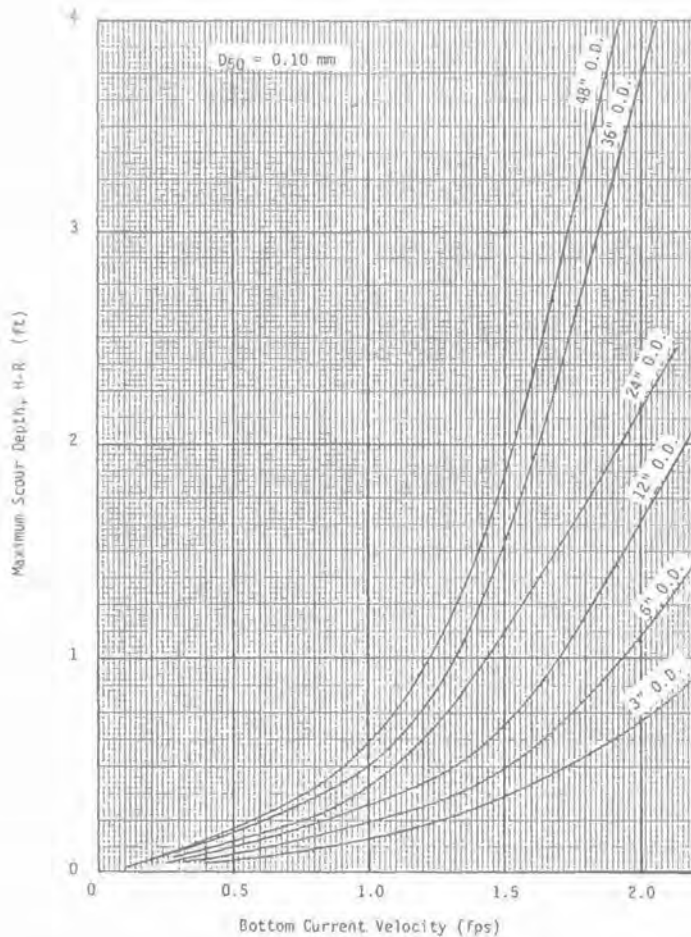


Figure 26c. Maximum scour depth as a function of bottom current velocity — $D_{50} = 0.13$ mm.

depth, beach slope, and wave characteristics such as height, period, and direction. A two-dimensional beach profile was used to investigate the required depth of burial for a pipeline through the surf zone.

The monochromatic wave generator was of the oscillating pendulum type with adjustable speed and eccentricity, which allowed the desired wave height and period to be obtained. A slope wave-absorbing structure made of perforated metal sheets

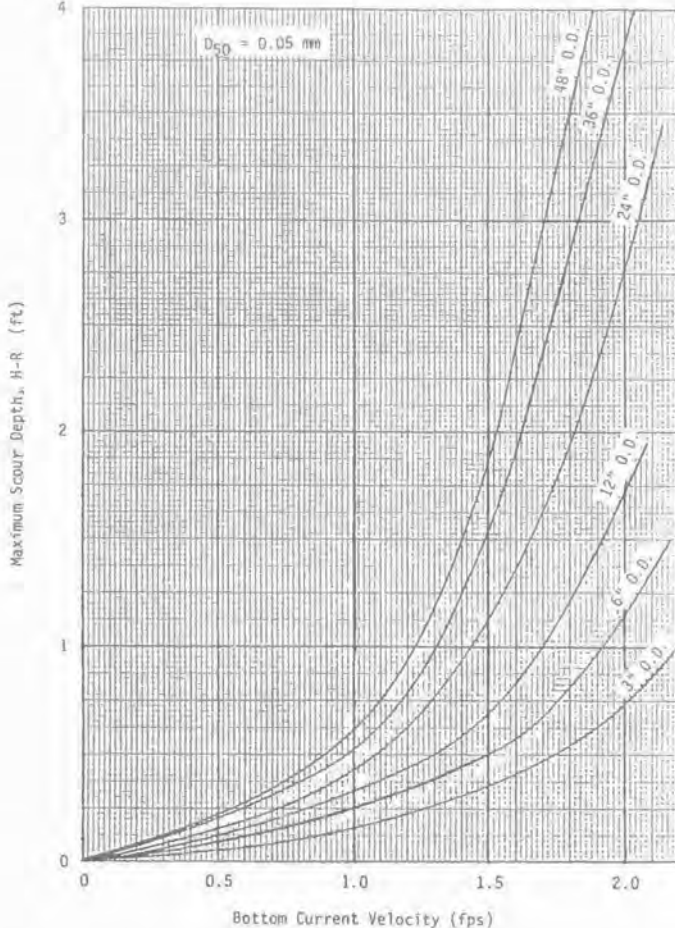


Figure 26d. Maximum scour depth as a function of bottom current velocity — $D_{50} = 0.10$ mm.

was placed behind the wave generator to reduce wave reflection. A wire mesh filter was placed in front of the generator paddle to reduce turbulence effects. A 30–40 mesh size Ottawa standard sand was employed to simulate the prototype beach.

The early tests were designed to determine “equilibrium” profiles of beaches for a variety of initial beach slopes and wave characteristics. Tests were conducted with initial beach slopes of 1:10, 1:20, 1:30, and 1:60 [11], and the beach was allowed to come to equilibrium in each case.

A sample dimensionless plot of beach equilibrium profiles for the initial slope of 1:20 is shown in Figure 27. The horizontal distance X (measured negatively sea-

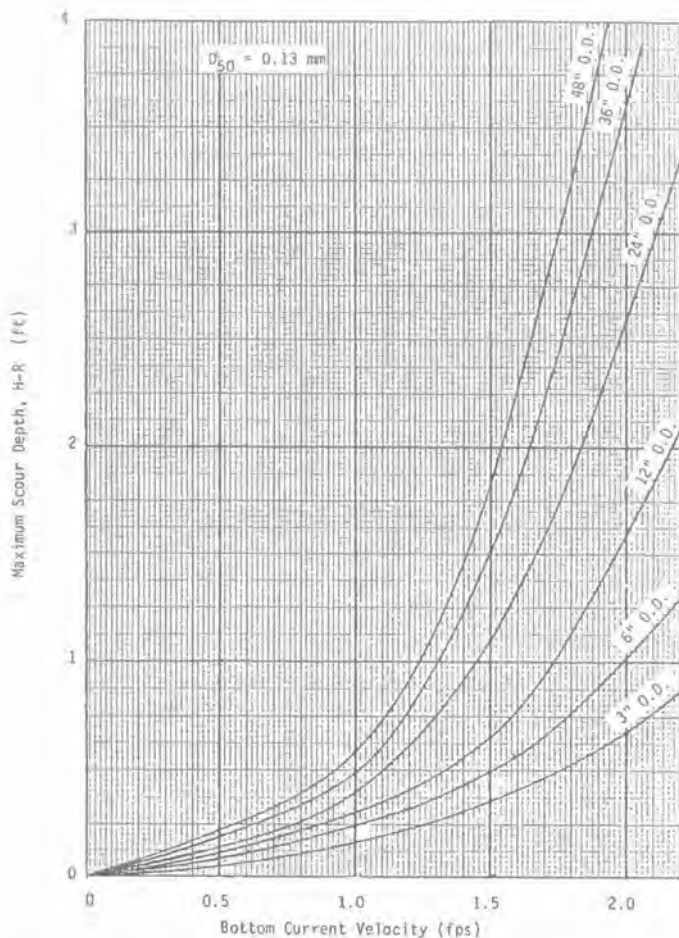


Figure 26e. Maximum scour depth as a function of bottom current velocity — $D_{50} = 0.05$ mm.

ward), was divided by the deep-water wavelength L_0 to render it dimensionless. Similarly, the vertical distance Y (measured negatively downward) was divided by the deep-water wave height H_0 to form a dimensionless number. The undulating patterns of berms and troughs observed in the laboratory resembled patterns observed in the field [6b]. Sample results of scour patterns observed at the model pipeline are presented in Figures 28 and 29.

The equilibrium profile characteristics T_{max} , B_{max} , h_T , and h_C (Figure 30) were used to correlate the results. Plots of h_T as a function of h_C were derived from field

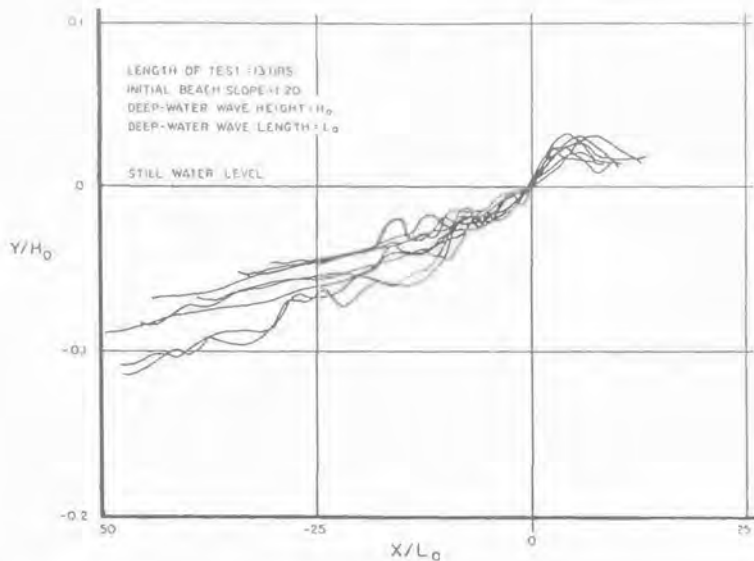


Figure 27. Dimensionless beach profiles; beach slope 1:20. (From Smith et al., 1976. Reprinted by permission.)

WAVE LENGTH / WATER DEPTH (L/d) = 5.2
 WAVE HEIGHT / WAVE LENGTH (H/L) = 0.051

TWO-DIMENSIONAL TESTS

TOP OF PIPE AT OCEAN BED (BURIAL = 0)

LENGTH OF TESTS (HRS.)

● 75 —————
 ■ 7 —————

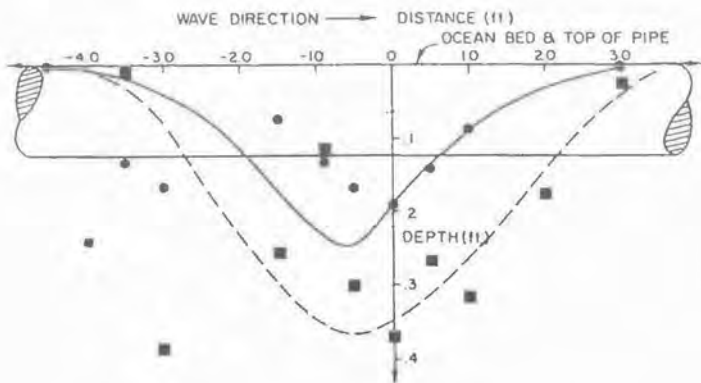


Figure 28. Sample result of scour; two-dimensional test.

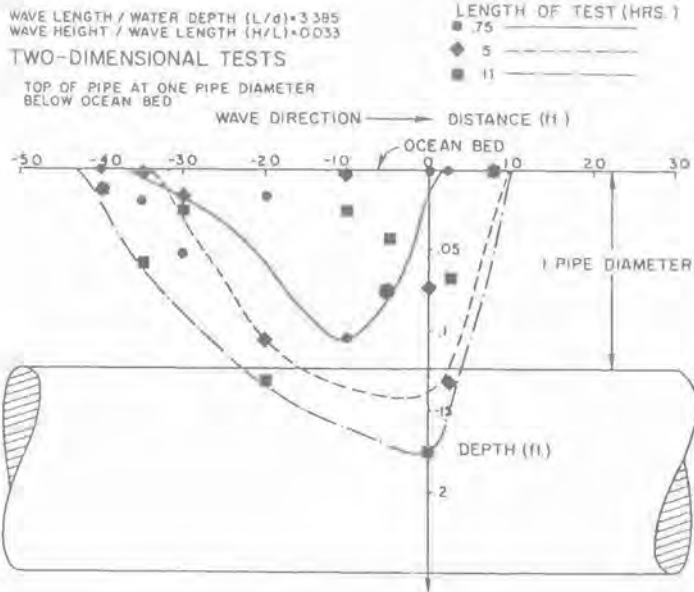


Figure 29. Sample result of scour, two-dimensional test; top of pipe; one pipe below ocean depth.

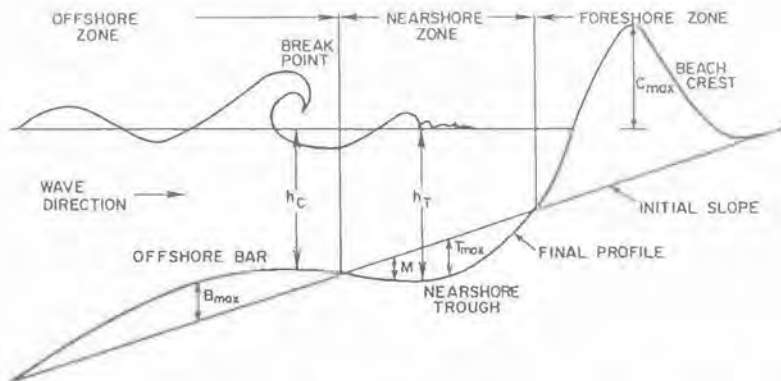


Figure 30. Definition sketch for T_{max} , B_{max} , h_C , and h_T ; B_{max} = maximum height of the offshore bar; T_{max} = maximum depth at the nearshore trough; h_T = vertical distance from water level to the nearshore trough; h_C = vertical distance from water level to the offshore bar. (From Herbich, 1970. Reprinted by permission.)

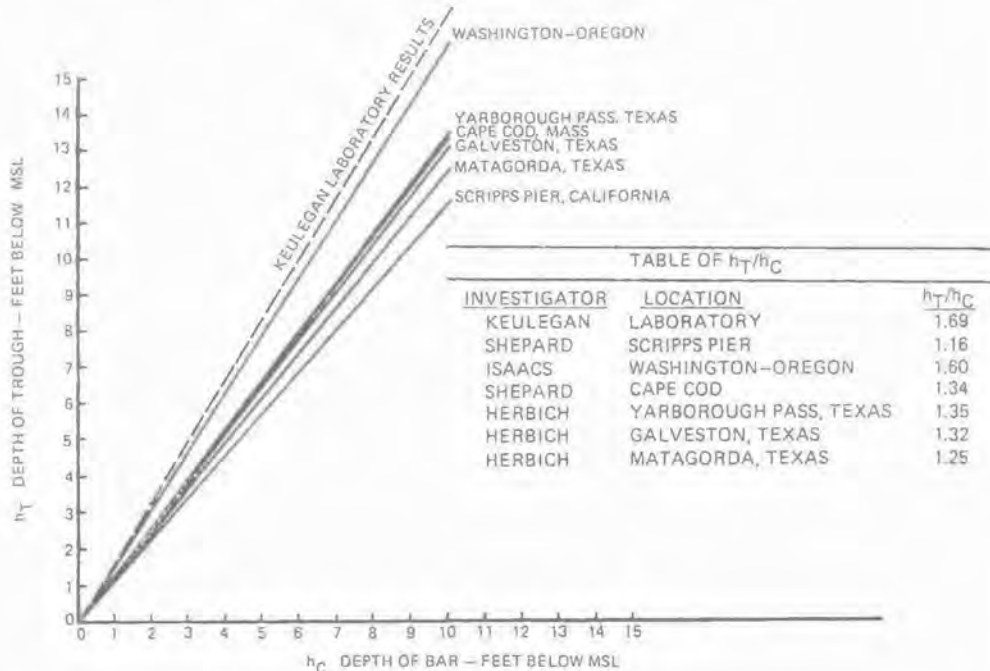


Figure 31. Relationship between depth of trough and depth of bar. (From Herbich, 1970. Reprinted by permission.)

and laboratory data as shown in Figure 31. The values of h_T/h_C observed in the field ranged from 1.16 at the Scripps Pier in California to 1.60 at the Washington-Oregon coast.

Laboratory studies at Texas A & M indicate that the beach slope affects the ratio of h_T to h_C , as indicated in Figure 32. For example, the h_T/h_C value with a 95% confidence interval is 1.80 ± 0.21 for a 1:10 slope, 1.49 ± 0.26 for a 1:20 slope, and 1.35 ± 0.09 for a 1:30 slope.

Qualitative agreement between laboratory and natural beaches was demonstrated by trial-and-error fitting, as shown in Figures 33 and 34. The required distortion of scales results in an unnatural repose angle at the foreshore. In addition, the wave parameters responsible for the natural profile were not available. However, the trial-and-error method is useful in determining a general scale factor. For example, a comparison between laboratory obtained profiles and field profiles near Sabine Pass, Texas, indicates a horizontal scale of 1:25 and a vertical scale of 1:8, or a

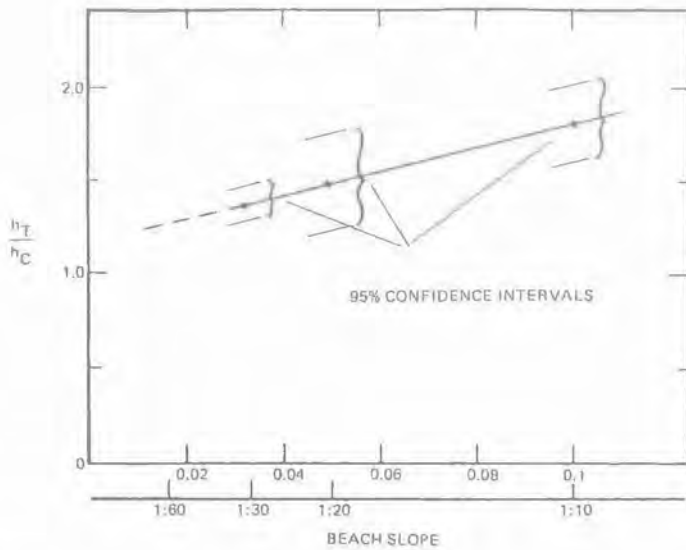


Figure 32. Ratio of h_T/h_C as a function of beach slope. (From Herbich, 1970. Reprinted by permission.)

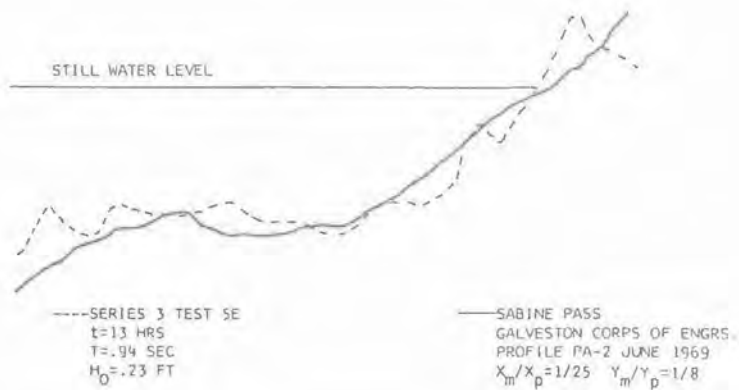


Figure 33. Comparison of laboratory and field profiles, Sabine Pass horizontal scale 1:25, vertical scale 1:8. (From Herbich, 1970. Reprinted by permission.)

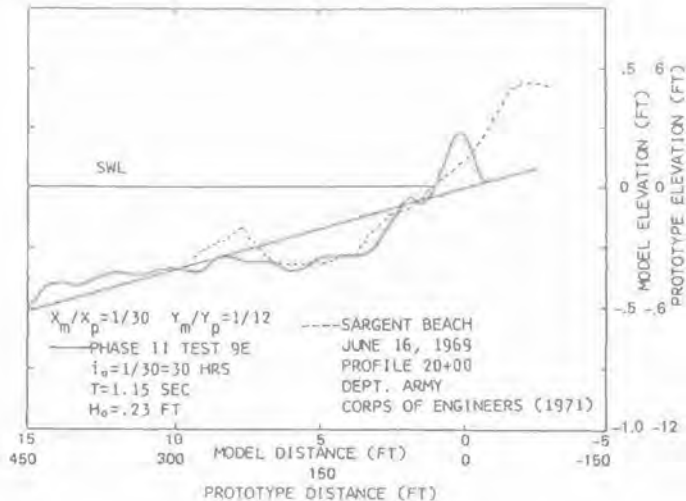


Figure 34. Comparison of laboratory and field profiles, Sargent Beach, Texas; horizontal scale 1:30, vertical scale 1:12, (SWL = still-water level.) (From Herbich, 1970. Reprinted by permission.)

distortion of about 3 to 1 (Figure 33). The comparison for Sargent Beach, Texas, shows a horizontal scale of 1:30 and a vertical scale of 1:12 (Figure 34).

Based on the results of the two-dimensional and three-dimensional tests, it appears that the pipe does not appreciably affect the beach profile. However, in many cases, local scour occurs around the pipeline due to pipe-sediment interaction.

A review of all test results indicates that sediment transfer over an equilibrium beach is altered when a pipeline is replaced on the beach. The three-dimensional tests have produced the following tentative conclusions:

1. A pipe placed at an angle of 60° to the wave crest will have a basically stable scour pattern seaward of the surf zone; however, considerable scour will result in the surf zone.
2. If the pipe is placed at a large angle (such as 60°) to the wave crest, burial of the pipe to a depth of one-half its diameter tends to produce significant scour until the pipe is uncovered.
3. Although "equilibrium" scour conditions appear to be reached after 13 hrs, tests conducted for a longer period (up to 60 hrs) indicate oscillations in relative scour and deposition over the pipe.

Offshore production pipelines in the United States have been generally in waters less than 400 ft deep [62]. However, with deeper offshore production drilling becoming more common, the footage of pipelines laid in deeper water is increasing at a dramatic rate. The first oil and gas discoveries in the North Sea were in the Southern Gas basin (about 53°N). As oil and gas production spread north-ward, the sea and weather conditions worsened and the water depths increased. The recent area being considered is in the Norwegian trench area of the North Sea, with water depths ranging from 750 to 900 ft. These depths would be 50% to almost 100% greater than any encountered earlier in the North sea [36].

The problems associated with submerged pipelines in intermediate or deep water are distinctly different from those encountered in shallow-water pipeline projects. The wave-induced drag and lift forces on a submerged pipe are considerable in shallow water. The water particle velocities are generally so high that fine sediments (clay and silt) have less chance to settle out of suspension and the shallow-water deposits are likely to be sandy. However, in deeper water, the wave-induced wave forces are less significant, and soft marine clays may occur at the mudline. The shallow-water and deeper-water routes have fundamental differences in soil properties such as stress histories, relative densities, rates of deposition, and in-situ pore pressures. These differences result in different design approaches and design considerations between shallow-water and deeper-water pipelines.

The entire North Sea is heavily fished with massive trawling equipment. The to determine the distance from the seawall to the first adjacent scour point. It and towed at speeds up to 5 knots. For this reason, many North Sea pipelines must be buried for protection against damage by trawlers. Burial in 400 to 600 ft water depth has resulted in the development of a second generation of pipe burial barges such as Brown & Root's *Bar 316* and *Bar 331* and Oceanics' *LB 27*. These barges are capable of cutting trenches 10 ft deep and burying pipe in water depths up to 550 or 600 ft. However, an entirely different burial method must be devised to bury many of the proposed pipelines across the 1,000–1,200-ft depths of the Norwegian trench.

Bottom characteristics and currents are important considerations in the North Sea. Scouring of sand by bottom currents can cause spanning as the pipeline is exposed. In September 1975, a mile-long section of the Brent System 36-in. trunkline in Yell Sound, Shetland lost its concrete jacket and floated to the surface [13]. The suspected cause was traced to high-velocity currents perpendicular to the pipeline, which scoured sediment, thus causing a span of 440 ft with a maximum distance from the seabed of 2 ft. Vortex shedding occurred, moving the pipeline up and down relative to the seabed, and the resulting friction and impact caused the concrete coating to break off. Although the pipe itself was undamaged, approximately 60% of the concrete coating was lost, and the increase in buoyancy caused the pipeline to float to the surface. The pipe was carefully flooded, guided back to the seabed, and weighted down with concrete weights to hold the line in place. Specially designed concrete saddle weights were later installed for permanent anchoring.

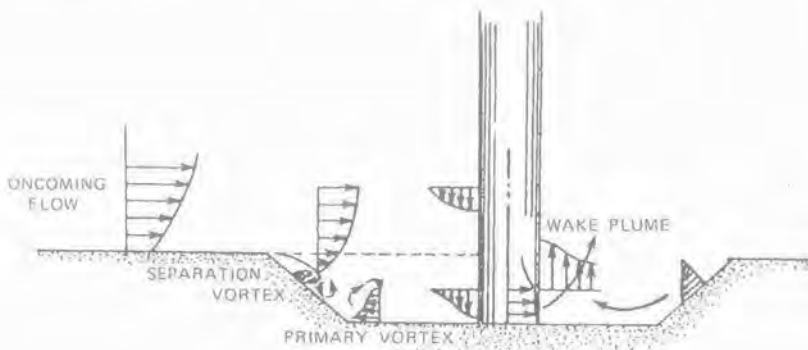


Figure 35. Diagram of various fields of turbulence associated with surge-induced flow.

Scour Around Piles*

Dynamics of Scour

A schematic view of the general hydrodynamic situation in the vicinity of a vertical obstruction reveals a pattern of secondary flows, or turbulence, that accounts for the scour of granular materials. The oncoming flow under a surge pulse is represented by the envelope of flow lines at the left (Figure 35). The scour pit surrounds the cylindrical pile, and the main scouring force is the primary vortex that develops in front of the cylinder. Since the velocity of the fluid increases with increasing height above the bed, a pressure gradient is established wherein a higher head is developed in the upper portion of the obstruction. The result of the fluid accumulation along the so-called "stagnation line" on the upstream face of the cylinder is a strong vertical fluid jet that descends along the upstream face of the obstruction. Erosion (associated with the primary vortex) creates a flat floor within the scour pit adjacent to the walls of the obstruction.

Secondary turbulence associated with the separation vortex forms a weak countervortex near the rim of the leading edge of the scour pit. Fluid at the sides of the cylinder accelerates to pass around the obstruction; this flow helps maintain the transport of grains thrown into suspension by the primary vortex. Palmer [38] indicates that the velocity in this region is twice that of the ambient field-surge velocity over the seafloor.

The pressure gradient at the rear of the obstruction is the reverse of that developed at the leading, or upstream, edge, and it increases with increasing height above the bed. This imbalance tends to lift sediment grains out of the scour pit in a turbulent wake plume.

* From Chapter 5, "Scour Around Piles," of *Seafloor Scour* (with permission from Marcel Dekker) [21].

Scour "equilibrium" is achieved for given parameters when the volume of material removed by the vortex turbulence is equal to the volume introduced into the pit through bed and suspended loads. At this point, a constant volumetric flux is achieved, and further enlargement of the pit requires longer periods of turbulent surge.

Scour Around Piles Caused by Currents

Any obstacle placed in the region of flowing water will cause the flow to divert around the object. Depending on the shape of the obstacle, type of flow, and local Reynolds number, the flow velocity will increase as the flow deflects around the object and the pressure will consequently decrease. Depending on the surface roughness, local Reynolds number, and boundary layer thickness, the flow will separate from the boundary, causing a wake to occur behind the pile.

The potential flow theory indicates that in the case of the unidirectional flow around a cylinder, the velocity of the flow at the cylinder wall 90° from the initial direction of flow will be twice the initial velocity of flow. Because the direction of flow is changing periodically in oscillatory wave flow, the separation may not occur unless the distance the water particles moves is several pile diameters long.

Scour depths around vertical structural members have been investigated very extensively in unidirectional flows in connection with studies of bridge piers. Several studies were presented by the National Cooperative Highway Research program [34], Anderson [2], Melville [32] and Breusers, et al. [9]. Anderson pointed out that the estimates of scour depths differ widely, particularly for the higher values of Froude Number and relative depth, and the various formula should not be extrapolated for flow conditions outside the range for which they are applicable.

Melville noted that in the ocean environment, the horseshoe vortex formed around the pile is the main mechanism for the scour process. Because scour caused by unidirectional flow occurs in relatively deep water where the wave-generated velocities are not present, the effect of water depth on scour depth is not significant [32].

Watson [57] observed that the strong tidal currents in the North Sea generate a vortex system that produces a local scour hole around the piles supporting an offshore platform. The scour hole assumed a shape of an inverted cone as the tidal currents change directions. Carstens [10] indicated that the scour becomes less extensive both in relative area and relative depth with increasing pile diameter.

Jain and Fischer [24] based on open-channel experiments (unidirectional flow) developed empirical scour formulas based on the following flow conditions:

1. Clear water scour. Sediment is removed from the scour hole and not replaced. Maximum scour occurs when the flow is no longer capable of moving the sediment out of the scour hole.
2. Incipient sediment motion. Flow velocity is approximately equal to the threshold velocity.
3. Sediment transporting scour. The sediment is continuously supplied to the scour hole from the general sediment transport. The maximum scour is reached when the sediment transport out of the scour hole equals the supply of sediment into the hole.

An experimentally-determined formula for scour depths [24] is as follows:

$$\frac{S_p}{D_p} = 1.86 \left(\frac{h}{D_p} \right)^{0.5} (N_F - N_{F_c})^{0.25} \quad (18)$$

where S = scour depth

D_p = pile diameter perpendicular to flow

h = mean flow depth

U = mean flow velocity

$N_F = U/\sqrt{gh}$ = Froude Number

$N_{F_c} = U_c/\sqrt{gh}$

U_c = critical velocity for initiation of sediment movement

g = acceleration due to gravity

The maximum clear-water scour is given by

$$\frac{S_p}{D_p} = 1.41 \left(\frac{h}{D_p} \right)^{0.3} (N_{F_c})^{0.25} \quad (19)$$

For design purposes

$$\frac{S_p}{D_p} = 2.0(N_F - N_{F_c})^{0.25} \left(\frac{h}{D_p} \right)^{0.5} \quad \text{for } (N_F - N_{F_c}) \geq 0.2 \quad (20)$$

and

$$\frac{S_p}{D_p} = 1.84(N_{F_c})^{0.25} \left(\frac{h}{D_p} \right)^{0.3} \quad (21)$$

for maximum clear water depth.

Jain and Fischer [24] also recommend that the scour depth for $0 \leq (N_F - N_{F_c}) \leq 0.2$ be assumed to be equal to the larger of the two values obtained from the previous two equations for design purposes.

Imberger [23] summarized results from several researchers for local scour around piles (Figure 36) and proposed the following equation:

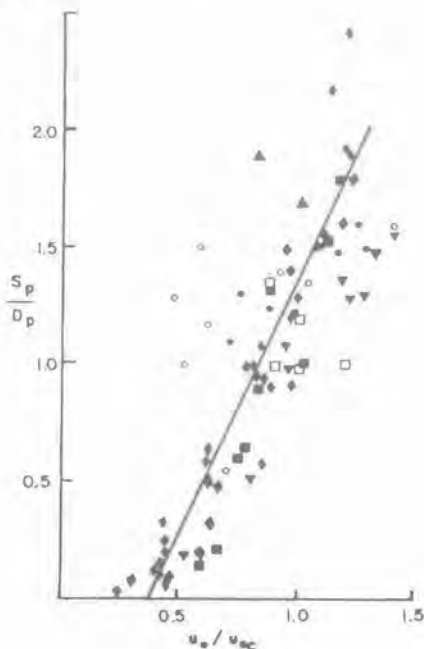
$$\frac{S_p}{D_p} = K \left(\frac{u_*}{u_{*c}} - 0.374 \right) \quad (22)$$

where K = coefficient = 2.18

u_* = shear velocity

u_{*c} = critical shear velocity

- - CHABERT & ENGELDINGER (1956)
- - BREUSERS (1971)
- ▲ - JAIN & FISCHER (1980)
- ▼ - SHEN et al (1969)
- - DADA (1981)
- - PRESENT (SAND)
- ◆ - PRESENT (SEDIMENT)



Dimensionless plot of scour depth against the shear velocity for cylinders without collars showing line of best fit from present results

Figure 36. Measurements of local scour around cylinders [23].

It has been suggested that the upper limit for the ratio of S_p/D_p can be estimated as 2.5.

The vortex system formed by flow around an obstacle is related to the shape and size of the obstacle [43]. The eddy structure formed is the basic mechanism of scour, and the depth of scour is a function of the pile Reynolds number N_{RP} :

$$N_{RP} = \frac{UD}{\nu} \tag{23}$$

where U = velocity
 D = pile diameter
 ν = kinematic viscosity

No successful theoretical development or mathematical simulation model of the scour problem has been developed to date, and reliance must be made on empirical or experimental studies.

Scour Around Piles Caused by Wave Action

The significant variables influencing the depth of scour around piles are as follows:

- h = still-water depth
- L = wavelength
- H = wave height
- T = wave period
- d_{50} = median grain diameter
- ρ_s = density of sand
- ρ = density of water
- ϕ = angle of repose of sand particles
- g = gravitational acceleration
- D = pile diameter
- C_s = span between piles
- U = free stream velocity
- \bar{S}_u = ultimate scour depth
- t = elapsed time

The functional relationship between the above variables for scour is

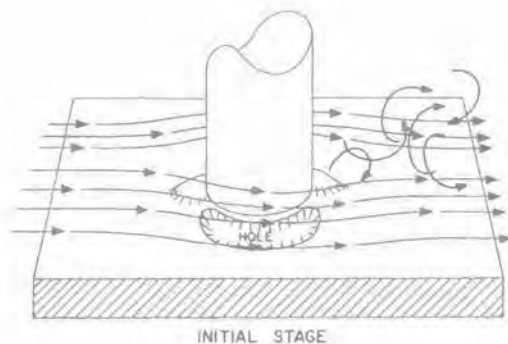
$$\frac{\bar{S}_u}{H} = f\left(\frac{H}{gT^2}, \frac{H}{L}, \frac{h}{L}, \frac{H}{h}, N_{RP}, N_s, \frac{\bar{S}_u}{d}, \frac{t}{T}, \phi, \frac{D}{C_s}\right) \quad (24)$$

where $N_{RP} = \frac{UD}{\nu}$ (25)

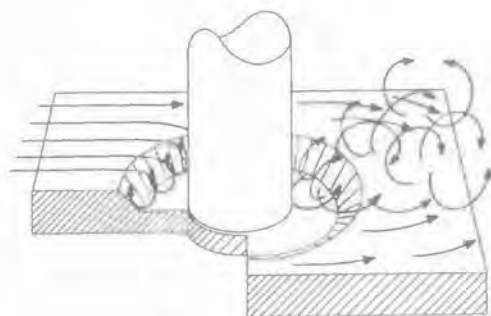
$$N_s = \frac{U}{\sqrt{(S_s - 1)gd}} \quad (26)$$

S_s = specific gravity of sand
 d = grain diameter

There were several experimental studies on scour due to oscillatory flow. Wells and Sorensen [59] and Das [14] have conducted experimental studies in the laboratory and Palmer [37, 38] conducted field studies around natural and artificial objects on the sea floor due to waves. The results of these studies show that the scour due to waves develops at the side of the cylinder and some deposition is observed against the upstream and downstream sides of the cylinder as shown in Figure 37. As the scour hole develops, these deposits are removed and the resultant scour hole is in the shape of an inverted cone with side slopes equal to the angle of repose of the sediment.



INITIAL STAGE



EQUILIBRIUM STAGE

Figure 37. Stages of wave-induced scour hole formation [35].

Niedoroda et al. [35] suggest a different wave scour mechanism because of a difference in boundary layer thickness. A relatively thick boundary layer (as thick as 6 meters) is developed by a steady current; however, in oscillatory flow only a thin boundary layer is presented. Scour in oscillatory flow is caused by acceleration of the primary flow past the obstruction, and the small- and large-wake flow patterns.

Chow and Herbich [12] investigated scour around six-, four-, and three-legged pile structures $D_{50} = 0.3$ mm and for sands with $D_{50} = 0.62$ mm. The relationship obtained between dimensionless ultimate scour \bar{S}_u/H and dimensionless wave height (or wave steepness) H/gT^2 indicates that the relative ultimate scour depth increases as the wave steepness increases. However, a point is reached where further increases in wave steepness result in a rapid decrease in scour due to the phenomenon of ripple formation. Further studies should be conducted with larger piles.

The tests also indicated that the relative scour depth tends to increase as the relative depth h/gT^2 decreases or as D/C_s increases. Correlations with the sediment number N_s and the pile Reynolds number N_{RP} indicate a rapid increase in \bar{S}_u/H to a maximum value, followed by a rapid decrease with further increases in N_s and N_{RP} .

When the parameter \bar{S}_u/H is plotted versus the number of waves, most of the tests show an initial rapid increase in the relative scour depth, but in most cases

the approximate ultimate conditions are reached after 1,200 waves. The majority of curves reach characteristic plateaus where the scour activity is dominant for a period of time, but decrease when ripples begin to form, until a state of equilibrium is reached. For all tests, the ultimate scour conditions were reached after 4,000 waves.

The general scour pattern was one of concentrated local scour around the pile, with ripple formations progressing in the direction of the wave propagation. The

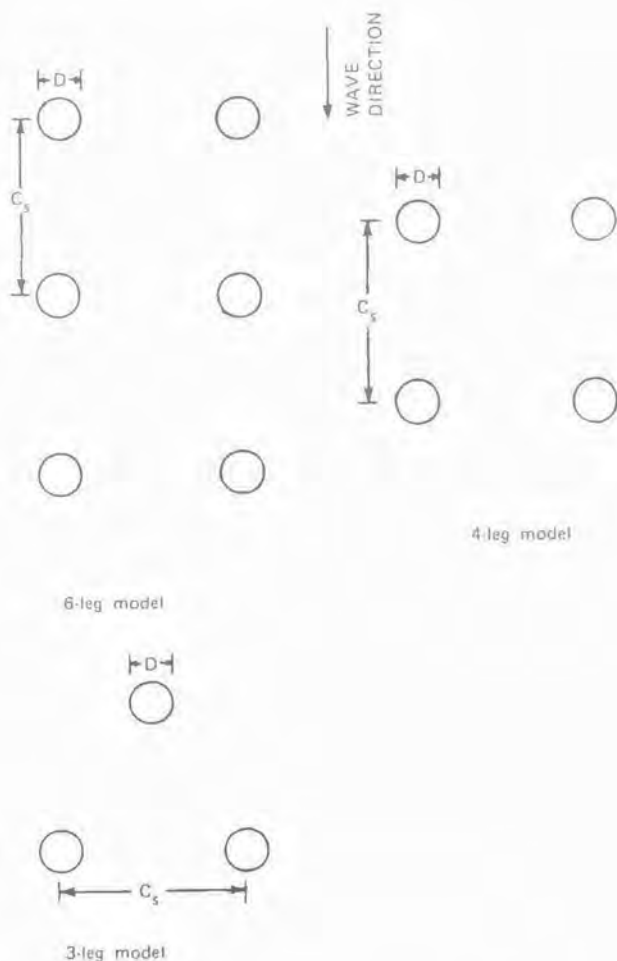


Figure 38. Experimental models.

formation of ripples is an important factor in the phenomenon of scour. When the absolute ultimate scour depth is estimated, the wave height of the ripple should be added to the local scour depth.

Scour data are presented for a six-, four-, and three-legged pile structure (Figure 38) and for sands with $d_{50} = 0.3$ mm (Figure 39) and $= 0.62$ mm [12].

Figure 40a shows the relationship between dimensionless ultimate scour \bar{S}_u/H and dimensionless wave height H/gT^2 for sand no. 1 ($d_{50} = 0.3$ mm), and Figure 40b shows the relationship between the same variables for no. 2 ($d_{50} = 0.62$ mm). Although further studies must be conducted with larger size piles, it appears that as the wave steepness increases the relative ultimate scour depth increases until a point is reached where, for further increases in wave steepness a rapid decrease in scour occurs. The rapid decrease in scour depth is associated with the phenomenon of ripple formation.

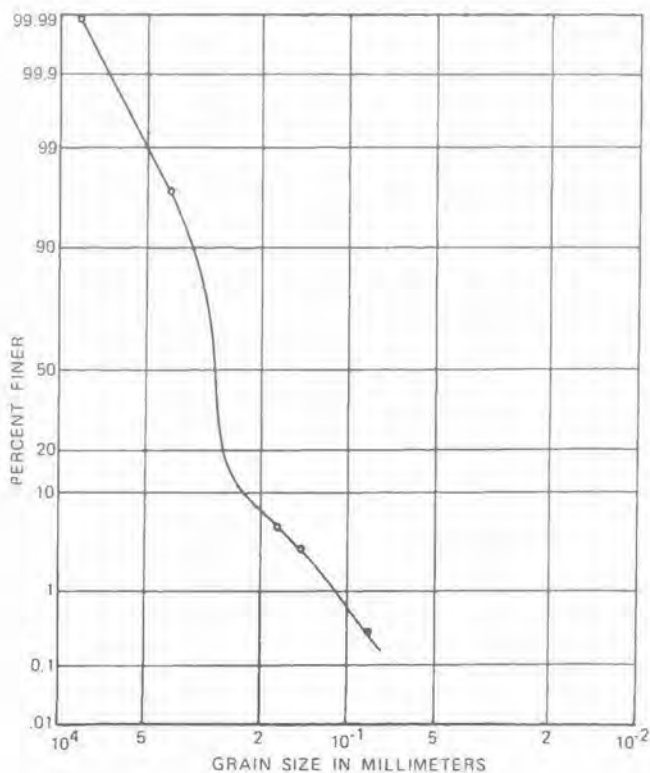


Figure 39. Sieve analysis of sand no. 1.

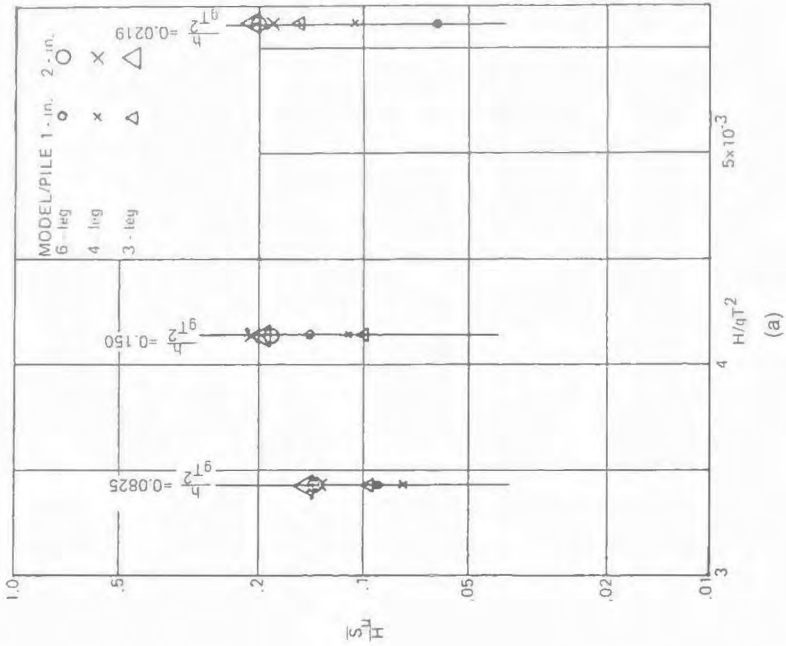


Figure 40a. Relative ultimate significant scour depth as a function of wave steepness for various values of relative steepness; median sand diameter = 0.3 mm [21].

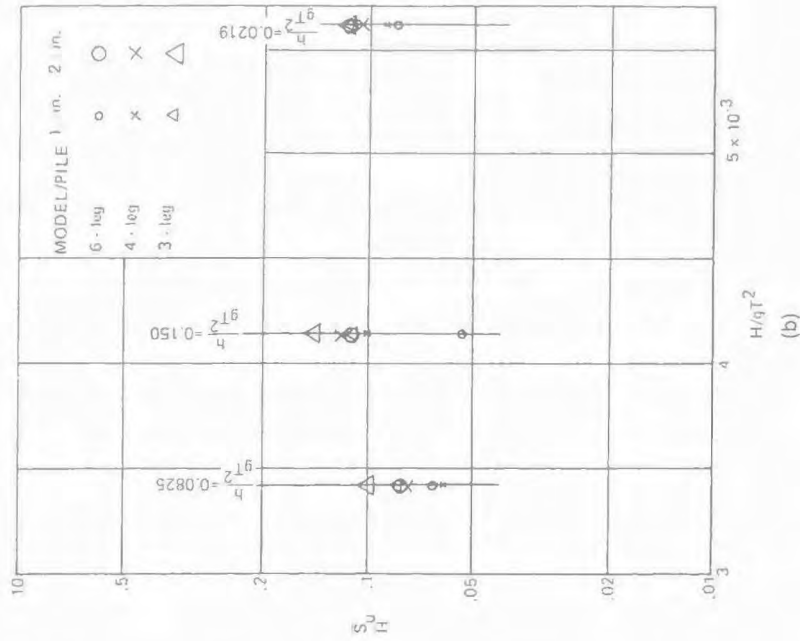


Figure 40b. Relative ultimate significant scour depth as a function of wave steepness for various values of relative steepness; median sand diameter = 0.62 [21].

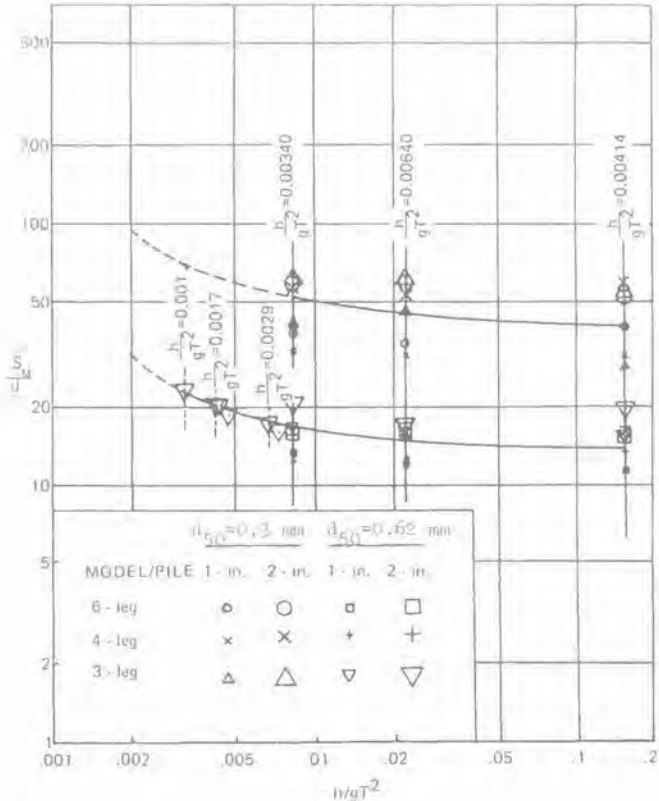


Figure 41a. Relative ultimate significant scour depth as a function of relative depth (from Herbich, et al. 1984).

Figure 41a indicates that as the relative depth decreases for each sediment size, the relative scour depth increases slowly at first until it reaches a relative depth of approximately 3.0×10^{-3} , where the relative scour depth increases rapidly with a decrease in sediment size. Figures 41b and 41c show the functional relationship between the relative ultimate significant scour depth and the sediment number N_s and pile Reynolds number N_{RP} , respectively. Both curves seem to have a rapid initial increase in \bar{z}_s/H , and the functional relationship is somewhat similar in both cases, as the relative scour depth increases rapidly at first to a maximum value. Any further increase in N_s and N_{RP} results in a rapid decrease in the ultimate scour depth. For a given density and viscosity of water, any further increase in the value of product of velocity and pile diameter, UD , will result in a decrease in scour depth.

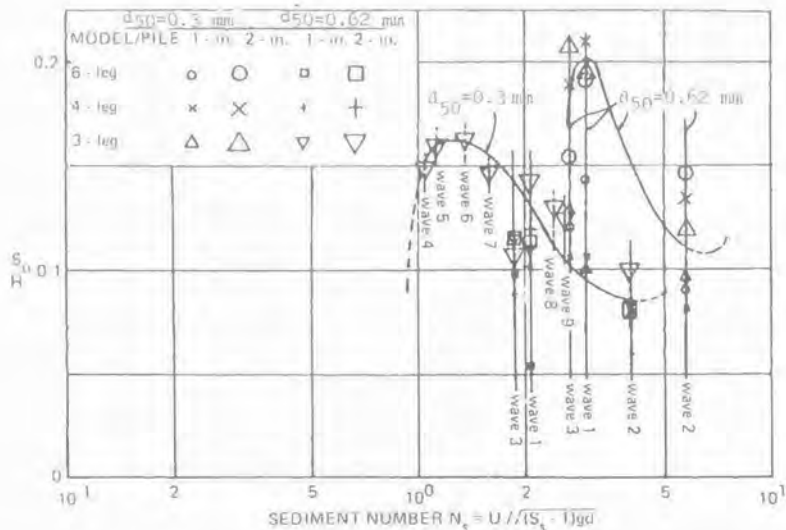


Figure 41b. Relative ultimate significant scour depth as a function of the sediment number (from Herbich, et al., 1984).

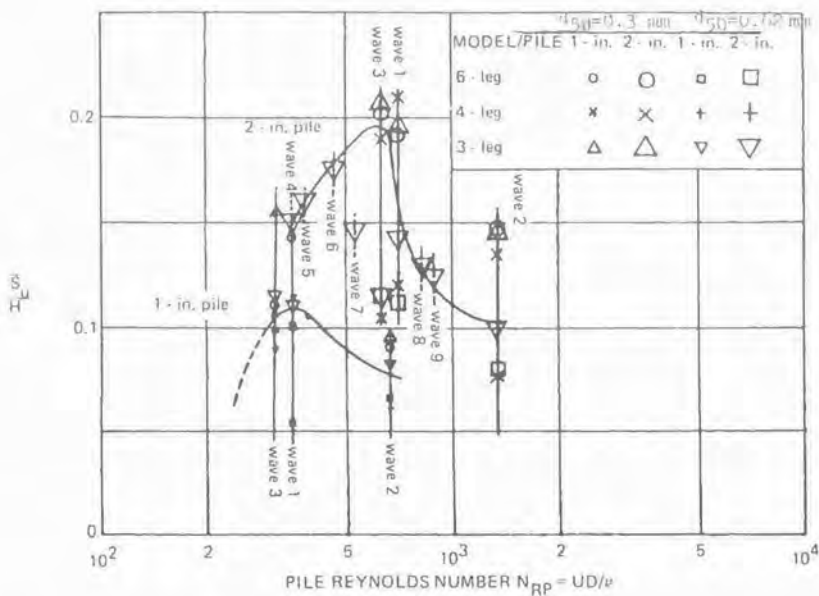


Figure 41c. Relative ultimate significant scour depth as a function of pile Reynolds number [21].

Bed Shear Due to Currents and Waves. This section gives a brief derivation of the resultant bottom shear stress due to steady and oscillatory motion. The shear stress is the result of the current and waves moving in the same direction. This procedure closely follows that of Bijker [6].

Using the mixing-length concept, the intensity of bed shear in a turbulent current may be written as

$$\tau_{\text{bim}} = \rho l^2 \left(\frac{\partial U_y}{\partial y} \right)_{\text{bottom}}^2 \quad (27)$$

where τ_{bim} = bed shear stress

ρ = fluid density

l = mixing length

U_y = velocity at a height y above the bed

For a rough bed,

$$l = Ky \quad (28)$$

for small values of y . The coefficient K has a value of 0.4. For a normal, fully turbulent flow, Equations 27 and 28 show that the variation of velocity outside the laminar sublayer to the bottom can be written as

$$\frac{\partial U_y}{\partial y} = \frac{U_*}{Ky} \quad (29)$$

where U_* = shear velocity = $\sqrt{\tau/\rho}$. From open-channel flow theory, it is shown that

$$U_* = \sqrt{\frac{\tau}{\rho}} = \sqrt{ghI} = \frac{U\sqrt{g}}{C} \quad (30)$$

where g = gravitational acceleration

h = water depth

I = slope of energy level

U = mean fluid velocity

C = Chezy coefficient

The velocity distribution calculated by integrating Equation 29 is shown in Figure 42a [6]. Assuming a straight-line velocity distribution from the origin up to y' , one obtains the following velocity gradient:

$$\frac{\partial U_y}{\partial y} = \frac{U_{y'}}{y'} \quad (31)$$

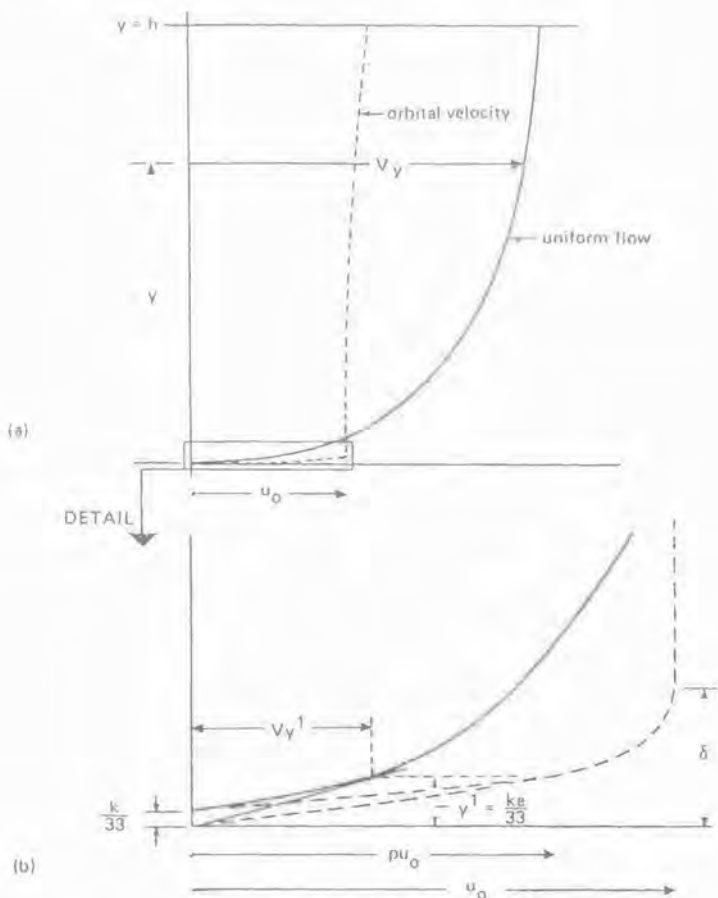


Figure 42. Velocity distributions of uniform and orbital motion [6].

where $U_{y'}$ = velocity at a distance y' above the bed. By combining Equations 28, 29, and 31, a relation of the following form results:

$$\tau_{y'} = \rho K^2 U_{y'}^2 \simeq \tau_{btm} \quad (32)$$

Because the velocity gradient used in Equation 32 is at a distance y' above the bed, the shear stress predicted by this equation is actually the stress at y' . It is the straight-line approximation of the velocity distribution that allows one to equate the shear stress at y' to the bottom shear stress.

A similar relation may be obtained by using the same procedure with orbital motion. The orbital motion velocity distribution is given in Figure 42b [6].

As a special note, y' is simply the distance at which the velocity equals U_*'/K . The straight-line approximation and the equation for the velocity distribution yield a value of $y' = k'e/33$, in which k' is a value for the bed roughness.

The primary task remaining is to find the orbital velocity at y' . Once this orbital velocity is known, the resultant of the orbital velocity and the steady velocity may be found. By entering this resultant velocity into an equation of the form of Equation 32, the bed shear may be calculated.

From Equations 29 and 31 the velocity at y' due to the steady current is

$$U_{cy'} = \frac{U\sqrt{g}}{CK} \quad (33)$$

As shown by Bijker, the wave induced velocity at y' is

$$U_{wy'} = P = Pu_b \quad (34)$$

where $P = 0.45$

$$u_b = \frac{\omega H}{2 \sinh 2\pi h/L} \sin(\omega t)$$

A more detailed discussion of the value of P is given by Bijker [6].

Referring to Figure 43 the resultant velocity at y' is simply the sum of the steady current and the oscillatory current. In vector notation, this relationship is expressed as

$$\bar{U}_{y'} = \bar{U}_{cy'} + \bar{U}_{wy'} \quad (35)$$

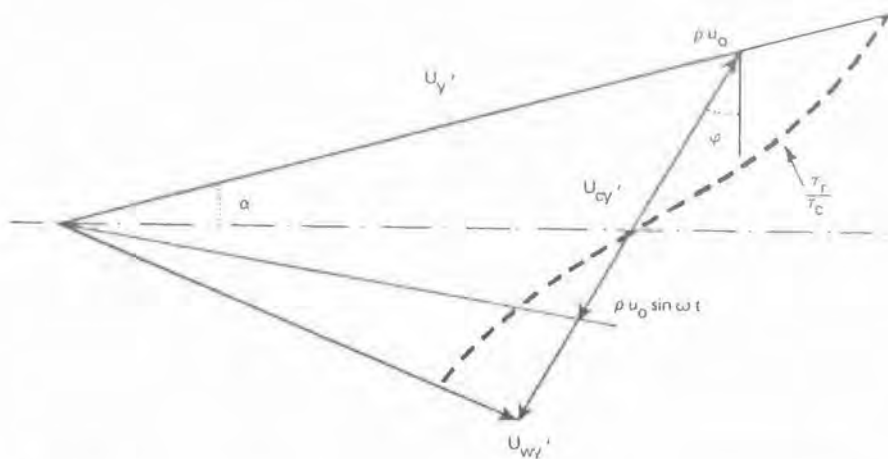


Figure 43. Velocity resulting from combined effect of uniform and orbital motion [6].

In scalar notation, the resultant velocity is

$$U_{y'} = U_{cy'} + U_{wy'} = \frac{U\sqrt{g}}{CK} + Pu_b \quad (36)$$

Therefore, the bed shear given by an equation of the same form as Equation 32 is

$$\tau_{bim} = \rho K^2 \left(\frac{U\sqrt{g}}{CK} + Pu_b \right)^2 \quad (37)$$

To find the time-averaged bottom shear stress, the following integration is performed:

$$\bar{\tau}_{bim} = \frac{2}{T} \int_{-T/4}^{T/4} \rho K^2 \left(\frac{U\sqrt{g}}{CK} + Pu_b \right)^2 dt \quad (38)$$

The resulting time-averaged bed shear stress due to a steady current and waves propagating in the same direction is

$$\bar{\tau}_{bim} = \frac{U^2 g \rho}{C^2} + \frac{P^2 u_0^2 K^2 \rho}{2} \quad (39)$$

where $u_0 = \frac{\omega H}{2 \sinh(2\pi h/L)}$ = wave-induced bottom velocity

$\omega = \frac{2\pi}{T_R}$ = radian wave frequency

T_R = relative wave period

H = wave height

h = water depth

L = wave length

The first term in Equation 39 is the stress contribution of the steady current, and the second term is the stress contribution of the wave motion.

The foregoing derivation is analogous to the derivation presented by Bijker [6]. The only difference is that Bijker's derivation is for waves propagating at some angle to the steady current rather than in the same direction as the current. Including the generality of waves propagating at any angle yields an integral somewhat more complex than that given in Equation 38. This complex integral is of the elliptical type and it is integrated numerically, whereas the integral given in Equation 38 has been integrated analytically.

Equation 39 is the result of a linear assumption made when the wave-induced horizontal bottom velocity is evaluated. In order to use nonlinear theory, the bottom velocities must be computed by means of the appropriate wave theory. From

Equation 37

$$\bar{\tau}_{\text{bim}} = \rho K^2 \left(\frac{U^2 g}{C^2 K^2} + \frac{2U\sqrt{g}Pu_b}{CK} + P^2 u_b^2 \right)$$

$$\bar{\tau}_{\text{bim}} = \frac{U^2 \rho g}{C^2} + \frac{2U\rho K P u_b \sqrt{g}}{C} + \rho K^2 P^2 u_b^2$$

Therefore,

$$\bar{\tau}_{\text{bim}} = \frac{U^2 \rho g}{C^2} + \frac{2U\rho K P \bar{u}_b \sqrt{g}}{C} + \rho K^2 P^2 (\bar{u}_b)^2 \quad (40)$$

The terms \bar{u}_b and \bar{u}_b^2 in Equation 40 can be obtained by using computer programs that calculate the bottom velocity at specific phase increments along the wave.

Chezy Coefficient

The Chezy coefficient plays an important role in evaluating the time-averaged bottom shear stress. Three methods may be considered. From Equation 30, the relationship between the Chezy coefficient and the current-induced bottom shear stress is as follows:

$$C = U \sqrt{\frac{g\rho}{\tau}} \quad (41)$$

The first method considered was to solve for the mean current-induced shear stress by equating it to the rate of change of fluid momentum along the sand bed. This method requires measuring the water surface elevation and velocity distribution at the upstream and downstream portions of the sand bed.

The second method considered was to calculate the horizontal velocity gradient at the bottom from the velocity distribution upstream of the pile. Assuming a Newtonian fluid, the bottom shear stress may be calculated directly from the velocity gradient.

The third method considered was to use data compiled by Lovera and Kennedy [29], equating the sand bed friction factor to the sand median diameter and Reynolds number. The Chezy coefficient is related to the bed friction factor as follows:

$$C = \sqrt{\frac{8g}{f}} \quad (42)$$

Figure 7 is the result of the accumulation of all data, and it shows the friction factor as a function of Reynolds number for many different sand sizes.

The lower limit for f is governed by the smooth boundary relation

$$f = \frac{0.316}{N_R^{1/4}} \quad (43)$$

where $N_R = \frac{UR}{\nu}$

R = hydraulic radius

Hence, the calculated friction factor (or Chezy coefficient) cannot be less than that predicted by the smooth boundary relation.

Dimensional Analysis. There are many significant variables influencing the ultimate scour depth at a cylindrical pile due to wave and current motion:

$$\Pi_7 = D/L \quad (44)$$

$$\Pi_8 = \frac{U'^2(\rho_s - \rho)}{\bar{\tau}} \quad (45)$$

$$\Pi_9 = \frac{S_u}{L} \quad (46)$$

$$\Pi_{10} = \frac{fL}{U} \quad (47)$$

Rearranging and combining the Π terms yields

$$\frac{\Pi_4}{\Pi_6 \Pi_5} = \frac{U'}{\sqrt{gd_{50}(\rho_s - \rho)/\rho}} = N_s \quad (48)$$

$$\frac{\Pi_4}{\Pi_6 \Pi_8} = \frac{\bar{\tau}}{gd_{50}(\rho_s - \rho)} = \tau' \quad (49)$$

$$\frac{\Pi_9}{\Pi_7} = \frac{S_u}{D}$$

$$\Pi_7 \Pi_3 = \frac{U'D(\rho_s - \rho)}{\mu} = N_R \quad (50)$$

$$\Pi_7 \Pi_{10} = \frac{fD}{U'} = S \quad (51)$$

Therefore, the functional relationship is as follows:

$$\frac{S_0}{D} = f\left(\frac{h}{L}, \frac{H}{L}, \frac{U^2 L (\rho_s - \rho)}{\mu}, \frac{\rho_s - \rho}{\rho}, \frac{U^2 (\rho_s - \rho)}{\bar{\tau}}, N_{s0}, \tau', N_{R1}, S\right) \quad (52)$$

Note that for steady motion, the dimensionless shear stress term τ' reduces to the sediment number N_s .

Scale Effects. The improper scaling of the sediment size is usually accepted in sediment model studies. Proper sediment size scaling would lead to a cohesive model sediment, and a cohesive sediment possesses properties vastly different from a non-cohesive sediment.

According to Bijker [6], the boundary layer resulting from a combination of currents and waves is directly proportional to the boundary roughness and thus to the boundary friction factor. This implies that the boundary layer thickness for the model and the prototype will be approximately the same. Defining a Reynolds number based on the boundary layer thickness leads to the ratio

$$\frac{N_{R_{m\delta}}}{N_{R_{p\delta}}} = \frac{U_m}{U_p} \quad (53)$$

where $N_{R_{m\delta}}$ = model Reynolds number based on boundary layer thickness

$N_{R_{p\delta}}$ = prototype Reynolds number based on boundary layer thickness

U_m = model fluid velocity

U_p = prototype fluid velocity

This ratio implies that the model boundary layer may be laminar, whereas the prototype boundary layer may be turbulent.

Experimental Studies. Machemehl and Abad [30] investigated the scour around a cylindrical pile due to the combined effect of waves and currents. The scour was measured as a volumetric unit and results reported in terms of dimensionless ratios. The relative scour volume is equal to

$$V_s / D_p h d \quad (54)$$

where V_s = volume of scour hole at time t

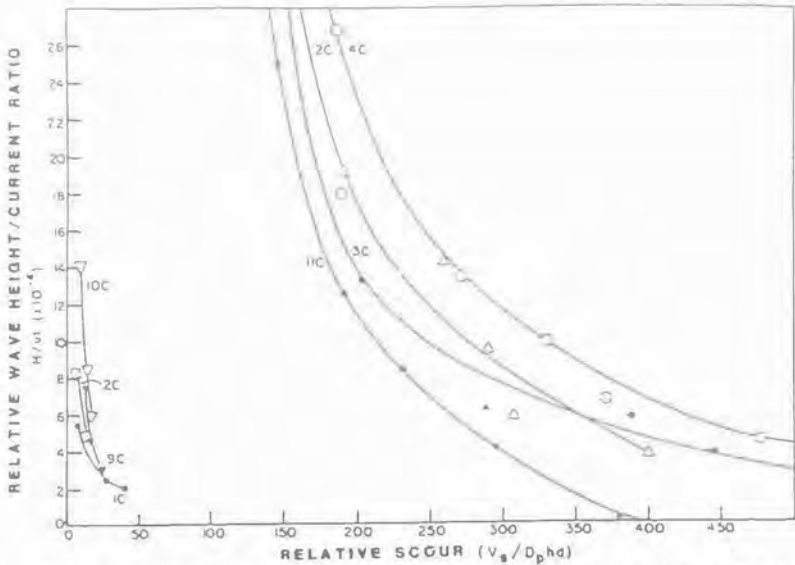
D_p = pile diameter

h = still water depth

d = mean diameter of sand particle

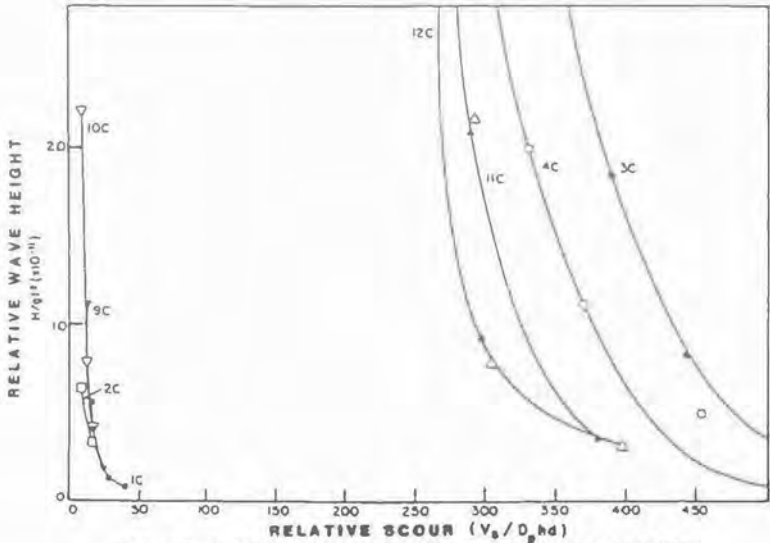
The relative wave height to current ratio is equal to

$$\frac{H}{ut} \quad (55)$$



(A) AS A FUNCTION OF RELATIVE WAVE HEIGHT/CURRENT RATIO

Figure 44. Relative scour for a single pile caused by waves and currents as a function of relative wave height/current ratio [30].



(B) AS A FUNCTION OF RELATIVE WAVE HEIGHT

Figure 45. Relative scour for a single pile caused by waves and currents as a function of relative wave height [30].

where H = wave height

u = free stream velocity

t = elapsed time

g = acceleration due to gravity

Figure 44 presents relative scour as a function of relative wave height to current ratio and Figure 45 shows the effect of relative wave height (H/gt^2) on the relative scour. The experiments with low velocities are clustered together at the smaller values of relative scour volume, while those with high velocities are clustered together at the higher values of relative scour volume. Thus the currents are the primary reason for scour.

General Scour Depth and Critical Conditions for the Initiation of Scour

For general scour, the scour depth is a result of interactions between dynamic forces (current and wave) and sediment type (size and density). It also depends on the magnitude of sediment movement and whether the sediment is being supplied to the area.

The necessary and essential conditions for general scour are:

1. The initiation of sediment motion, that is, when the actual velocity exceeds the critical velocity for movement.
2. Sufficient capacity of current and waves to transport the sediment to the downstream or upstream area.
3. Insufficient sediment from the upstream or downstream area to replenish the sediment in the scoured area (i.e., the amount of sediment removed exceeds the amount of sediment deposited in the scoured area).

General scour occurs in a larger area, while local scour is generally observed around obstructions to flow.

The purpose of the analysis for general scour depth was to obtain an experimental relationship between scour depth and dynamic and sediment variables. In the analysis, all variables were combined to form dimensionless parameters.

The "general" relative scour depth S_{a0}/h can be expressed as follows:

$$\frac{S_{a0}}{h} = F_1 \left(N_F, \frac{H}{L}, U_r, N_s \right) \quad (56)$$

where N_F = Froude number, $\frac{V^2}{gh}$

$\frac{H}{L}$ = wave steepness

U_r = Ursell parameter, $\frac{HL^2}{h^3}$

N_s = sediment number = $\frac{V_{f,w}^2}{[(\rho_s - \rho)/\rho]g^2h^4d_{50}}$
= $\frac{[V + (1/T - V/L)HL/2h]^2}{[(\rho_s - \rho)/\rho]g^2h^4d_{50}}$

From the general scour tests the following relationships were observed:

$$S_{u_0} \propto V \quad \text{and} \quad S_{u_0} \propto V_{t,w}$$

$$S_{u_0} \propto \frac{1}{h}$$

$$S_{u_0} \propto H$$

$$S_{u_0} \propto L$$

$$S_{u_0} \propto \frac{1}{d_{50}}$$

Equation 56 may be rewritten

$$\frac{S_{u_0}}{h} = F_1 \left(N_F, \frac{H}{L}, U_r, N_s \right) = F_1(\alpha) \quad (57)$$

$$\text{where } \alpha = \frac{V^2 H^2 L [V + (1/T - V/L)HL/2h]^2}{[(\rho_s - \rho)/\rho] g^2 h^4 d_{50}}$$

The correlation analysis for the relationship between relative general scour depths S_{u_0}/h and parameter α was performed on most of the results. The following correlation was obtained:

$$\log_{10} \left(\frac{S_{u_0}}{h} + 0.05 \right) = -0.6631 + 0.3649 \log_{10} \alpha \quad (58)$$

or

$$\frac{S_{u_0}}{h} = 0.2172 + \alpha^{0.3649} - 0.05 \quad (59)$$

(Correlation coefficient $r = 0.949$.) Figure 46 presents the correlation line ABC, line AB describes the no-scour case and line BC covers the scour case.

Point B, where the two lines AB and BC cross, is important. Point B represents a critical condition for the initiation of scour, that is:

when $\alpha < 0.02$, the sand bed will not scour

when $\alpha > 0.02$, the sand bed will scour

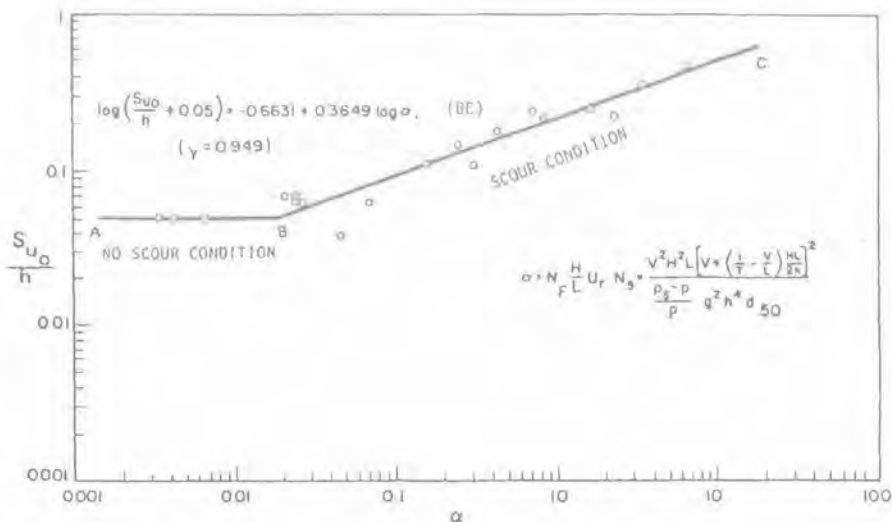


Figure 46. The correlation curve between relative scour depth S_{u0}/h and parameter α [56].

Analysis of “Total” and Net “Local” Scour Depth

When an obstruction is placed on the sand bed, the scouring process around the obstruction will begin as soon as the velocity of current and wave-induced current exceeds the critical velocity of sediments, even if no general scour occurs.

The local scour depth around a cylinder, S_u , can be expressed as follows:

$$S_u = F_2(V_{tw}, h, \rho, H, L, T, d_{50}, \rho_s, D, \nu, t) \quad (60)$$

where V_{tw} = combined velocity of current and wave

h = still-water depth

ρ = water density

H = wave height with current

L = wave length with current

T = wave period with current (i.e., “absolute” wave period)

d_{50} = mean diameter of sand (50% finer)

ρ_s = sand density

ν = kinematic viscosity of water

t = time to produce scour

Because the scour depth is considered as ultimate or largest, the scour time t can be ignored.

The following dimensional parameters were selected for the analysis of experimental data:

1. The current Froude number, N_F : a ratio of kinetic energy $(1/2)\rho V^2$ to potential energy ρgh :

$$N_F = \frac{V^2}{gh} \quad (61)$$

In the scour process, the kinetic energy is one of the major dynamic factors causing movement of sand. However, the potential energy is also of importance, particularly when considering the water depth (i.e., the greater the depth, the lesser the chance of sediment movement).

2. Wave steepness, H/L : the greater the vertical amplitude of water particles, the greater the lifting action of sediment.
3. Ursell parameter, $U_r = HL^2/h^3$: it indicates the magnitude of wave energy that is transmitted to the sand bed.
4. Sediment number, $N_s = V_{rw}^2/[(\rho_s - \rho)/\rho]gd_{50}$, where V_{rw} is the combined velocity of current and wave. Thus,

$$N_s = \frac{[V + (1/T - V/L)HL/2h]^2}{[(\rho_s - \rho)/\rho]gd_{50}} \quad (62)$$

5. The pile Reynolds number, $N_{RP} = VD/v$. The importance of N_s and N_{RP} was shown by Carstens [10], Chow and Herbich [12], and Shen et al. [43]. The analysis of data summarized in Table 2 indicates the following relationships:

$$S_u \propto V$$

$$S_u \propto \frac{1}{h}$$

$$S_u \propto L$$

$$S_u \propto H$$

$$S_u \propto \frac{1}{d_{50}}$$

$$S_u \propto D$$

Equation 60 can be made dimensionless by dividing S_u by h :

$$\frac{S_u}{h} = F_2\left(N_F, \frac{H}{L}, U_r, N_s, N_{RP}\right) = F_2(\beta) \quad (63)$$

Table 2
Variables Influencing the Ultimate Scour

Symbol	Description	Units		Dimensions
		English	Metric	
h	Water depth	ft	m	L
H	Water height	ft	m	L
L	Water length	ft	m	L
ν	Kinematic viscosity	lb-sec/ft ²	N-sec/m	M/LT
g	Gravitational acceleration	ft/sec ²	m/sec ²	L/T ²
ρ	Fluid density	slugs/ft ³	kg/m ³	M/L ³
$\rho_s - \rho$	Sediment-fluid density difference	slugs/ft ³	kg/m ³	M/L ³
d_{50}	Sand median diameter	ft	m	L
U'	$U + \langle u_0 \rangle$	ft/sec	m/sec	L/T
D	Pile diameter	ft	m	L
$\bar{\tau}$	Time-averaged bed shear stress	lb/ft ²	N/m ²	M/L ²
f	Shedding frequency	sec ⁻¹	sec ⁻¹	1/T
S_u	Ultimate scour depth	ft	m	L

$$\text{where } \beta = N_F \frac{H}{L} U' N_s N_{RP} = \frac{V^3 H^2 L [V + (1/T - V/L)HL/2h]^2 D}{[(\rho_s - \rho)/\rho] g^2 \nu d_{50} h^4}$$

Using the Buckingham II theorem with 13 variables and 3 dimensions results in 10 Π terms. Selecting L, U' , and $\rho_s - \rho$ as the repeating variables, the following terms evolve:

$$\begin{aligned} \Pi_1 &= h/L \\ \Pi_2 &= H/L \\ \Pi_3 &= U' L (\rho_s - \rho) / \mu \\ \Pi_4 &= U'^2 / gL \\ \Pi_5 &= (\rho_s - \rho) / \rho \\ \Pi_6 &= d_{50} / L. \end{aligned}$$

The following correlation for the relationship between the relative local scour depths S_u/h and parameter β was obtained (Figure 47).

$$\log_{10} \frac{S_u}{h} = -1.4071 + 0.2667 \log_{10} \beta \quad (64)$$

(Correlation coefficient $r = 0.970$.) It was mentioned earlier that S_u includes two components, general scour and net local scour; therefore the above correlation is for the total scour.

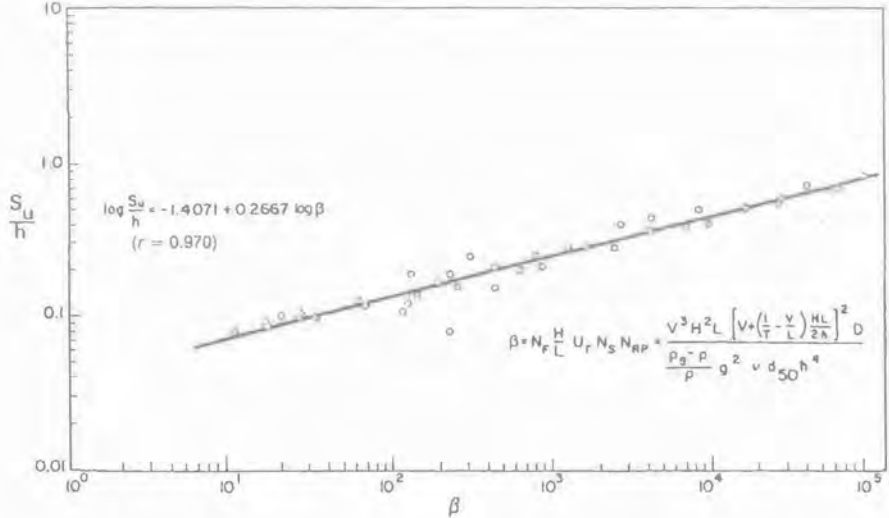


Figure 47. The correlation curve between relative scour depth s_u/h and parameter β [56].

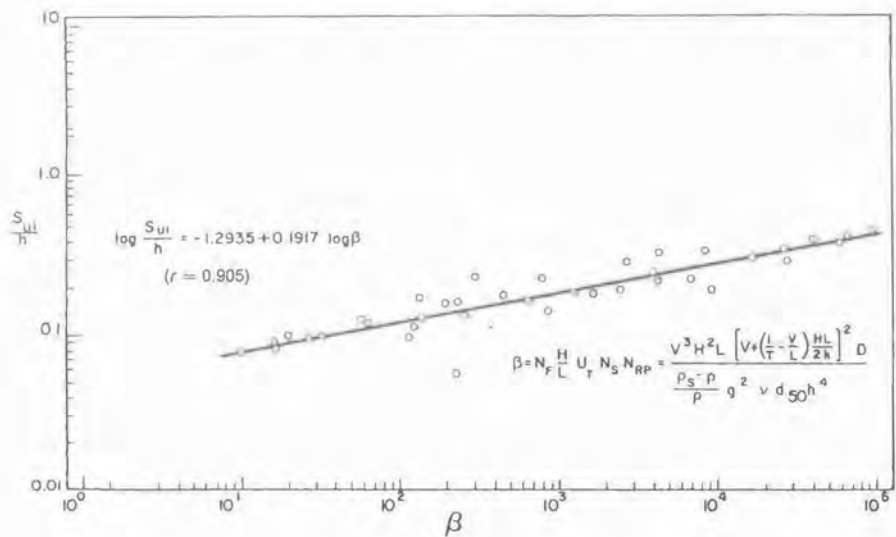


Figure 48. The correlation curve between relative scour depth s_{u1}/h and parameter β .

In order to obtain a relationship between net local scour depth S_{u_0} and parameter β , the total scour depth data were treated as follows:

1. The parameter for all 39 test runs, α , was calculated using Equation 57.
2. The general scour depth S_{u_0} was calculated using Equation 59 or Figure 46. Note that $\alpha < 0.02$ and $S_{u_0} = 0$.
3. The net local scour depth S_u was obtained as follows:

$$S_{u_i} = S_u - S_{u_0} \quad (65)$$

4. The correlation was obtained from

$$\frac{S_{u_i}}{h} = F_3(\beta) \quad (66)$$

The following relationship was obtained between S_u/h and β (Figure 48).

$$\log_{10} \frac{S_{u_i}}{h} = -1.2935 + 0.1917 \log_{10} \beta \quad (67)$$

(Correlation coefficient $r = 0.905$.)

Summary

1. The parameter for all 39 test runs, α , which was calculated using Equation 57,

$$\alpha = N_F \frac{H}{L} U_r N_s = \frac{H^2 LV^2 [V + (1/T - V/L)HL/2h]^2}{[(\rho_s - \rho)/\rho] g^2 h^4 d_{50}} \quad (68)$$

can be taken as a complex (composite) relationship that includes the dynamic factors of current and wave as well as sediment size (including the initiation condition of sediment motion).

2. Subject to experimental limitation, the general scour of sand bed will not occur when $\alpha < 0.02$.
3. When $\alpha > 0.02$, the sand bed will erode; the relative general scour depth is given by:

$$\log_{10} \left(\frac{S_{u_0}}{h} + 0.05 \right) = -0.6631 + 0.3649 \log_{10} \alpha \quad (69)$$

4. For the scour around a pile under a combined action of current and waves, the parameter

$$\begin{aligned} \beta &= N_F \frac{H}{L} U_r N_s N_{RP} \\ &= \frac{H^2 LV^3 D [V + (1/T - V/L)HL/2h]^2}{[(\rho_s - \rho)/\rho] v g^2 h^4 d_{50}} \end{aligned} \quad (70)$$

can be taken as a complex (composite) relationship which includes the dynamic factors, sediment size, and pile size.

5. When $\alpha < 0.02$, only the local scour around a pile will occur. Based on the experimental data the relative local scour depth is given by

$$\log_{10} \frac{S_{ul}}{h} = -1.2935 + 0.1917 \log_{10} \beta \quad (71)$$

6. When $\alpha > 0.02$, the scour around a pile will be the total scour, including general and net local scour. Based on the experimental data the relative total scour depth is given by the following relation:

$$\log_{10} \frac{S_u}{h} = -1.4071 + 0.2667 \log_{10} \beta \quad (72)$$

and the relative net local scour depth is given by Equation 71.

When scaling these data to prototype conditions, it is suggested that both Reynolds scaling and Froude scaling be considered. The choice of which scour depth prediction to use is left as an engineering judgment.

Scour About a Single, Cylindrical Pile Due to Combined Random Waves and a Current

The scour phenomenon begins with the incipient motion of sediment particles. Incipient sediment motion is defined to be "an instantaneous condition reached when the resultant of all the active forces on the particle intersects the line connecting the bed particle contact points," [16]. There are three types of active forces acting on a sediment particle. Two of these forces, the drag and lift forces, are due to the fluid motion. These forces are in turn balanced by the sediment particle mass.

A thorough understanding of these forces is required to comprehend fully the processes of incipient motion, bedload transport, and bed form development; all of which depend on the collective response of initially stationary bed particles to fluid forces.

In oscillatory flow generated by waves, the scour hole initiates at the side of the cylinder, and sometimes sediment deposition is found to occur against the upstream and downstream sides of the cylinder. Once fully developed, the scour hole is a radially symmetric frustrum of an inverted cone having side slopes at the angle of repose of the sediment [37].

The mechanics of scour due to waves and currents are quite complicated and this type of scour occurs in almost all ocean environments. The scale and shape of the scour hole depends on the relative magnitude of the unidirectional velocity and the oscillatory flow velocities.

Scour experiments were conducted by Eadie and Herbich [15] in a 120-ft long (36.6 m), 3-ft deep (0.91 m) and 2-ft (0.61 m) wide, two-dimensional, glass-walled wave flume. The test area was located approximately 40 ft (12.2 m) from the wave generator. The entire test area measured 40 ft (12.2 m) in length and was divided

into several sections. An 8-ft (2.4 m) long, 5-in. (0.13 m) deep test sediment bed was bordered on each end by an 8-ft long (2.4 m) 10-in. (2.7 m) high false bottom. At the leading edge of the test area, a 16-ft (4.9 m) long ramp was used to gradually bring the wave up to the new depth at the top of the false bottom. A 1.5 in. (0.04 m) diameter aluminum pile was positioned along the centerline of the sediment bed.

Currents were produced using a centrifugal pumping system. The flow rate was monitored using a Fischer and Porter electromagnetic flow meter. The pump discharge entered the wave flume just forward of the wave generator and was diffused using a louvered grate. A Thermo-Systems model 1050 hot film anemometer was used to measure the vertical velocity distribution of the combined waves and currents.

The random wave generator used was a Seasim modular wave making system. This system consisted of a servo control system amplifier, a programmable spectrum random signal generator, an autocompensating wave height gauge, and a paddle type sea wave simulation rolling seal modular wave generator. All test runs used a 1.5 in. (0.04 m) diameter pile placed in a bed of glass microbeads. The microbeads had a mean diameter (D_{50}) of 0.1 mm and a specific gravity of 2.45. Four different wave spectra were generated: Darbyshire, Pierson-Moskowitz, Jonswap (wave period = 8 secs) and Jonswap (wave period = 10 sec).

At the onset of each test, the sediment bed was leveled to a 5 in. (0.13 m) uniform thickness. After achieving the required water depth, the proper flow rate was established. The desired water level was maintained by regulating a 10-in. discharge valve located at the rear of the tank. The sediment bed was once again leveled as the above variables remained constant. The previously programmed signal generator then started generating the desired wave spectrum. Maximum scour depth was recorded at various intervals throughout each run, the time increment increasing as the test progressed. Each test was completed when equilibrium in the measured maximum scour depth was attained. After draining the tank, the patterns were photographed and sediment elevations, taken in the form of a rectangular grid, were established with the point gauge to determine equilibrium scour depth.

The functional relationship for scour may be expressed as:

$$\frac{S_d}{h} = f(S_d/H_{1/3}, S_d/D, S_d/D_{50}, N_{RP}, N_F, N_{FP}, N_{ES}, N_S) \quad (73)$$

$$\text{where } N_{RP} = \frac{UD}{v}$$

$$N_F = u/\sqrt{gh}$$

$$N_{FP} = u/\sqrt{gD}$$

$$N_{ES} = u/\sqrt{2S_d g}$$

$$N_S = U/\sqrt{gD_{50}(\rho_s - \rho)/\rho}$$

On various dimensionless plots, data from experiments conducted by Armbrust and Wang were used in combination with data obtained from the random wave-current interaction experiments. Regression analysis was performed on the plots in order to construct the appropriate curves. Logarithmic regression analysis was used on the semi-logarithmic plots, and power regression analysis was used on the full

logarithmic plots. The " r^2 " term adjacent to each curve represents the correlation coefficient for each curve.

It was discovered that a relationship exists between scour depth and sediment number (N_s), (Figures 49a and 49b) as well as between scour depth and the pile Reynolds number (N_{RP}), (Figures 49c and 49d). However, scour depth is not dependent on N_s , or N_{RP} alone, but is also dependent on pile diameter as well as sediment size.

By plotting the relative scour depth (S_d/h) against the product of the pile Reynolds number and the sediment number ($N_{RP}(N_s)$), all data points collapsed onto a single curve regardless of variance in pile diameter or sediment size (Figure 49e). It appears that because all data collapse onto a single curve, the type of wave train used for model studies, either monochromatic or random, is insignificant in the prediction of scour depth about a single cylindrical pile. However, the geometric shape of the scour hole differs with the type of wave train generated. By using a dimensionless plot (Figure 49e), it appears as though predictions of scour depth could be made for situations in which the pile diameter or mean sediment size varied without using scaling factors. Before any conclusions can be made, field data are required to evaluate the need, if any, for scale effects.

Scour Patterns. The rate of scour hole development by wave-current interaction was faster than that due to a steady current alone. Scour development is very rapid initially, the scour rate then decreases until the equilibrium scour depth is reached.

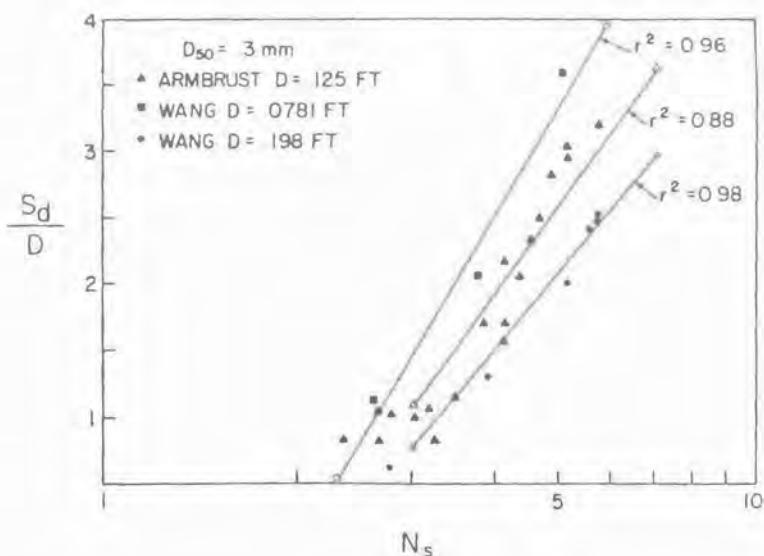


Figure 49a. Relative scour depth, S_d/h , vs. sediment number for a constant sediment size and various pile diameters [15].

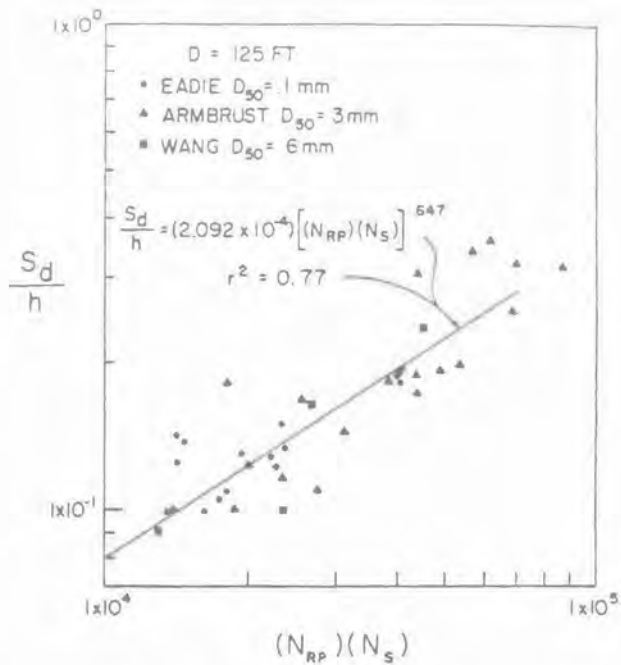


Figure 49b. Relative scour depth, S_d/h , vs. sediment number times pile Reynolds number for a constant pile diameter and various sediment sizes [15].

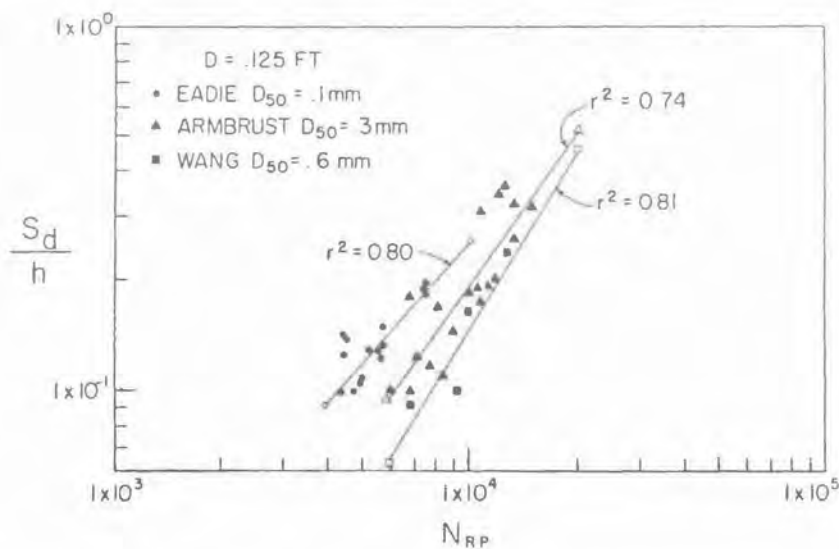


Figure 49c. Relative scour depth, S_d/h , vs. pile Reynolds number for a constant pile diameter and various sediment sizes [15].

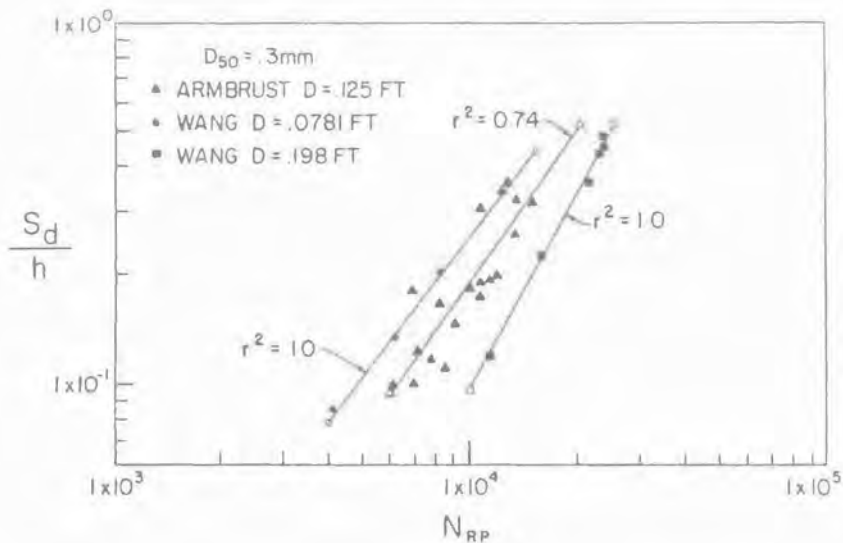


Figure 49d. Relative scour depth, S_d/h , vs. pile Reynolds number for a constant sediment sizes and various pile diameters [15].

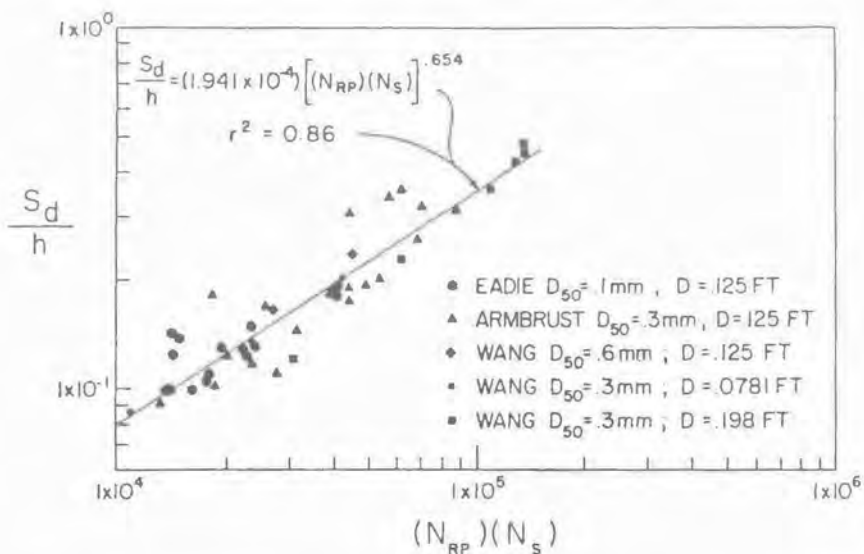


Figure 49e. Relative scour depth, S_d/h , vs. sediment number times pile Reynolds number for various sediment sizes and pile diameters [15].



Figure 50a. Initial stages of scour development [15].

Figure 50a shows a typical pattern of scour development in its initial stages, approximately the first 2 to 5 minutes of test. Figures 50b and 50c are the typical scour patterns that occur due to wave-current interaction 30 minutes and 2 to 3 hours after test commencement, respectively.

In all cases, the scour hole due to wave-current interaction was similar in shape to the scour hole formed by a steady current. This shape resembles an inverted



Figure 50b. Scour pattern 30 minutes after test commencement [15].



Figure 50c. Scour pattern 2–3 hours after test commencement [15].

cone. A typical example of a scour hole formed by a steady current is shown in Figure 50d. Figures 50e–d depict the scour pattern formed by the same current used in Run 4 (Figure 50c), combined with four different random wave spectra. As stated previously, the equilibrium scour hole associated with the wave-current interaction was deeper when compared to the equilibrium scour hole formed by a



Figure 50d. Typical scour cavity due to a steady current $h = 1.67$ ft (0.36 m); $U_c = 0.485$ fps (0.148 mps); $D = 0.125$ ft; $S_d = 0.14$ ft (0.043 m) [15].



Figure 50e. Scour pattern due to random waves and current—Run 13. $h = 1.167$ ft (0.36 m); $U_c = 0.485$ fps (0.148 mps); $U = 0.498$ ft/sec (0.1518 mps); wave spectrum—Darbyshire; $H_{1/3} = 0.1724$ ft (0.053 m); $D = 0.125$ ft (0.038 m); $S_d = 0.143$ ft (0.044 m) [15].

steady current alone. The size and shape of the equilibrium scour hole associated with wave-current interaction was at times greater than, approximately equal to, or less than the size and shape of the scour hole due to a steady current alone. These results differ from the prediction made by Niedoroda and Dalton [35]. They



Figure 50f. Scour pattern due to random waves and current—Run 14. $h = 1.167$ ft (0.36 m); $U_c = 0.485$ ft/sec (0.148 mps); $U = 0.491$ ft/sec (0.150 mps); wave spectrum—Pierson-Moskowitz; $H_{1/3} = 0.1527$ ft (0.047 m); $D = 0.125$ ft (0.038 m); $S_d = 0.149$ ft (0.045 m) [15].

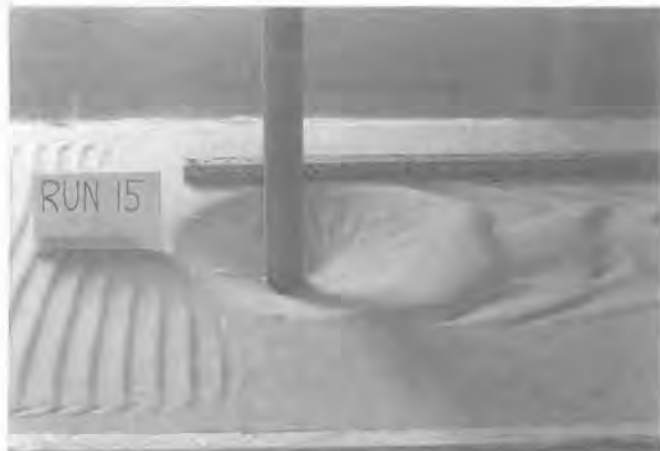


Figure 50g. Scour pattern due to random waves and current—Run 15. $h = 1.167$ ft (0.36 m); $U_c = 0.485$ ft/sec (0.148 mps); $U = 0.504$ ft/sec (0.154 mps); wave spectrum—Jonswap ($T = 8$ sec); $H_{1/3} = 0.1631$ ft (0.050 m); $D = 0.125$ ft (0.038 m); $S_d = 0.174$ ft (0.053 m) [15].

stated that the scour hole size and shape for combined waves and currents should not be as great as that developed by a steady current alone.

The general scour pattern was one of localized scour around the pile. A vortex formed around the pile due to disturbed flow and suspended the sediment. The sediment was carried farther downstream under the combined effects of waves and



Figure 50h. Scour pattern due to random waves and current—Run 16. $h = 1.167$ ft (0.36 m); $U_c = 0.485$ ft/sec (0.148 mps); $U = 0.508$ ft/sec (0.155 mps); wave spectrum—Jonswap ($T = 10$ sec); $H_{1/3} = 0.1550$ ft (0.047 m); $D = 0.125$ ft (0.038 m); $S_d = 0.155$ ft (0.047 m) [15].

currents than it was with a steady current alone. Initially, the sediment suspension appeared to become greater as the scour hole developed, possibly due to a strengthening of the vortex system surrounding the pile. Because of the disturbance of flow caused by the pile, trailing ripples formed immediately behind the pile extending in the direction of wave propagation as the test progressed.

In all cases, the maximum scour depth occurred downstream of the pile, approximately 1/4 in. from the pile, and at an angle of approximately 40° to the left or right of an imaginary line drawn through the pile and parallel with the wave flume walls.

The random waves and currents may be summarized as follows:

1. Scour development was very rapid initially. The scour rate then decreased until an equilibrium scour depth was reached.
2. Scour development due to current and wave action occurred faster than scour due to a steady current alone.
3. The equilibrium scour depth caused by wave-current interaction is approximately 10% greater than the scour depth caused by a steady current alone.
4. The shape of the scour hole due to waves and currents and the shape of the hole due to current alone are similar. The shape resembles an inverted cone.
5. A relationship exists between scour depth and sediment number (N_s). However, scour depth is not dependent on N_s alone, but is also dependent on pile diameter and sediment size.
6. A relationship also exists between scour depth and the pile Reynolds number (N_{RP}). Again, scour depth is not dependent on (N_{RP}) alone, but is also dependent on pile diameter, as well as sediment size.
7. By plotting the relative scour depth (S_d/h) against the product of the pile Reynolds number and sediment number, ($N_{RP})(N_s)$, all data points collapse onto a single curve regardless of variance in pile diameter or sediment size.

Although the amount of data is limited, due to the fact that all data could be collapsed onto one curve when plotting S_d/h versus ($N_{RP})(N_s)$, (Figure 49e), it appears as though the type of wave train used for model studies, either mono-chromatic or random, is insignificant in predicting scour depth about a single, cylindrical pile. However, when attempting to predict the geometry of the scour hole, the irregularity of the wave train becomes very significant. Armbrust stated that the pattern of scour for wave-current interaction is no longer conical in shape, but the pattern is irregular due to the wave particle orbital motion. The data in this study clearly indicate a conical scour pattern for random wave-current interaction. Although these results are different from those of Armbrust, they agree with field data, as well as with the predictions of Niedoroda and Dalton. The fact that the geometric shape of the scour hole differs with the type of wave train used, may become important in the prediction of scour depth around multiple pile cases.

The conclusions resulting from this study were found for a flow in which the steady current was greater than the oscillatory flow produced by the waves. If the magnitude of the two flows in relation to one another change, the flow patterns will also change and the geometry of the scour hole may very likely differ from results found in this study.

Rance [42] conducted laboratory experiments of scour around large diameter objects subject to waves and currents. The large diameter objects were defined when the diameter was greater than one tenth of the wavelength. Cylindrical, square, and hexagonal piles were employed to evaluate the effect of structural shape on scour. Rance reported that an angular column has the same effect as an equivalent circular cylinder of the same cross-sectional area. The general pattern of erosion and accretion depends on the wave and current direction with respect to the structure. In Figure 51 the measured depth and the extent of scour are expressed as a percentage of the structure diameter for a square structure (Figure 51a) and for a hexagonal structure (Figure 51b). Estimated scour around large diameter objects is shown in Figure 52. The estimates appear to be independent of geotechnical and oceanographic conditions [42].

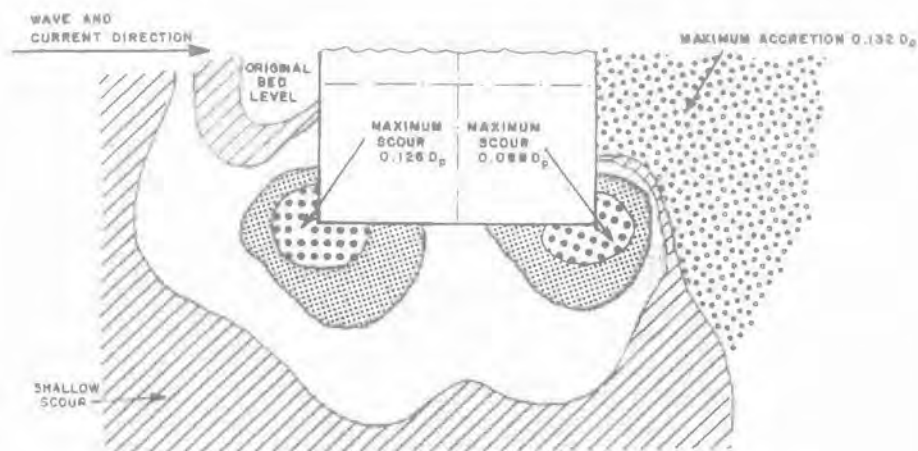
Local Scour Around Pile Groups Due to Waves and Currents

As shown in an earlier study by Chow and Herbich [12], the scour depth increases if the ratio of pile diameter to center-to-center span length between the piles increases from about 0.12 to 0.25. Breusers [8], based on model experiments with a 3-legged platform, showed an increase in scour over that for an isolated pile if the spacing is less than three diameters.

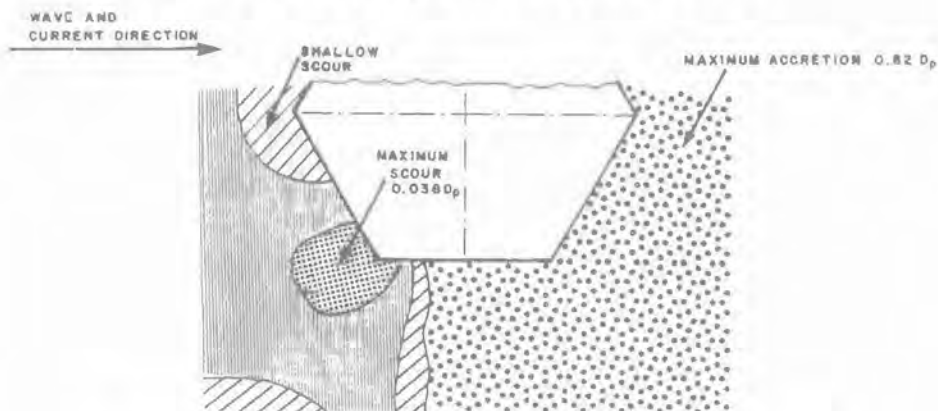
Model experiments with three different arrays of pile groups due to currents alone and the combined action of waves and currents were conducted by Lee [27]. Tests conducted with currents alone indicated that the ultimate scour depth increases with larger velocities, with pile diameters and finer sediment sizes. The results were plotted in dimensionless form as functions of the sediment number, the pile Reynolds number, and the pile Froude number. Experiments with combined waves and currents indicate that the critical sediment number required to cause incipient scour was smaller than that for currents alone. A relationship between the relative scour depth S_p/D_p and the product of sediment number and the pile Reynolds number $(u^2 D_p) / \sqrt{(S-1)gd}v$ is shown in Figure 53 for 1-, 3-, 4-, and 6-legged platforms (where S_p —scour at the pile; D_p —pile diameter; S —specific gravity of the sediment).

The scour depth tends to increase with increasing current and pile diameters. The finer the sediment, the larger the scour depth. The scour due to superimposed waves and currents is larger than that due to current alone, and much larger than that due to waves alone. It may thus be concluded that most of the scour is caused by the current.

Experiments were also conducted at Delft Hydraulic Laboratory [51] to evaluate scour around groups of two and three cylinders (Figure 54). The maximum scour was observed to be 1.2 to 1.5 times the diameter of the cylinder for the case of currents only. The currents and waves from the perpendicular direction produced maximum scour depth of the same magnitude, however, the area of scour was more extensive. For currents and waves at an angle of 120° to each other the maximum scour depth was 1.0 to 1.1 times the cylinder diameter. The scour depth was independent of the velocities greater than threshold velocities for initiation of bedload



(A) SQUARE STRUCTURE WITH LEADING FACE



(B) HEXAGONAL STRUCTURE WITH LEADING CORNER

LEGEND

-  SCOUR DEPTH (s_p)/STRUCTURE DIAMETER (D_p) < 0.01
-  $0.03 > s_p / D_p > 0.01$
-  $0.06 > s_p / D_p > 0.03$
-  $s_p / D_p > 0.06$
-  ACCRETION (RANGES NOT SPECIFIED)

0 0.1 0.2
SCALE - METRES

Figure 51. Typical scour patterns for a square structure (a) and for a hexagonal structure (b) [42].

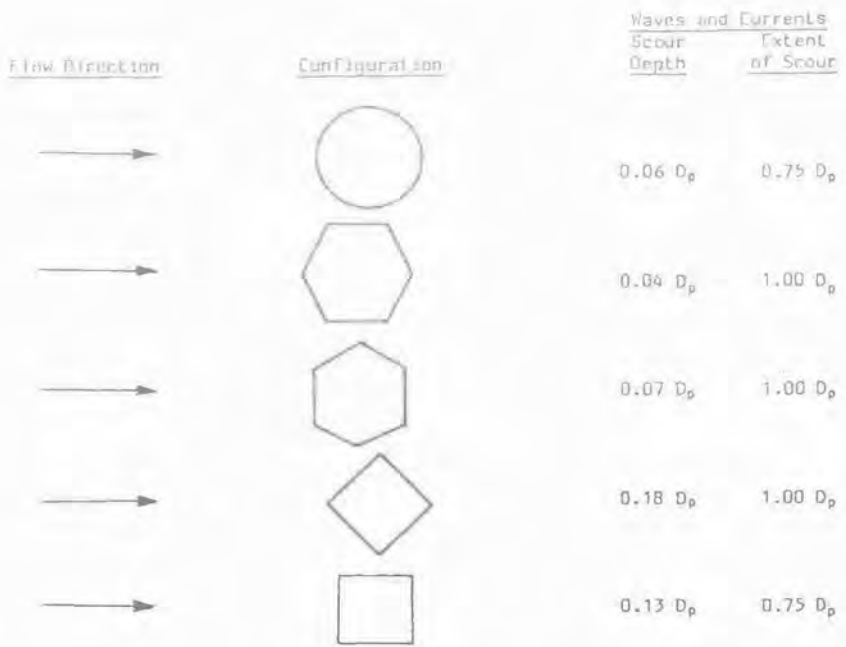


Figure 52. Scour around objects with diameters larger than a tenth of a wavelength [42].

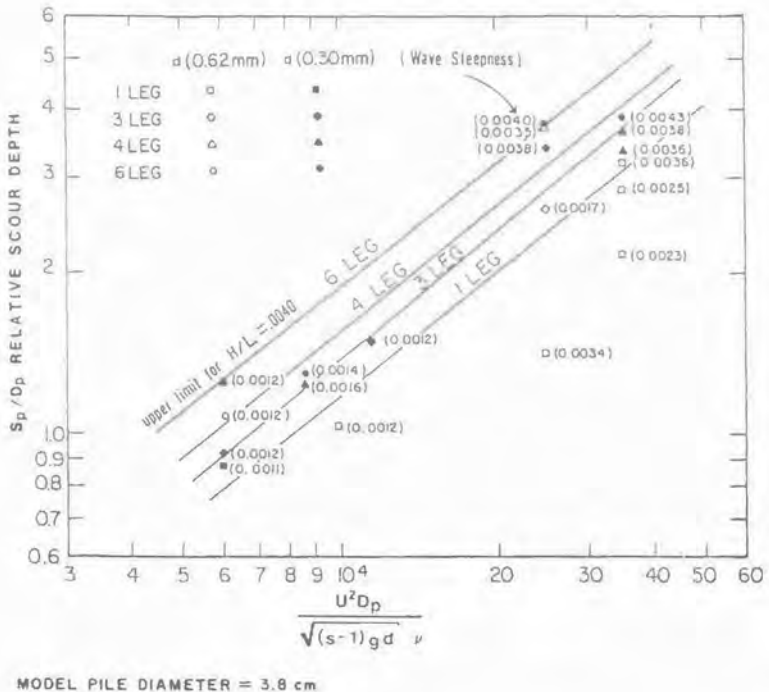


Figure 53. Relative scour depth caused by waves and currents for 1-, 3-, 4-, and 6-legged platforms [27].

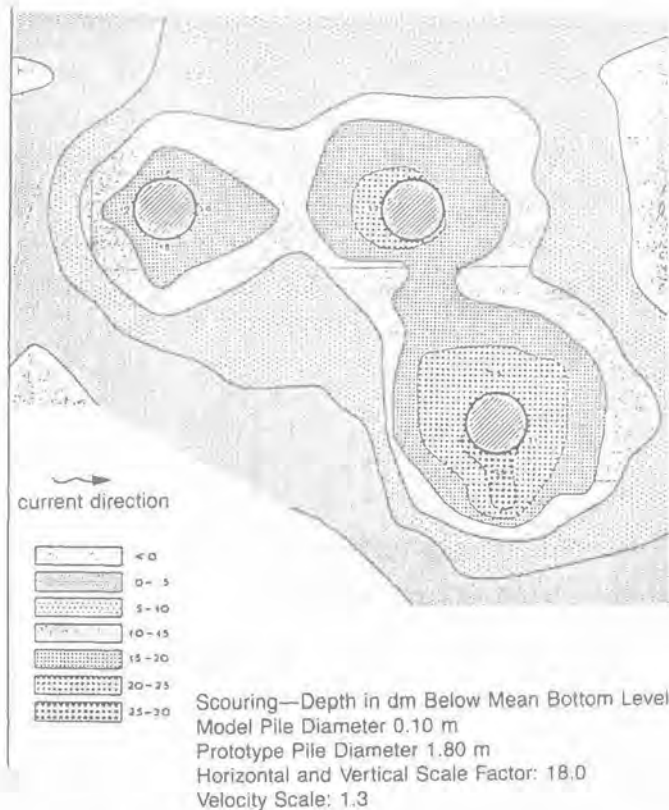
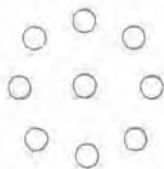


Figure 54. Scour pattern around a group of three piles [51].

transport, however, the equilibrium scour depth was achieved sooner at greater velocities.

For multiple pilings, the scour patterns can be treated as independent if the hydrodynamic characteristics of the individual horseshoe vortices are not affected by the proximity of the adjacent pilings. As the spacing between pilings decreases, a point is reached when a cluster of pilings would act as a single piling with a much greater effective diameter (Figure 55).

Model tests to evaluate scour around the pontoons of a semi-submersible drilling rig due to currents alone were conducted by Wilson and Abel [60]. The extent of scour was sufficient to produce undermining and settlement of the rig pontoons. The presence of waves was found to influence the scouring process and accelerate the rate of scour.



- a) Piling Spacing Such That Effective Diameter is Greater Than That of Individual Piling.
- b) Effective Diameter Approximately Equal to that of Circumscribing Circle.

Figure 55. Effective diameter for pile clusters.

Criteria for Local Scour Around Piles

Single Piles. Scour around single piles is caused by waves and currents, most of the scour (perhaps up to 90%) is caused by the current. Because most of the information on scour is based on model experimentation and there are only few documented field measurements, general criteria, or guidelines are empirical in nature. The design depth of scour is usually taken equal to twice the pile diameter and the lateral extent of the scour hole is dependent on the natural angle of repose of granular sediments as shown in Figure 56. Estimated dishpan scour should be added to the local scour in arriving at the total scour depth.

Groups of Piles. Wave-induced scour around multiple piles observed by Palmer [37, 38] indicate that the individual scour holes around each pile eventually coalesce and form larger scour patterns. Lambe and Whitmen [26a] noted that the limit of scour hole interference for a sand with a submerged natural angle of repose of 27° is a center-to-center piling spacing of approximately 9 diameters.

Dishpan Scour

In addition to the local scour around piles, a more extensive scour has been observed around platforms in the North Sea [53, 57] and in the Gulf of Mexico [39–41]. Dishpan scour may be defined as a general scour around the whole platform probably caused by diffraction of waves and bottom current turbulence around the platform. It results in a deep smooth-bottom saucer much larger than the structure [39]. A general lowering of seabed occurs around the platform with scour pattern taking the shape of an elongated elliptical bowl perpendicular to the predominant current direction. Dimensions of dishpan scour were reported by Posey and Sybert [39], Watson [57], and Van Dijk [53] and are summarized in Table 3.

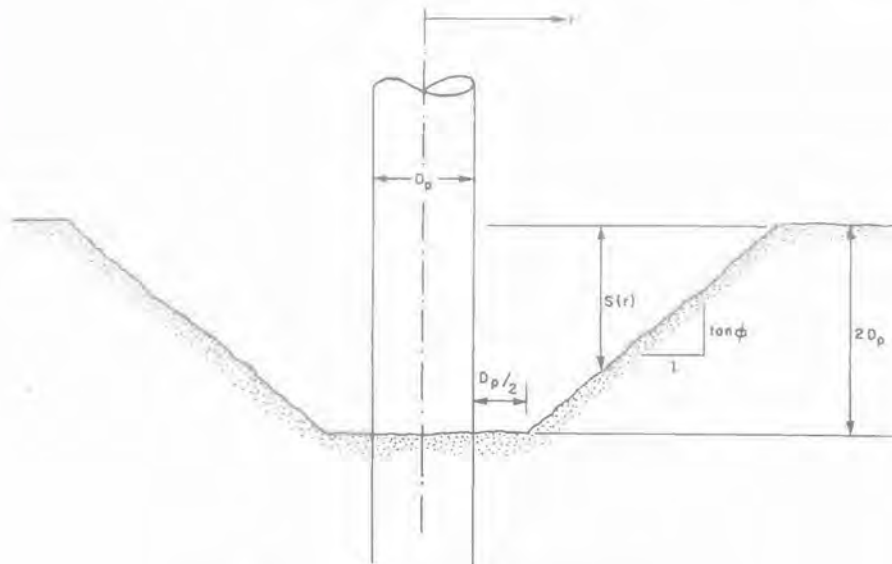


Figure 56. General criteria for scour around a single pile.

Table 3
Reported Dimensions of Dishpan Scour

Dimension	Posey and Sybert [39]	Watson [57]	Van Dijk [53]
Area:	Gulf of Mexico	North Sea	North Sea
Water depth:	11.6 to 13.7 m	40 m	30 to 35 m
Platform geometry:	5 individual platforms, 12 vertical legs of 0.25 m diameter in a rectangle of 12.1 by 27.3 m	2 platform complex with 14 vertical legs of 1.0 m diameter	2 platform complex
Sediment size:	0.08–0.1 mm or finer	unknown	unknown
Scour depth below seabed level:	2.3 to 4.0 m	3.0 m	5.5 m
Distance from platform leg:	15 m	152 m	43 by 49 m
Scour pattern:	unknown	Elliptical bowls elongated at right angles to the predominant current direction	unknown

The extent of the dishpan scour is given by Watson [57] for the North Sea platform (Figure 57a) and for the Gulf of Mexico by Posey [41] (Figure 57b). Angus and Moore [3] have also reported that both local scour and dishpan scour occurred simultaneously around offshore platforms in the North Sea.

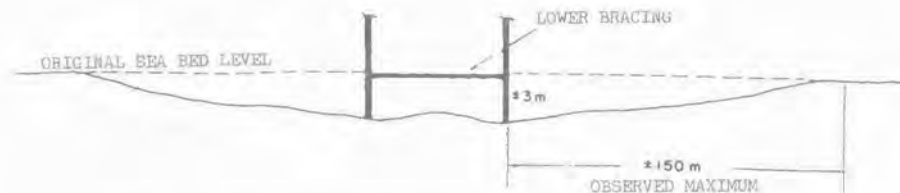


Figure 57a. Extent of dishpan scour at a North Sea platform [57].

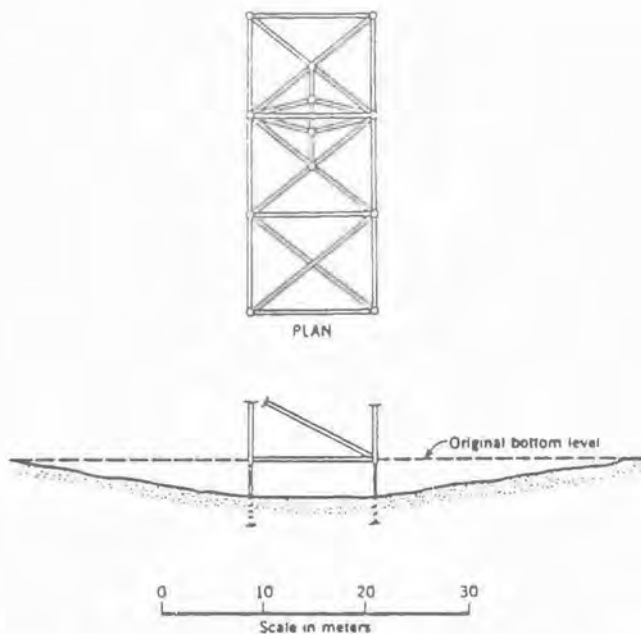


Figure 57b. Extent of dishpan scour at a Gulf of Mexico platform [41].

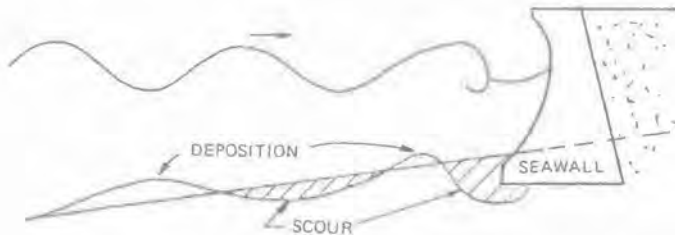


Figure 58a. Changes in beach profiles in front of seawalls.

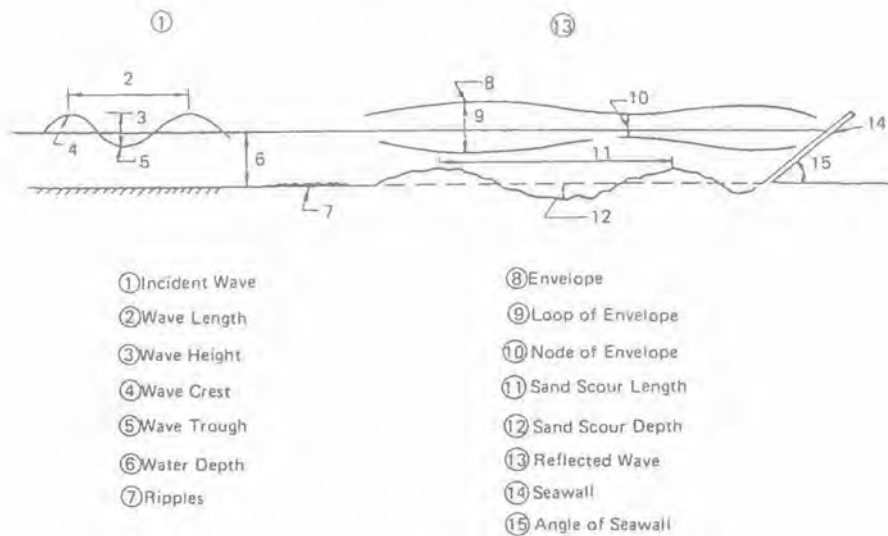


Figure 58b. Terminology.

Scour in Front of Seawalls*

The Eighteenth International Congress on Navigation (Rome, 1953) divided seawalls into two types: those from which waves are reflected and those on which waves break. It is generally agreed that any intermediate type producing a combination of reflection and breaking sets up severe erosive action of the granular seabed in front of the wall (Figure 58a).

* From Chapter 7, "Scour in Front Seawalls," *Seafloor Scour* (with permission from Marcel Dekker, Inc.) [21].

However, it has also been observed that erosion can and does occur at locations where waves do not break. For example, a protective wall may be fronted by a beach and submerged to a depth sufficient to prevent wave breaking. The design engineer of a seawall must know the depth to which protective sheet-piling must be driven to prevent the overturning of the wall due to erosion or scouring of the sand at the toe of its foundation.

When a system of oscillatory, incident waves progresses toward the seawall and hits the seawall, another system of waves is formed by the reflection of waves from the seawall. These two wave systems form a third wave system as the reflected wave is superimposed on the incident wave. The velocity components of the new wave system are given by the summation of the velocity component vectors of the incident and reflected waves (Figure 58b).

Experimental Studies

Wave Channel. A sketch of the experimental setup is shown in Figure 59. A simulated seawall made of plexiglas was located some 52 ft from the wave generator and was constructed so that the angle θ measured from the horizontal could be equal to 15° , 30° , 40° , 67.5° , or 90° (vertical).

A false bottom was constructed under and in front of the wave generator and set at the same depth as the sand bed [17].

The monochromatic wave generator was of the oscillating-pendulum type. The stroke, period, and pendulum settings were adjustable so that the desired wave characteristics could be obtained. A wave absorber was installed behind the wave generator, and wave filters were used in front of the generator. Parallel-wire capacitance-type wave probes and an electronic wave recorder were used.

Beach Material. The material used to simulate the prototype beach was a white silica sand quarried at Melville, N. J. and is of the type commonly found on many beaches. While other researchers have experimented with the use of low-density crushed plastic as a simulated beach material, the sand selected had the advantage

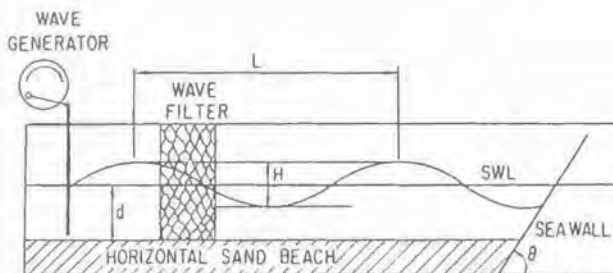


Figure 59. Sketch of test facility.

of more nearly representing natural beaches. Before being placed in the wave channel, the sand was well washed to eliminate the finer particles, which tend to suspend in water and thus obscure visual observations (Figure 59). The median diameter of sand was 0.019 in. (0.4825 mm).

The scour wavelength λ was measured from crest to crest. The extent of scour B was also measured, as shown in Figure 60. Neither of these varied significantly with time (or number of waves to pass over the scoured area), but both had a fixed relationship to water wavelength.

The depth of scour S was measured from the original sand bed level (indicated by the previously drawn reference line) to the point of maximum scour, on the outside of the wave channel, because the depth of scour was fairly uniform along the width of the channel. The depth of scour was measured at every scour formation at certain intervals of time. By dividing the time interval by the wave period, the number of waves to pass over the scour formation, N , was then determined.

Each test was run until the ultimate depth S was reached, that is, until the depth of scour did not increase with any further increase in the number of waves passing over and becoming a constant value. This usually took anywhere from a few hours to a few days for each test.

The variables significant to this problem are (1) the wave height H , (2) the wavelength L , (3) the wave period T , (4) the depth of water d , (5) the seawall angle θ , and (6) the number of waves to act on the beach, N .

Additional variables to be considered are the specific gravity and porosity of the sand and the diameter of the particles. Unfortunately, only one type of sand was employed, so the material properties were constant in this study.

Denoting by X all the unknown scour parameters—such as the scour depth S , extent B , and location λ —and making use of the relationships between T , L , and

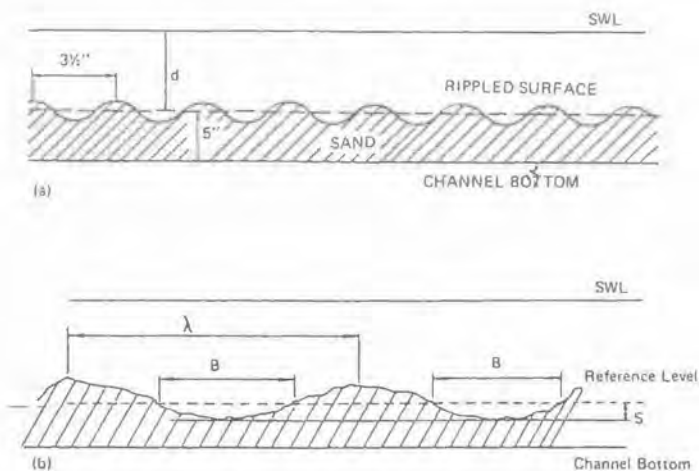


Figure 60. (a) Typical ripple formation; (b) Typical scour formation.

d to eliminate the effects of T, an expression that contains significant parameters is

$$f(X, H, L, d, \theta, N) = 0 \quad (74)$$

When ultimate conditions are reached, so that S, B, and λ are no longer influenced by N, Equation 74 becomes

$$F(X, H, L, d, \theta) = 0 \quad (75)$$

θ already appears as a dimensionless variable. Since there are now only four independent dimensional variables left, with one independent dimension three dimensionless ratios can be formed; thus Equation 75 can be transformed to

$$\frac{X}{H} = f_1\left(\frac{H}{d}, \frac{L}{d}, \theta\right) \quad (76)$$

or

$$\frac{X}{L} = f_2\left(\frac{H}{d}, \frac{L}{d}, \theta\right) \quad (77)$$

Wave Reflection. It is obvious that the magnitude of beach scour also depends on wave reflection from the seawall.

The reflective capacities of impermeable beaches were described theoretically by Miche [33] and studied by Straub and Herbich [45]. Miche considered the ideal case of a perfectly smooth barrier forming an angle α with the horizontal and analytically developed a formula for the maximum wave steepness in deep water that will be totally reflected by such a barrier:

$$\delta_{OM} = \sqrt{\frac{2d}{\pi}} \frac{\sin d}{\pi} \quad (78)$$

where δ_{OM} is the maximum wave steepness (in deep water), which will be totally reflected by a smooth barrier. From this he deduced that waves steeper than δ_{OM} would be partially reflected and those flatter than δ_{OM} would be totally reflected. The part theoretically reflected (R') has then the following value:

$$R' = \frac{\delta_{OM}}{\delta_{OI}} \quad (79)$$

where $R' \leq 1$

δ_{OI} = incident wave steepness in deep water

The magnitude of wave reflection as a function of beach slope computed from Miche's theory was partially verified by Straub and Herbich [45], and the actual values of wave reflection coefficient for various beach slopes were published.

Considering a sinusoidal wave, the wave reflections may be measured in the following manner.

Let the incident wave be

$$\eta_I = a \sin\left(\frac{2\pi}{\lambda} x - \frac{2\pi}{T} t\right) \quad (80)$$

and the reflected wave

$$\eta_R = b \sin\left(\frac{2\pi}{\lambda} x + \frac{2\pi}{T} t\right) \quad (81)$$

where η = surface elevation

a, b = wave amplitudes

x = distance along a horizontal axis

t = time

For the clapotis

$$\eta = \eta_I + \eta_R \quad (82)$$

At the nodes ($x = 0, \lambda/2, \lambda, \text{etc.}$),

$$\eta = (a - b) \sin \frac{2\pi}{T} t \quad (83)$$

At the loops ($x = \lambda/4, 3\lambda/4, \text{etc.}$)

$$\eta = (a + b) \cos \frac{2\pi}{T} t \quad (84)$$

An envelope of incident and reflected waves is developed with definite loops and nodes. The reflection coefficient is equal to

$$\frac{H_L - H_n}{H_L + H_n} = C_R$$

where H_L = height at the loop

H_n = height at the node

Mechanics of Sediment Movement

If the mean diameter of a sediment particle (50% finer by weight) is d , and u_* is the local fluid velocity parallel to the bottom, then the drag force just sufficient to initiate movement of a bed particle

$$F_D = C_D \rho \frac{u_*^2}{2} \frac{\pi d^2}{4} \quad (85)$$

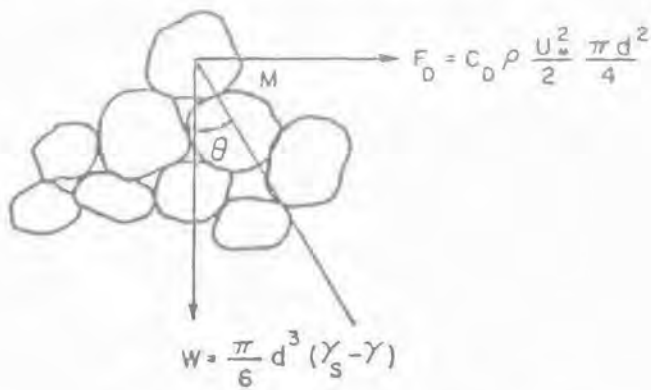


Figure 61. Initial movement of a sand particle.

where C_D = coefficient of drag
 ρ = density of the fluid

Consider a particle P as shown in Figure 61 θ is the angle of repose. The moment that is just sufficient to initiate movement of the particle about M must equal the moment of its own weight about point M [18]:

$$F_D = C_D \rho \frac{u_*^2}{2} \frac{\pi d^2}{4} = \frac{\pi}{6} d^3 (\gamma_s - \gamma) \tan \theta \quad (86)$$

where γ_s = specific weight of sediment
 γ = specific weight of fluid
 C_D = coefficient of drag, which is a function of Reynolds number N_R

Boundary Layer Along a Flat Sand Bed

The mechanics of sediment movement were discussed in the previous section and u_* was defined as the local horizontal velocity parallel to the bottom. However, the sand particle is so small that the boundary layer effect must be considered. Fortunately, the boundary layer along a flat plate is the simplest case of the application of Prandtl's boundary layer theory.

Based upon the cnoidal wave theory and laboratory observations (Figure 60), it is reasonable to assume that the fluid flow pattern between the sand bed and water surface (within the scour wavelength) is uniform and steady, or that $\partial v / \partial y = \text{constant}$. Following Prandtl's development the thickness of boundary layer may be expressed as

$$\delta = \left(\frac{v x}{U} \right)^{1/2} \quad (87)$$

or

$$\eta = y \left(\frac{U}{\nu x} \right)^{1/3} \quad (88)$$

where $\eta = y/\delta$ is defined as a dimensionless term.

From the definition of stream function, we have

$$u_* = \frac{\partial \Psi}{\partial y} = \frac{\partial \Psi}{\partial \eta} \frac{\partial \eta}{\partial y} = U f'(\eta) \quad (89)$$

or

$$\frac{u_*}{U} = f'(\eta) \quad (90)$$

The solution of this equation was obtained by Howarth [22].

The mechanics of the scouring process may be explained in the following. When the experiment is started with a flat sand bed, the horizontal velocity component under the node is affected more than the horizontal velocity component under the loop, so that the primary scour occurs under the nodes of the envelope. A few hours later (usually 1 to 3 hr) the crests of the sand formation move under the nodes of the envelope. This relative position will normally last throughout the duration of the experiment.

From Equation 86, for a particular grain size of sand, the most important variable is u_* . In other words, u_* , the local velocity parallel to the bottom, is the main factor determining the depth of scour. Because the wave is generated from rest, the equation of continuity is valid in this case. It is then logical to say that when scour depth increases, the local velocity must decrease until a certain point when the ultimate scour depth is reached. This does not imply that scour and sediment transfer come to a halt; it is only a limit that is approached asymptotically.

Figure 62 shows a side elevation of sand bed. Section a represents the initial condition (before the scour) and section b represents the condition when the ultimate scour is reached.

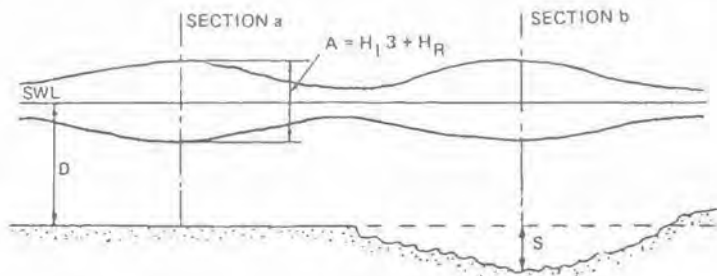


Figure 62. Geometry of sand scour [18].

The continuity equation may be written between section a and section b,

$$U_a \left(D - \frac{1}{2} A \right) = U_b \left(D - \frac{1}{2} A + S \right) \quad (91)$$

or

$$U_b = U_a \frac{D - (1/2)A}{D - (1/2)A + S} \quad (92)$$

This equation must be modified to take account of reflection, which is a function of the slope of the seawall. When the two wave systems approach from opposite directions and are superimposed, the velocity components may be added vectorially. Introducing Equation 89, we have

$$f'(\eta)(1 - C_r)U_b = (1 - C_r)f'(\eta)U_a \frac{D - (1/2)A}{D - (1/2)A + S} \quad (93)$$

where C_r is the reflection coefficient, defined as

$$C_r = \frac{A - B}{A + B} = \frac{H_R}{H_I} \quad (94)$$

Substituting Equation 93 into Equation 88 and simplifying, the following expression for "ultimate" scour depth is obtained:

$$S = \left(D - \frac{1}{2} A \right) \left\{ (1 - C_r) u_* \left[\frac{3}{4} C_D \rho \frac{\cot \theta}{d(\gamma_s - \gamma)} \right]^{1/2} - 1 \right\} \quad (95)$$

where $A = H_I + H_R$.

Dimensional Analysis

The following dimensionless terms may be obtained from the dimensional analysis:

$$\frac{S}{K}, \frac{\lambda}{L}, \frac{T}{t}, N_R, \frac{V^2 \rho}{d(\gamma_s - \gamma)}, N_F, C_r$$

where the following functional equation may be written:

$$f \left(\frac{S}{K}, \frac{\lambda}{L}, \frac{T}{t}, N_R, \frac{V^2 \rho}{d(\gamma_s - \gamma)}, N_F, \theta, \alpha, C_r \right) = 0 \quad (96)$$

$$\frac{S}{K} = f_1 \left(\frac{\lambda}{L}, \frac{T}{t}, \frac{1}{N_R}, \frac{V^2 \rho}{d(\gamma_s - \gamma)}, \frac{1}{N_F}, \theta, \alpha, C_r \right) \quad (97)$$

For the sake of comparison Equation 95 may be rewritten in the following form:

$$\frac{S}{K} = (1 - C_r) \left(\frac{3}{4} C_D \right)^{1/2} \left[\frac{V^2 \rho}{d(\gamma_s - \gamma)} \right]^{1/2} (\cot \theta)^{1/2} - 1 \quad (98)$$

It is obvious that Equations 97 and 98 are very similar. However, it must be pointed out that Equation 95 should be used only for the ultimate scour depth.

General Observations

For almost every case tested, ripples were observed to form in the sand bed soon after the start of each test. These ripples continued in existence and became superimposed upon the larger-scale effects of scouring. Very even and regular in appearance, the ripples were sinusoidal in shape. For all tests the pitch length of the ripples, measured from crest to crest, was $3\frac{1}{2}$ in., and the overall height was approximately 1 in.

Bagnold [5] has presented some data for the natural pitch length of quartz sand in oscillating water waves, and this value of $3\frac{1}{4}$ in. compares favorably with his findings.

Manohar [31] has presented an interesting experimental finding relating the ripple-height-to-length ratio with a parameter similar to the Einstein sediment function. However, no comparison is possible because the maximum ratios he obtained are much lower than the ones obtained in this study.

Soon after the appearance of the ripples, it was observed that the sand bed began to erode appreciably at uniform intervals such that the sand bars and troughs were created throughout the length of the sand bed.

Depth of Scour. The relationship between the \bar{S}/H (where \bar{S} is the average of the one-third greatest depths of scour recorded) and N (number of waves) is indicated in Figures 63 and 64. The results show that in every case the depth of scour initially increased very rapidly with increasing N , but became independent of N as it attained its ultimate value. The constant \bar{S}/H is termed the ultimate depth of scour, \bar{S}_u/H . It was established that after ultimate depth of scour was attained a further increase in the number of waves did not affect the relative depth of scour, but that does not imply that scouring and particle movement came to a standstill. Actually, after ultimate conditions were established, a state of equilibrium existed so that particles removed by wave action were replaced through deposition of particles held in suspension.

There is definite evidence that \bar{S}/H was always greater for the 30° seawall than for the 15° seawall. Tests on seawalls of 90° , 67.5° , and 45° indicated that all relative depths of scour lie on one smooth curve. This seems logical because it has been

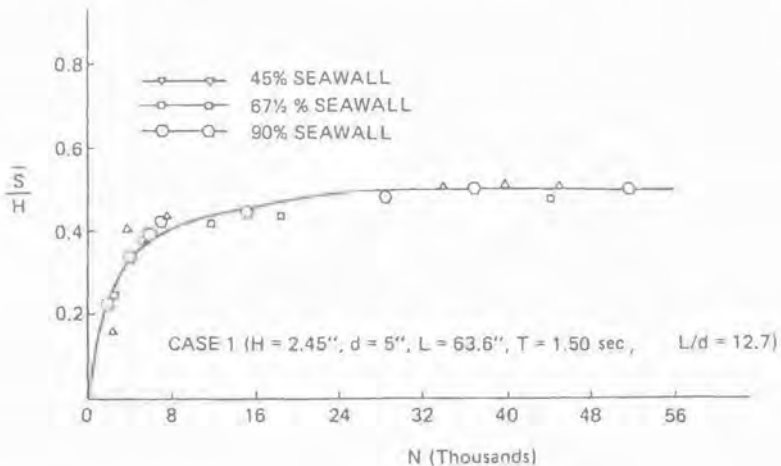


Figure 63. Relative depth of scour \bar{S}/H as a function of number of waves, Case 1.

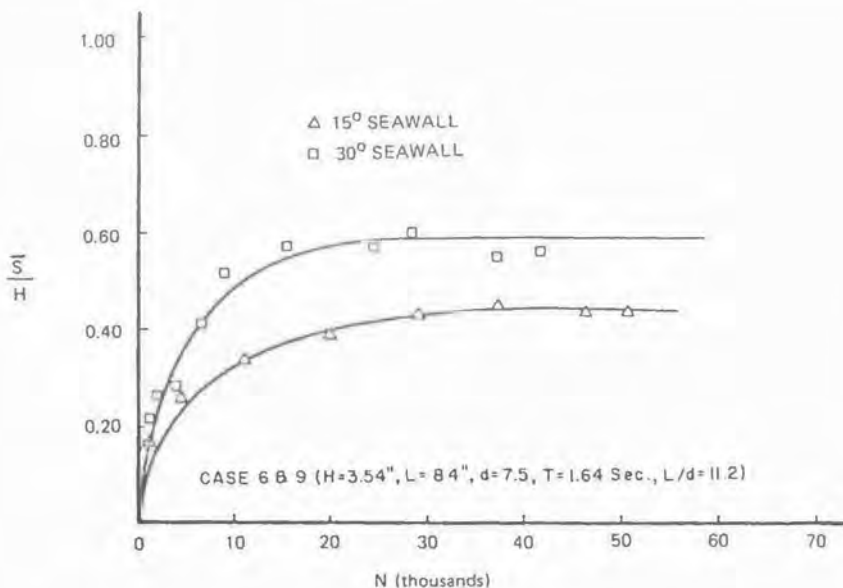


Figure 64. Relative depth of scour \bar{S}/H as a function of number of waves.

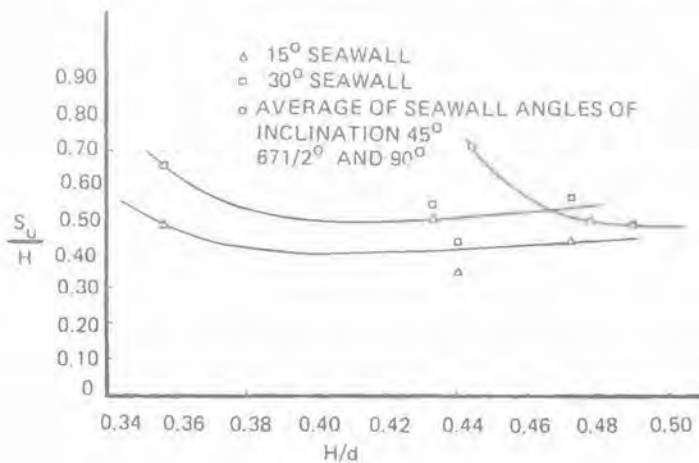


Figure 65. Ultimate relative depth of scour \bar{S}_u/H as a function of relative wave height H/d . (from Herbich, Murphy and Van Weele, 1965).

observed that the difference in reflection coefficient between the 15° seawall and the 30° seawall is much larger than the difference in reflection between the 90°, 67.5°, and 45° seawalls.

Effect of Wave-Height-to-Water-Depth Ratio (H/d). Figure 65 presents the results of the study to evaluate the effect of H/d .

Due to the steep slope of the curves at low H/d , it may be that the curves continue to rise as H/d decreases to a value lower than 0.35, to eventually approach a limit of incipient sand movement. It appears that the limit occurs at H/d of 0.32.

As H/d increases, the \bar{S}_u/H decreases for both the 15° and the 30° seawalls. Either the gradual increase in \bar{S}_u/H continues or the value of \bar{S}_u/H becomes constant as the limit of wave breaking is reached. According to the solitary wave theory, the point of wave breaking occurs at H/d of 0.78.

Effect of Wavelength-to-Water-Depth Ratio (L/d). Figure 66 shows the effect of L/d on \bar{S}_u/H for the 15° seawall and partly for the 30° seawall.

Although there are not enough data available for a rigorous investigation of the relationship, some observations may be drawn. First, a low ultimate relative depth of scour occurs for both the 15° and the 30° seawalls somewhere between $L/d = 7$ and $L/d = 10$. Second, the values of \bar{S}_u/H increase more rapidly for L/d values greater than 9.

Effect of Reflection Coefficient. As reflection coefficient C_R increases, the ultimate depth of scour for the 30° seawall increases linearly up to a value of C_R of approximately 45% (Figure 67). Beyond that point the linearity ceases to exist and the curve flattens at a C_R of 54% where a constant value of \bar{S}_u of 2.01 is reached. After

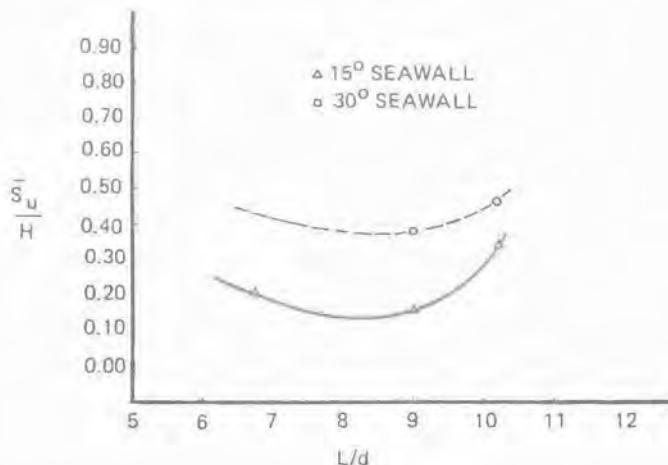


Figure 66. Ultimate relative depth of scour \bar{S}_u/H as a function of relative wave length L/d . (from Herbich, Murphy and van Weele, 1965).

54% is attained, it appears that any further increase in reflection coefficient does not have an effect on the ultimate depth of scour.

An estimated plot was also prepared for the 15° seawall (Figure 68). For the 15° seawall values of \bar{S}_u were available but data for R were not taken, and the reflection coefficient was estimated from data presented by Straub and Herbich [45]. Figure 68 indicates that the 15° seawall followed a trend similar to that of the 30° seawall.

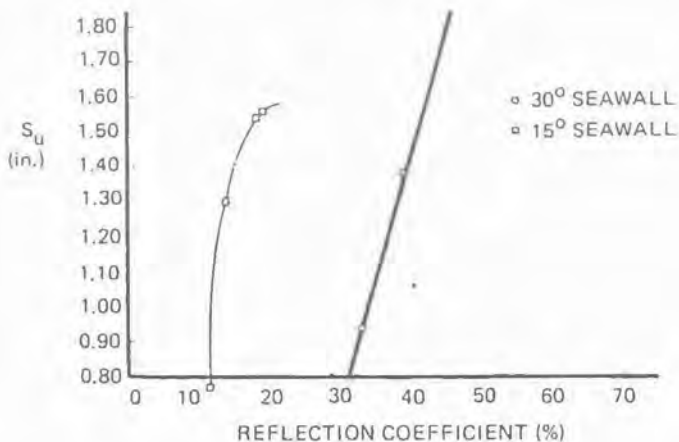


Figure 67. Ultimate relative depth of scour \bar{S}_u/H as a function of relative wave height H/d . (from Herbich, Murphy and van Weele, 1965).

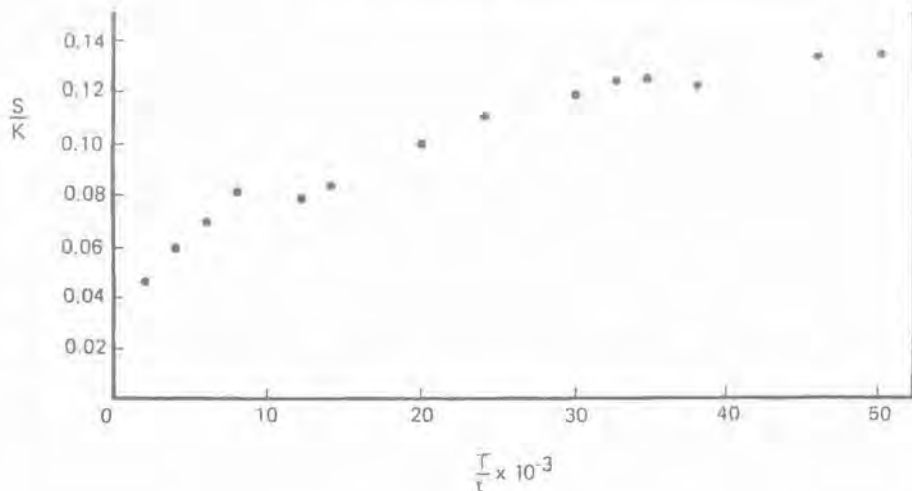


Figure 68. Relationship between \bar{S}/K and T/t [18].

Scour Formations. At the end of every test the extent of scour B and the distance between adjacent scour formations λ were measured. Every case provided strong evidence that λ is one-half of the wavelength L , whereas B is one-fourth of the wavelength (Figure 60).

Besides obtaining this $(1/2)L$ scour pattern, Bagnold [5] was also able to obtain scour patterns spaced at intervals of $2L$ using crushed plastic and extremely fine sand as the bed material.

Although λ completely defines the distance between scour locations, it is difficult to determine the distance from the seawall to the first adjacent scour point. It was observed that there was a very slow but perceptible advance of the entire scour formation in the direction of wave travel as the number of waves acting on the bed increases. The most that can be stated is that at any time there will always be scouring within a distance of at least $(1/4)L$, or less from the face of the wall.

Results

1. All experiments performed indicate there may be a limit of scour depth that is approached asymptotically. The scour depth increases very rapidly during the first few hours and then the erosive process slows down and reaches a state of what other investigators called ultimate scour depth. Figure 68 is a plot of S/K as a function of T/t , where S is the average scour depth taken within a range of 15 ft in front of the seawall. The term T/t is actually the number of waves generated.
2. Fluctuations in values of measured wave height and wave reflection were observed throughout the test; these are shown in Figure 69. It should be noted that the average wave height was used in all calculations. The comparison in

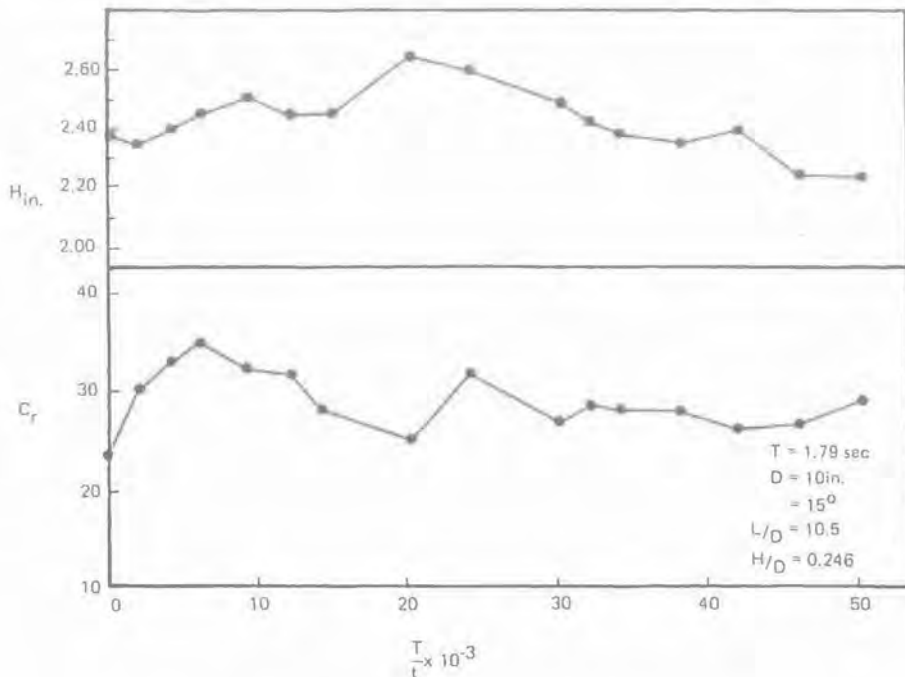


Figure 69. Fluctuation of H and C_r as a function of T/t [18].

Table 4 was made between theoretically calculated values and experimental results.

3. Scouring of natural flat sand beaches occurs in a narrow range defined between boundary limits of wave breaking and incipient sand movement. The

Table 4
Calculated Values vs. Experimental Results

Experiment	Calculated value from Eq. (7.21) (in.)		Average scour depth \bar{S} (in.)	Maximum scour depth S_{max} (in.)
	$y = \frac{1}{2}\delta$	$y = 5d$		
A1	-1.13	0.585	0.457	0.50
A2	1.56	1.664	1.103	1.50
A3	1.22	1.950	1.170	1.55
A5	1.35	1.272	1.300	1.80
A6	1.09	1.170	1.420	1.80
A7	1.21	2.380	1.373	1.45

limit of wave breaking may be taken as $H/d = 0.78$ from the solitary wave theory. The limit of incipient sand motion was approximately defined as $H/d = 0.43$ for 45° , 67.5° , and 90° seawalls and $H/d = 0.33$ for the 15° and 30° seawalls for the conditions studied.

5. For wave conditions within these limits it was found that the depth of scour initially increases with increasing number of waves acting on the bed, but reaches a constant value when the ultimate depth of scour is attained.
6. For all cases the predominant scouring pattern had a spacing between crest λ equal to one-half the wavelength L , and the depth of scour B was one-fourth of the wavelength.
7. The ultimate depth of scour is a function of the reflection coefficient. The depth of scour increases with increase in reflection coefficient up to a high value of wave reflection.
8. Because of all the seawalls studied the coefficient of reflection is lowest for the 15° seawalls, the depth of scour was also the least.
9. The relative ultimate depth of scour was approximately the same for the 45° , 67.5° , and 90° seawalls, as there is little difference between coefficient of reflection for these seawalls.

The calculated values were based on two assumptions: (a) $y = 1/2$ and $\delta = 1.72(ux/U)^{1/2}$ and $\eta = y(U/(L/2))^{1/2}$ (column 2) and (b) $y = 5d$ (column 3).

The agreement between theoretically predicted values and experimentally obtained values is considered good.

Uncertainties Involved in Scour Predictions

There are several uncertainties involved in predicting scour, as indicated throughout this book. The uncertainties can be enumerated on the basis of prediction accuracy for several variables:

1. Information regarding the soil characteristics is difficult to obtain economically. Many disturbed and undisturbed soil samples may be taken, but the soil conditions may be different between the locations where the samples are obtained. Also, in a dynamically active area the ocean floor may be undergoing erosion or deposition, and samples taken during the winter season, for example, may not be representative of the ocean-floor characteristics of the summer.
2. Information regarding the magnitude and frequency of waves for any given location may not be available or may be difficult to obtain. A wave monitoring program, which must be carried out for at least 12 months, is expensive. Wave characteristics may also be obtained by hind-casting methods from the synoptic weather charts, but the accuracy for any given location may not be as good as desired.
3. Information regarding the magnitude and frequency of currents for any given location may not be available or may be difficult to obtain. The general circulation patterns in the oceans are known, but the magnitude of currents near the ocean floor is not generally available. In addition, there are current

reversals during the year and unless a long-term (12 months) current monitoring program is undertaken, the one-time current measurement may be misleading.

4. Wave-structure interaction for a given structure is complicated, and the equations developed to determine forces rely on the estimates of velocities and accelerations obtained as in (1).
5. Scour patterns for a given structure and given waves and currents have generally been determined from small-scale models in the laboratory. The results of these tests can at best be qualitative rather than quantitative. Field tests are expensive and very few have been conducted.

References

1. Alexander, H. Personal communication, 1977.
2. Anderson, A. G. "Scour at Bridge Waterways—A Review," Report No. FHWA-FD-75-89, Federal Highway Administration, Washington, DC, 1974.
3. Angus, N. M. and Moore, R. L. "Scour Repair Methods in the Southern North Sea." OTC Paper 4410, Offshore Technology Conference, 1982.
4. Armbrust, S. L. "Scour about Cylindrical Pile due to Steady and oscillatory Motion." M.S. thesis, Texas A&M University, 1982, College Station, Texas.
5. Bagnold, R. A., "Sand Movement by Waves: Some Small-scale Experiments with Sand of very low density," *J. Inst. Civ. Eng.* 27–28: 447, 1964.
6. Bijker, E. W. "The Increase of Bed Shear in a Current due to Wave Motion." Delft Hydraulics Laboratory Publication No. 46, 1967, Delft, The Netherlands.
7. Bijker, E. W. "Wave-Seabed-Structure Interaction," Proc. 1st Behaviour of Offshore Structures Conference, 1976, pp. 830–845.
8. Breusers, H. N. C. "Local Scour Near Offshore Structures," Proc. Offshore Hydrodynamics Symposium, 1971, Oosterveld, M.W.C., Wageningen, Netherlands. pp. X, 1–X, 16.
9. Breusers, H. N. C. and Nicollet, G., Shen, H. W. "Local Scour Around Cylindrical Piers," *J. Hydraulic Research*, Vol. 15, No. 3, 1977, pp. 211–252.
10. Carstens, M. R. "Similarity Laws for Localized Scour." *J. Hydraulics Div.*, Proc. ASCE. Vol. 92, No. 1443, 1966, pp. 13–36.
11. Chao, J. L. and Hennessy, P. V. "Local Scour Under Ocean Outfall pipelines," *J. Water Pollut. Contr. Fed.*, Vol. 44, no. 7, 1972, pp. 1443–1447.
12. Chow, W. Y. and Herbich, J. B. "Scour Around a Group of Piles," Proceedings of the Offshore Technology Conference, Houston, 1978 Texas, Paper No. 3308.
13. Daniels, M. and Swank, J. C. "Northern North Sea Pipelines—The Brent System," *Proc. Offshore Technol. Conf., OTC 2601*, Houston, 1976.
14. Das, M. M., "A Literature Review on Bed-Load Transport Due to Wave Action and Localized Scour in Noncohesive Sediments;" in *A literature review on Erosion and Deposition of Sediment near Structures in the Ocean* (by H. A. Einstein and R. L. Wiegel), Univ. of California, Berkeley, 1970.
15. Eadie, IV, R. W., Herbich, J. B. "Scour about a Single, Cylindrical Pile Due to Combined Random Waves and a Current", Proc. 20th Coastal Engr. Conf., ASCE, 1986, pp. 1858–1870.
16. Eagleson, P. S., and Dean, R. G. "Wave Induced Motion of Bottom Sediment Particles," Paper no. 3225, T. ASCE, Vol. 126, Part I, 1961, pp. 1162–1189.
17. Herbich, J. B., Murphy, H. D., and Van Weele, B., "Scour Flat Sand Beaches Due to Wave Action in Front of Seawalls," Proc. Coastal Engineering, Santa Barbara Speciality Conference, ASCE, 1965.

18. Herbich, J. B., and Ko, S. C., "Scour of Sand Beaches in Front of Seawalls," Proc. Coastal Engineering, ASCE, Chapter 40, 1968.
19. Herbich, J. B. "Comparison of Model and Beach Scour Patterns," *Proc. Coastal Eng.*, ASCE, Washington, D.C., Chap. 30 1970.
20. Herbich, J. B. *Offshore Pipeline Design Elements*, 1981, Marcel Dekker, Inc. 233 pp.
21. Herbich, J. B., Schiller, Jr., R. E., Watanabe, R. K., and Dunlap, W. A. *Seafloor Scour: Design Guidelines for Ocean-Founded Structures*, Marcel Dekker, New York, 1984, 336 pages.
22. Howarth, L. "The Solution of the Laminar Boundary Layer Equations," *Proc. Royal Society (London)*, A164, 1938, 547.
23. Imberger, J. "Scour Behind Circular Cylinders in Deep Water," Proc. 18th Coastal Engineering Conference, Vol. 2, ASCE, 1972.
24. Jain, S. C. and Fischer, E. E. "Scour Around Circular Bridge Piers at High Froude Numbers," Report No. FHWA-RD-79-104, Federal Highway Administration, Washington, DC, 1979.
25. Jonsson, I. G. "Wave Boundary Layers and Friction Factors, Proc. 10th Coastal Engineering Conference, Vol. 1, 1966, pp. 127-148.
26. Kjeldsen, S. P., Gjorsvik, O., Bringaker, K. G., and Jacobsen, J. "Local Scour Near Offshore Pipelines," Proc. 2nd Int. Conf. on Port and Ocean Engineering under Arctic Conditions, 1973, pp. 308-331.
- 26a. Lambe, T. W. and Whitman R. V. *Soil Mechanics*, John Wiley & Sons, Inc., New York, 1969.
27. Lee, T. Y., "Scour Around a Group of Circular Piles Caused by Waves and Currents," unpublished M. S. thesis, Ocean Engineering, Texas A&M University, 1983.
28. Li, H. "Stability of Oscillatory Laminar Flow Along a Wall," Technical Memorandum No. 47, Beach Erosion Board, San Francisco, 1954.
29. Lovera, F., and Kennedy, J. F. "Friction-Factors for Flat-Bed Floors in Sand Channels," *Proc. ASCE*, Vol. 95, 1969, pp. 1227-1234.
30. Machemehl, J. L. and G. Abad. "Scour Around Marine Foundations," OTC Paper 2313, Offshore Technology Conference, 1975, pp. 691-702.
31. Manohar, M., "Mechanics of Bottom Sediment Movement Due to Wave Action," Technical Memorandum No. 75, Beach Erosion Board, U.S. Army Corps of Engineers, 1955.
32. Melville, B. W. "Local Scour at Bridge Sites," Dept. of Civil Engineering, Report No. 117, University of Auckland, New Zealand, 1975.
33. Miche, M., "The Reflecting Power of Maritime Works Exposed to Wave Action," *Annales de Ponts et Chaussées* (in French) 1951.
34. National Cooperative Highway Research Program. "Scour at Bridge Waterways," Highway Research Board, 1970.
35. Niedoroda, A. W., Dalton, C., and Bea, R. G. "The Descriptive Physics of Scour in the Ocean Environment," OTC paper 4145, Offshore Technology Conference, Vol. IV, 1981, pp. 297-304.
36. O'Donnell, J. P. "Pipeline Problems in the North Sea Get Solutions After Costly Research Efforts," *Offshore*, October 1975, pp. 69-71.
37. Palmer, H. D. "Wave-induced Scour on the Seafloor." *Proc. Civ. Eng. Oceans II*, ASCE, 1969, pp. 703-716.
38. Palmer, H. D. "Wave-induced Scour Around Natural and Artificial Objects," Ph.D. thesis, 1970, University of Southern California.
39. Posey, C. J., and Sybert, J. H. "Erosion Protection of Production Structures," Proc. 9th Convention, Int. Assoc. Hydraul. Res., 1961, pp. 1157-1161.
40. Posey, C. J. "Protection Against Under scour, OTC Paper 1304 Offshore Technology Conference, 1970.

41. Posey, C. J. "Protection of Offshore Structures Against Under scour." *J. Hydraul. Div., Proc. ASCE*, Vol. 97, No. HY7, 1971 pp. 1011-1016.
42. Rance, P. J. "The Potential for Scour Around Large Objects. Scour Prevention Techniques around Offshore Structures," Seminar held in London, Dec. 16, 1980. Society for Underwater Technology. pp. 41-53.
43. Shen, H. W., Schneider, U. R., and Roper, A. T. "Analytical Approach to Local Scour," Proceedings of the 12th Congress of the International Association for Hydraulic Research, Vol. 3, Sec. C18-C19, 1967.
44. Smith, D. C., IV, Herbich, J. B. and Spence, T. W. "Factors Influencing Equilibrium of a Model Sand Beach," TAMU-SG-77-203, Texas A&M University, College Station.
45. Straub, L. G. and Herbich, J. B., "Experimental Studies of Wave Filters and Absorbers," St. Anthony Falls Hydraulic Laboratory Project Report No. 44, University of Minnesota, Minneapolis, 1956.
46. Straub, L. G., Herbich, J. B., and Bowers, C. E., "An Experimental Study of Wave Absorbers," Project Report No. 54, 1957. St. Anthony Falls Hydraulic Laboratory, University of Minnesota, Minneapolis.
47. Straub, L. G., Herbich, J. B., and Bowers, C. E., "Laboratory Tests of Permeable Wave Absorbers," *Proc. Coastal Engineering Conference*, Chapter 44, 1958.
48. Streeter, V. L. *Fluid Mechanics*. 5th ed. 1971, McGraw Hill, New York.
49. Task, P. D. *Recent Marine Sediments*, American Association of Petroleum Geologists, 1939, Menasha, Wisc.
50. Teramoto, S., Tagaya, K., Yatagai, K., Marase, Y. and Niomiya, K. "Study on Scouring of Sit-on-Bottom Type Offshore Structure," *Technical Review*, Vol. 10, no. 1, ser. no. 26, 1973, Hiroshima, Japan.
51. Delft University, "Drilling-Platform Mobiloil, Scouring Around Spuds," Report on Model Investigation, Waterloopkundig Laboratorium, Delft, 1965.
52. Van Ast, W., de Boer, P. L. "Ontgroning onder een pijpleiding door stroming en l of golven," unpublished Master's thesis (in Dutch), Civil Eng. Dept., Delft Institute of Technology, 1973.
53. Van Dijk, R. N. "Experience of Scour in the Southern North Sea," *J. Soc. Underwater Technol.*, Vol. 7, No. 1, 1981, pp. 18-22.
54. Venezian, G., Personal communication, 1981.
55. Vincent, G. E. "Contribution to the Study of Sediment Transport on a Horizontal Bed Due to Wave Action." *Proc. 6th Conf. Coastal Eng., ASCE*, 1975, pp. 326-335.
56. Wang, R. K., and Herbich, J. B., "Combined Current and Wave Produced Scour Around a Single Pile," Texas Engineering Experiment Station, Report No. COE 269, 1983, Texas A&M University, College Station, Texas.
57. Watson, T. "Scour in the North Sea," Preprints, 2nd Annual European Meeting, Soc. Pet. Engrs of AIME, London, England, Paper No. 4314, 1973.
58. Wells, D. R., and Sorensen, R. M., "Scour Around a Circular Pile Due to Oscillatory Wave Motion," TAMU-SG-70-208, Report No. COE 113, 1970, Texas A&M University, College Station, Texas.
59. Wells, D. R. and Sorensen, R. M. "Scour Around a Circular Cylinder Due to Wave Motion," *Proc. 12th Coastal Engineering Conference*, Ch. 79, 1970, pp. 1263-1280.
60. Wilson, N. D. and Abel, W. "Seafloor Scour Protection for a Semi-Submersible Drilling Rig on the Nova Scotian Shelf," OTC Paper 1891, Offshore Technology Conference, 1973, pp. 631-646.
61. Yang, C. T. "Incipient Motion and Sediment Transports," *Proc. ASCE, J. Hydraul. Div.*, Vol. 99, no. HY10, 1973, pp. 1679-1704.
62. Yen, B. C., Allen, R. L. and Shatto, H. H. "Geotechnical Input for Deep-Water Pipelines," *Civ. Eng. Oceans*, Vol. 1, 1975, p. 504.